The development of a vibration absorber for vibrating screens

by

Nicolaas Francois du Plooy

submitted in partial fulfilment of the requirements for the degree

M.Eng

in the Faculty of Engineering
University of Pretoria

Pretoria

December 1999

The development of a vibration absorber for vibrating screens

by

Nicolaas Francois du Plooy

Supervisor : Prof. PS Heyns
Department : Mechanical and Aeronautical Engineering
Degree : M.Eng

Summary

High levels of vibration are essential for the proper operation of vibrating screens. However, this motion imparts high dynamic loads on their support structures leading to premature failure or costly construction. Various methods exist for the attenuation of these forces, but they require undesirable addition of weight to the screen assembly, which can be as much as 130% of the screen mass. More appropriate methods are pendulum, hydraulic and liquid inertia vibration absorbers. These devices can provide similar isolation at only a fraction of the weight increase of current screen isolation methods. The liquid inertia vibration absorber's unique properties make it ideal for the attenuation of screen forces, as this study will show.

A mathematical model describing the motion for the vibration absorber was derived. This led to an equation describing the force transmissibility, which was used to show which parameters influence the absorber's performance. The model was extended to take into account the effect of conical port inlets/outlets, which were used to reduce the viscous damping. The effect of viscous damping was quantified using computational fluid dynamics. The mathematical model was used to show how an optimal set of parameters could be found.

Two design procedures were developed for the vibration absorber and were then used to design an experimental absorber. The experimental absorber was used to validate the mathematical model. Several practical considerations for the design were discussed and solutions suggested. The stiffness of the absorber was estimated using finite element modelling. Two elastomeric springs of different hardnesses were fitted to the absorber. The softer spring achieved a transmissibility of 16% by 42 Hz. The main stumbling block in reducing the transmissibility even further is the reduction of the damping.

The experience gained from the experimental absorber was used to suggest how an absorber could be applied to a screen. An absorber isolating at 12.5 Hz was designed for this purpose. A theoretical design study investigated two possible configurations of absorber fitment. When the absorber was fitted directly to the screen the force transmitted was reduced 7.2 times. Fitting the absorber to the sub-frame gave similar transmissibility results to that of a screen fitted with a sub-frame only, but the mass ratio was only 15%.

The outcome of this study is a thorough understanding of liquid inertia vibration absorbers as well as a procedure for their optimal design.

Keywords: Vibration absorber, vibrating screen, elastomer mechanical properties, sub-frame, transmissibility, isolation frequency, liquid inertia.

Die ontwikkeling van 'n vibrasie-absorbeerder vir vibrerende siwwe

deur

Nicolaas Francois du Plooy

Studieleier : Prof. PS Heyns
Departement : Meganiese en Lugvaartkundige Ingenieurswese
Graad : M.Ing

Opsomming

Hoë vlakke van vibrasie is belangrik vir die werking van vibrerende siwwe. Hierdie vibrasie veroorsaak egter hoë dinamiese kragte wat na die fondasie van die sif oorgedra word. Die kragte kan vroegtydige faling of hoë aanvanklike konstruksiekoste tot gevolg hê. Verskeie metodes bestaan wat gebruik kan word om die kragte te verminder, maar dit vereis dat groot hoeveelhede massa by die struktuur gevoeg word. Die massa kan tot 130% van die sifmassa beloop. Meer toepaslike metodes is die gebruik van pendulum, hidrouliese en vloeistof traagheid vibrasie-absorbeerders. Hierdie toestelle kan soorgelyke isolasie verskaf teen 'n fraksie van die massaverhoging van huidige metodes. Hierdie studie toon dat die vloeistof traagheid vibrasie-absorbeerder unieke eienskappe het wat dit idiaal maak vir die attenuasie van sifkragte.

'n Wiskundige model wat die beweging van die sif beskryf is opgestel. Dit het gelei tot die afleiding van die krag transmissie vergelyking, wat gebruik is om aan te toon watter veranderlikes die gedrag van die absorbeerder sal beïnvloed. Die model is uitgebrei om ook die invloed van koniese poort inlate/uitlate in ag te neem. Hierdie inlate is gebruik om die viskeuse demping van die absorbeerder te verminder. Die effek van die viskeuse demping is bepaal deur van berekeningsvloeidinamika gebruik te maak. Die wiskundige model is gebruik om aan te toon hoe die optimale stel parameters bepaal kan word.

Twee ontwerpmetodes is ontwikkel wat gebruik is om 'n eksperimentele absorbeerder te ontwerp. Die absorbeerder is gebruik om die wiskundige model te verifieer. Verskeie praktiese probleme met die ontwerp is bespreek en oplossings is voorgestel. Die styfheid van die veer is bepaal deur gebruik te maak van 'n eindige-element model. Twee poliuretaan vere van verskillende hardhede is in die absorbeerder gegiet. Die sagter veer het 'n krag

transmissie van 16% by 42 Hz getoon. Die krag transmissie kan verder verminder word deur die demping te verlaag.

Die ondervinding wat opgedoen is met die eksperimentele absorbeerder is gebruik om voor te stel hoe 'n absorbeerder op 'n sif gebruik kan word. 'n Absorbeerder wat by 12.5 Hz isoleer is vir die doel ontwerp. 'n Teoretiese ontwerp studie van twee absorbeerder en sif konfigurasies is aan die hand gedoen. Wanneer die absorbeerder direk op die sif geïnstalleer word kan die krag wat na die fondasie oorgedra word met 7.2 keer verminder word. Wanneer die absorbeerder onder 'n subraam geïnstalleer word kan dieselfde resultate as vir 'n sif met net 'n subraam verwag word, maar dan teen net 'n 15% verhoging in massa.

Die resultaat van die studie is 'n deeglike analise van vloeistof traagheid vibrasie absorbeerders en 'n metode vir hul optimale ontwerp.

Sleutelwoorde: Vibrasie-absorbeerder, vibrerende sif, meganiese eienskappe van poliuretaan, subraam, krag transmissie, isolasie frekwensie, vloeistof traagheid.

Acknowledgements

I would like to thank:

- Prof. PS Heyns for his guidance and encouragement
- My parents for their unfailing support
- Mr. PJ Venter of the CFD laboratory for his advice regarding the flow analysis
- Staff of the LGI for their help with the tests.

Table of contents

CHAPTER 1

Introduction and literature review

1.1 Introduction

Many modern industrial machines rely on vibration for their operation. Oscillatory motion is essential for screens, rock drills, compactors etc. Their proper operation demands high levels of vibration, usually to the detriment of their support structures and operators.

The combined forces imparted by the vibration of several vibratory screens simultaneously, may for example cause fatigue failure of the supporting structures and plant buildings, or may alternatively require much more expensive civil engineering infrastructure than is really necessary (Greenway, 1983).

Various techniques exist which can be employed to reduce this vibration. The most common method is the use of low stiffness and damping isolators. This method is limited by the permissible static deflection of the isolating springs. Other methods include the use of sub-frames and counterweights. These methods add a lot of mass and cost to the structure. Sub-frames will also increase the transient response of the system and counterweights will require more force to achieve the desired acceleration. This study will specifically show how vibration absorbers can be employed to reduce the amount of vibration transmitted to the support structure.

Vibration absorbers are devices used to attenuate the vibration of a primary system by adding a secondary spring and mass system (Rao, 1990). The absorber reduces the response at a tuned isolation frequency. At the isolation frequency the inertia of the secondary system is utilised to cancel the forces normally transmitted to the structure or the operator's hands. Such devices can therefore be used on machines that are primarily operated at a dominant frequency of excitation, like vibrating screens or rock drills.

A literature survey revealed that this subject has been investigated thoroughly. The most suitable absorber concept found was the Liquid Inertia Vibration Eliminator developed for helicopter rotor head vibration attenuation (Halwes, 1980). This concept uses hydraulic amplification of the absorber mass through a proper geometric arrangement. This feature is exploited to achieve isolation without the weight penalty of current screen isolation methods.

The second chapter will be devoted to finding the equations describing the absorber's isolation properties. An experimental absorber was built and tested. The design is documented in chapter three and the experimental results subsequently. In chapter five a comparison of the isolation and absorbing techniques available for screens is presented.

1.2 Vibrating machines

A wide variety of vibrating machines are used in industry to achieve a range of material handling functions. This study will specifically investigate vibrating screens. An introduction to vibrating screens is therefore necessary. This introduction will include the classification of vibrating machines, which will be used to narrow down the area of investigation. The screen motion can be characterised by angle, stroke length, frequency and stroke pattern. The motion is important since it will influence the feed rate and screening effectiveness. The motion requirements will be discussed in the paragraph on bulk solid movement theory. It is also necessary to define the terminology used in the screening industry. The basic elements of a screen will be listed. This will include the different configurations used for the isolation and forcing of screens. Next these elements will be constructed into a single degree-of-freedom mathematical model. This model will be used to show what the requirements for screen isolation are.

1.2.1 Classification of vibrating machines

Vibrating machines can be classified as follows (Frolov & Goncharevich, 1991):

- Vibrating mixers, separators and installations for compaction and loosening of disperse mediums.
- Vibration transport and processing machines.
- Vibrating elevators.
- Vibrating crushers.
- Vibration machines for strengthening treatment (i.e. surface hardening).

Frolov & Goncharevich define vibrating screens as "a variety of vibrating separators with perforated sieving surfaces". Screening units perform a function of scalping, de-dusting, grade sizing, washing or de-liquefying (Heyns & Van Niekerk, 1997). Grade sizing or classification can be done by size, shape, density, friction coefficient or other specific properties of the particles that constitute the medium. The medium can also be classified in more than one class by using multiple sieving surfaces.

Although this work will concentrate specifically on vibrating screens, the techniques developed will also be applicable to other vibrating machines operating at a constant excitation frequency.

1.2.2 Bulk solid movement theory

Particles are moved or conveyed over the screening surface through a series of hops. This motion is achieved by the application of either a circular, elliptical or uni-directional stroke as illustrated by figure 1.1.

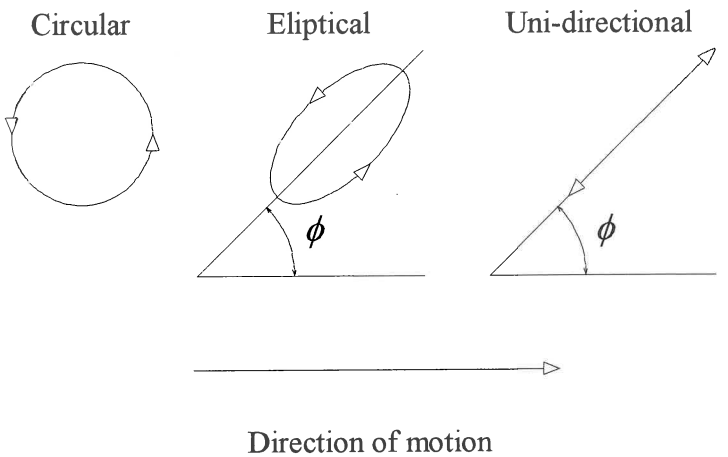

Figure 1.1 Stroke patterns (Dumbaugh, 1984)

Linear strokes are generally more efficient than either circular or elliptical strokes. A stroke angle of 30° is generally used for vibratory conveying while angles of 45° achieve better results for screening. In practice these may vary significantly according to the specific unit's function. The feed rate is a function of the stroke length and the frequency. High feed rates will diminish screening effectiveness.

Screens can be mounted on steep declines in which case a circular or elliptical stroke pattern should be used. Most often they are, however, mounted horizontally and a linear stroke pattern will be the most efficient.

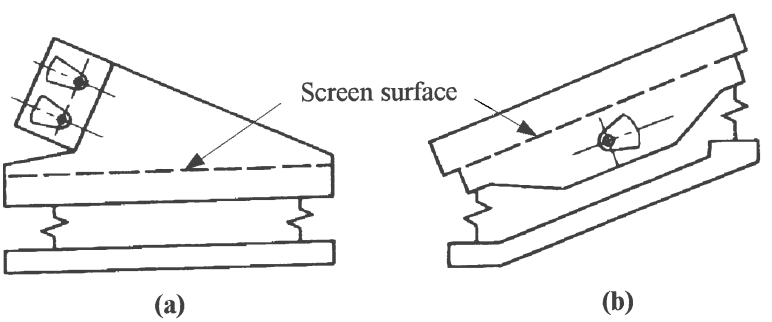

Figure 1.2 (a) Horizontal and (b) inclined screen mounting methods (Frolov & Goncharevich, 1991)

Accelerations of 3.5g are best for the conveying materials. For effective screening accelerations of between 4 and 5g are necessary (Dumbaugh, 1984). The acceleration can be achieved by varying the frequency or the stroke amplitude. Large amplitude and low frequency are used for large-sized materials and low amplitude, high frequency to size fine feeds.

1.2.3 Basic elements and configurations of vibrating screens

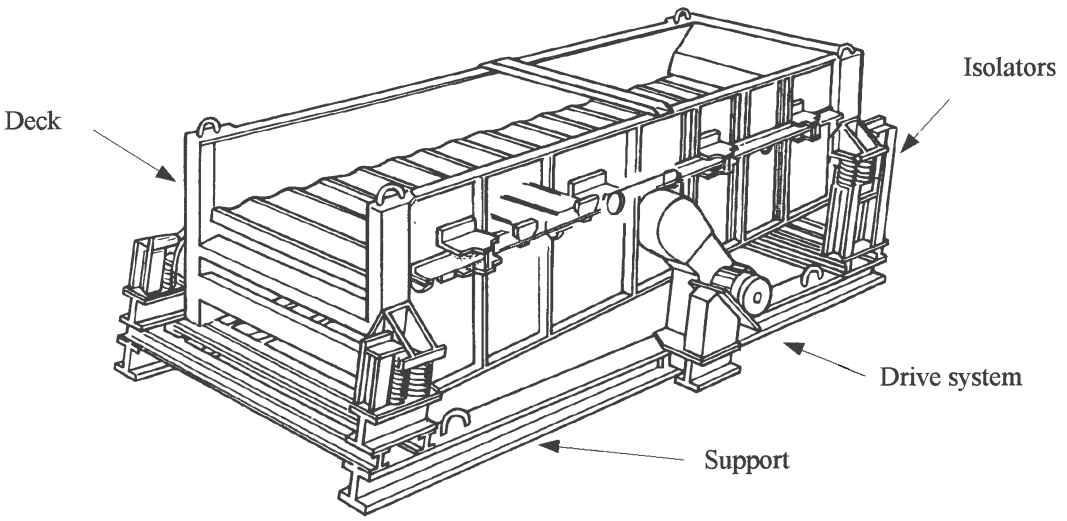

Figure 1.3 Screen elements (Frolov & Goncharevich, 1991)

The following basic elements can be identified:

- The member that contains the bulk solid is called the trough, pan, screen body or deck. More than one screening deck can be utilised to classify materials into several groups.
- The screen is exited by the vibratory drive system. Drive systems can either be linear electromagnetic shakers, rotating eccentric masses or eccentric link exciters (figure 1.4). Because of its simplicity, rotating eccentric masses are very commonly used for driving screens. To achieve linear motion, contra-rotating masses are used as shown in figure 1.2(a). Often two drives are used, one fixed with a horizontal and one with a vertical forcing direction, resulting in a 45° forcing angle.
- The screen is supported by isolation springs. Isolation springs can be either elastomeric, steel or air springs.
- The screen may be equipped with a counterweight or a sub-frame to reduce the amount of force transferred to the support

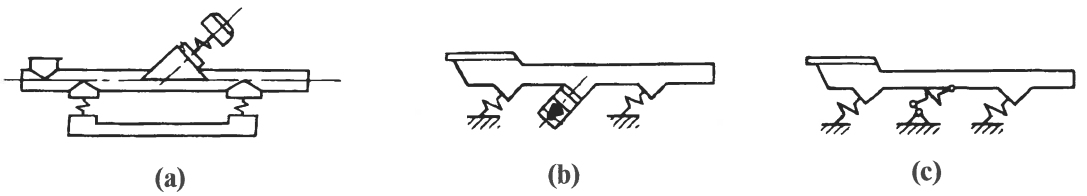

Figure 1.4 Vibratory drive systems (a) electromagnetic shaker (b) rotating eccentric masses (c) eccentric link (Frolov & Goncharevich, 1991)

1.2.4 Screen isolation assembly requirements

The objective of vibration isolation is the reduction of dynamic loads transferred to the supporting structure and the reduction of energy losses. To understand how isolator properties affect each of these it is necessary to derive a simple, single degree-of-freedom mathematical model as shown in figure 1.5.

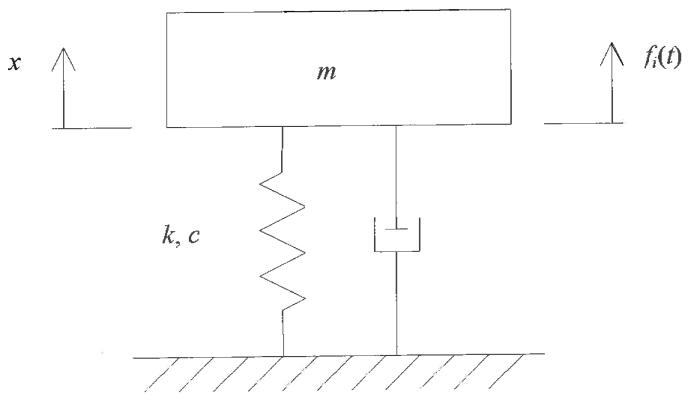

Figure 1.5 A single degree-of-freedom model of a vibrating screen

Effective isolation has the objective of low transmissibility of dynamic forces. The transmissibility is defined in terms of the applied and transmitted forces. The equation of motion is:

$$m\ddot{x} + c\dot{x} + k = f_i(t) \tag{1.1}$$

By substituting the assumed harmonic response and its derivatives, equation 1.1 can be transformed to the frequency domain (Rao, 1990):

$$\frac{X}{F_i} = \left[-\omega^2 m + i\omega c + k\right]^{-1} \tag{1.2}$$

The force transmitted to the support structure is the sum of the spring and damping forces:

$$F_o = (k + i\omega c)X \tag{1.3}$$

The transmissibility of the system is the ratio of force transmitted to the foundation (F_o) to that of the excitation force (F_i) and is shown in equation 1.4:

$$T_r = \left|\frac{F_o}{F_i}\right| = \left\{\frac{1+\left[2\zeta\frac{\omega}{\omega_n}\right]^2}{\left[1-\left(\frac{\omega}{\omega_n}\right)^2\right]^2+\left[2\zeta\frac{\omega}{\omega_n}\right]^2}\right\}^{\frac{1}{2}} \tag{1.4}$$

Equation 1.4 may be written in non-dimensional form using the well-known definitions:

$$\omega_n = \sqrt{\frac{k}{m}} \tag{1.5}$$

$$c_c = 2\sqrt{km} \tag{1.6}$$

$$\zeta = \frac{c}{c_c} \tag{1.7}$$

ω/ω_n is known as the frequency ratio.

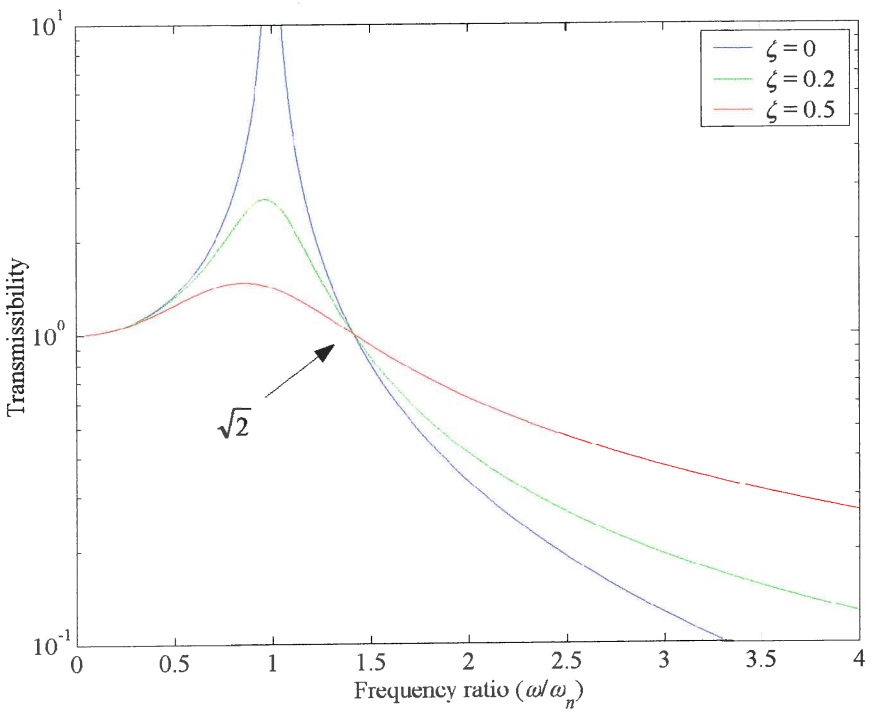

Figure 1.6 The influence of damping on the transmissibility of an isolator

For the design of a screen's isolating assembly the following requirements could be listed. (not all of these can be met simultaneously):

1. The low transfer of dynamic forces during steady state operation requires:
   - Low damping.
   - Low natural frequency, which will require low stiffness (equation 1.5).
2. The low transfer of dynamic forces during transient operation requires high damping.
3. Low static deflection requires high stiffness.
4. 4 to 5g acceleration.
5. The stresses in the springs must be low enough not to cause fatigue failure of the isolating assembly.
6. Low excitation force requires operation close to resonance.
7. Low power requirements necessitates the minimum dissipation of energy i.e. low damping.

1.3 Vibration control for vibrating screens

Vibration can be reduced in the following ways (Rao, 1990):

1. By controlling the natural frequencies of the system and avoiding resonance under external excitation.
2. By preventing excessive response of the system, even at resonance, through the introduction of damping or an energy-dissipating mechanism.
3. By reducing the transmission of excitation forces from one part of the machine to another through the use of vibration isolators.
4. By reducing the response of the system with the addition of a vibration absorber.

Agnes (1997) suggested a more basic definition and categorised all isolation attempts as either:

1. The addition of modes as will be done when adding an absorber to a system or by replacing a rigid connection with an isolator.
2. The modification of modes. This will include the addition of damping or changes in mass or stiffness.

Both these methods can either be active or passive.

A more practical classification is (Heyns & Van Niekerk, 1997):

1. Passive isolation
2. Vibration absorbers
3. Active vibration control
4. Semi-active isolation

For the purposes of this study it is suggested that vibration can either be absorbed by an inertial mass or a structure can be isolated from it. Each of these methods can be implemented in passive, semi-active or active sense. Contemporary vibration control strategies for vibrating screens use passive vibration isolators and passive vibration absorbers. The application of these methods will be discussed shortly.

1.3.1 Passive vibration isolation

Vibration isolation is achieved through the insertion of a resilient member (isolator) between the vibrating mass and the foundation as shown in figure 1.5. This method is commonly used in industry because of its relatively low cost. From figure 1.6 it is clear that operational frequencies higher than $\sqrt{2}\ \omega_n$ and low damping will result in the lowest transmissibility.

A low natural frequency is therefore desirable. This can be achieved through the use of low stiffness isolators. The natural frequency is, however, limited by the static deflection as explained by the following equation:

$$f_n = \frac{1}{2\pi}\sqrt{\frac{g}{\delta_{st}}} \tag{1.8}$$

where g is the gravitational acceleration constant.

Riddle *et al.* (1984) of the Structural Dynamics Research Corporation, in a report requested by the Anglo American Corporation, suggested that the deflection must be less than 15% of the free length for rubber isolators. For a typical screen with rubber isolators of 250 mm, δ_{st} will be 37.5 mm. Steel coil springs can be designed to have static deflections of up to 125 mm, but low axial stiffness is associated with low lateral stiffness, which can cause excessive lateral movement (Heyns & Van Niekerk, 1997). The effect of static deflection on the natural frequency is summarised in table 1.1.

Table 1.1 Natural frequency lower limits

Spring type	Static deflection [mm]	Natural frequency [Hz]
Steel coil	125	1.41
Rubber	37.5	2.57

Riddle *et al.* (1984) suggested that the natural frequency must be less than 30% of the operating frequency. A natural frequency of 25 to 33% of the operating frequency was suggested by Greenway (1983). The amount of damping is dependent on the type of isolator

used. The three types of isolators that are commonly used are steel coil springs, cylindrical solid rubber springs and Neidhart springs. Their properties are summarised in table 1.2.

Table 1.2 Comparison of isolator assemblies with a frequency ratio of 4

	Damping ratio	Isolation[1] [%]
Helical steel springs	$\eta = 0.01$	93.33
Type AB Neidhart systems[2]	$\zeta = 0.16$	89.21
Typical solid rubber spring[3]	$\eta = 0.2$	93.20

[1] $100(1 - |T_r|)$, [2] Mackie *et al.* (1997), [3] Riddle *et al.* (1984)

Pneumatic springs are known to render natural frequencies of lower than 1 Hz and may be effective, but since they are not very robust and reliable damping estimates could not be obtained they were not included in this comparison. Although steel springs provide a high amount of isolation they are prone to corrosion related fatigue failure and their low damping can be problematic during transient operation.

It would generally be advantageous for a screen to have low damping since it operates at a fixed frequency that is well above the natural frequency. A certain amount of damping is, however, required to control vibration during transients.

1.3.2 Passive vibration absorbers

The dynamic vibration absorber is a device, generating inertia, which reduces the vibration level of a protected structure (Korenev & Reznikov, 1993). Vibration absorbers can be used to achieve total isolation of a primary mass at a specific frequency by employing a secondary spring-mass system (Rao, 1990). For screens, vibration absorbers are either implemented as counterweights or sub-frames (figure 1.7). Riddle *et al.* (1984) restricted their sub-frame mass to less than 1.3 times the screen mass. Counterweights usually have weight equal to that of the screen. Both of these methods add undesirable weight to the screen assembly. Additionally the sub-frame can increase the screen motion during transients. The response should generally be less than 125% that of the response without a sub-frame.

(a) (b)

Figure 1.7 (a) A screen with a counterweight and (b) a screen with a sub-frame

The transmissibility of a system fitted with a counterweight can approach zero. A typical sub-frame design will transmit less than 10% of the screen spring force. In this study it is suggested that vibration absorbers are best suited to reduce dynamic forces and will therefore be discussed in more detail.

1.4 Vibration absorbers

1.4.1 The classic vibration absorber

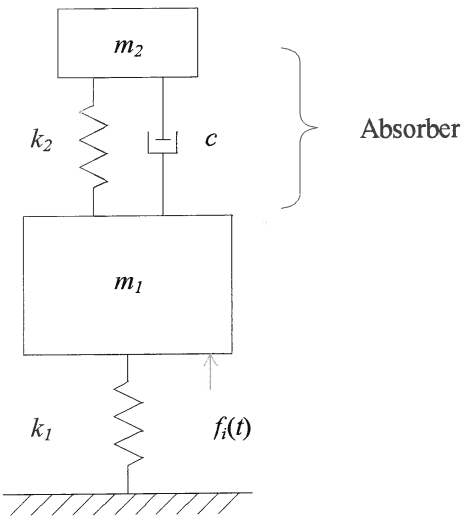

Figure 1.8 The damped dynamic vibration absorber

The classic vibration absorber was patented by Frahm in 1909. A vibration absorber consists of a primary system to which a secondary mass is added. The objective of the absorber is to minimise the motion of the primary mass. This is achieved by tuning the natural frequencies of the absorber to coincide with the excitation frequency. The result is a two degree-of-freedom system with zero response at the tuned frequency if no damping is present. This system also has two resonance frequencies, one just below and one just above the design frequency, which might reduce its effectiveness in practical applications with broad band excitation. Damping reduces the absorber's response at the resonant frequencies while also decreasing the effectiveness at the design frequency as can be seen on figure 1.9.

For most applications the added weight of the absorber will be undesirable. The mass ratio will therefore be much less than one. This implies a low stiffness and therefore a large displacement amplitude of the secondary mass. The allowable amplitude of the absorber motion will be the constraint for reducing the secondary mass. Another consideration is the effect of the mass ratio on the sensitivity to mistuning. Figure 1.10 shows that a large secondary mass will be advantageous if the primary mass is subject to changes in the

excitation frequency. In the study of vibration absorbers it is convenient to define the following ratios:

$$\mu = \frac{m_2}{m_1} \tag{1.9}$$

$$f = \frac{\omega_a}{\omega_n} \tag{1.10}$$

$$g = \frac{\omega}{\omega_n} \tag{1.11}$$

$$\omega_n = \sqrt{\frac{k_1}{m_1}} \tag{1.12}$$

$$\omega_a = \sqrt{\frac{k_2}{m_2}} \tag{1.13}$$

$$\zeta = \frac{c}{2m_2\omega_n} \tag{1.14}$$

The two important characteristic parameters for a vibration absorber are μ, the absorber's relative mass and f, the tuning ratio. The natural frequency of the primary mass is ω_n and of the absorber it is ω_a. The transmissibility is (Heyns & Van Niekerk, 1997):

$$\left|\frac{F_o}{F_i}\right| = \left\{\frac{(2\zeta gf)^2 + (g^2 - f^2)^2}{(2\zeta gf)^2\left[1 - g^2(\mu+1)\right]^2 + \left[\mu f^2 g^2 - (g^2-1)(g^2-f^2)\right]^2}\right\}^{\frac{1}{2}} \tag{1.15}$$

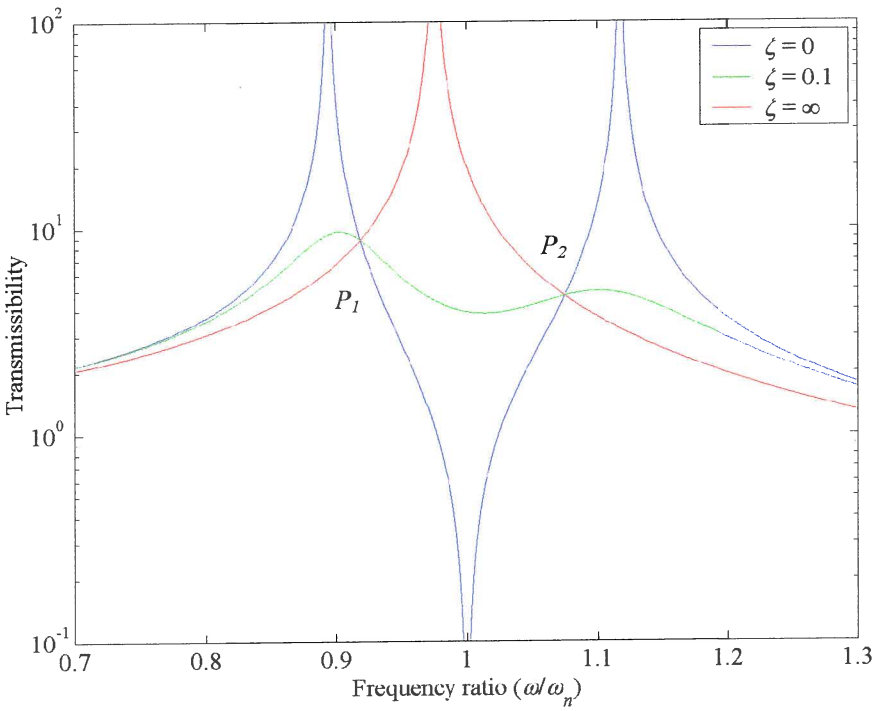

Figure 1.9 The influence of damping on the transmissibility of an absorber ($\mu = 1/20$ and $f = 1$)

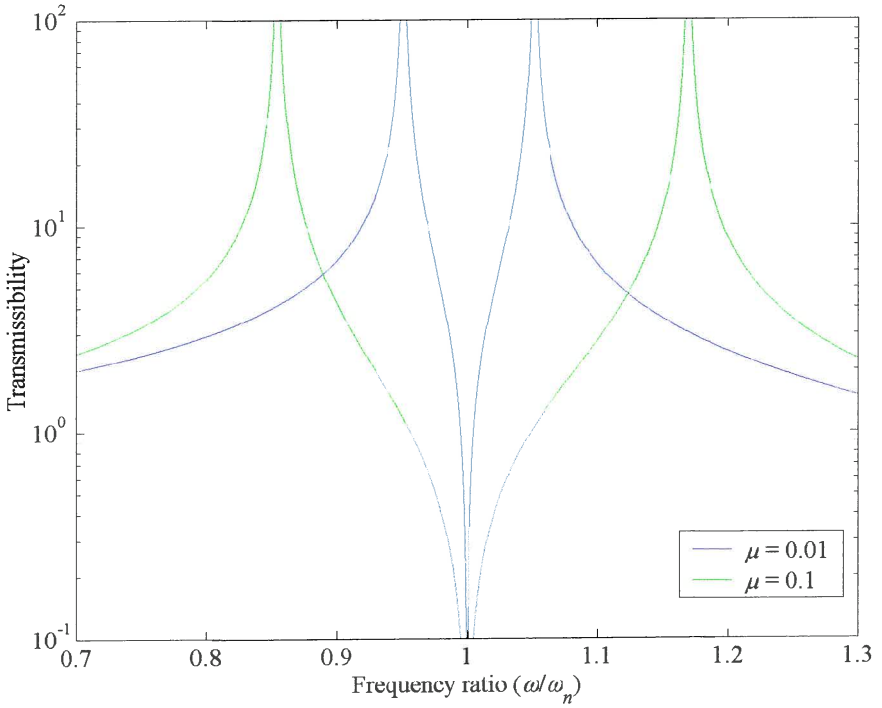

Figure 1.10 Transmissibility as a function of the mass ratio, μ ($f = 1$)

Den Hartog (1956) showed that all the curves for different damping ratios pass through the same points P_1 and P_2. Changing the ratio of natural frequencies (f) can shift the amplitude of these two points, one point going up and the other going down. The most favourable case is when the two amplitudes are equal. This was found to be (Den Hartog, 1956):

$$f = \frac{1}{1+\mu} \tag{1.16}$$

The optimum damping ratio is (Brock, 1946):

$$\zeta = \sqrt{\frac{3\mu}{8(1+\mu)}} \tag{1.17}$$

Optimal values for damped primary systems under wide band excitation are more difficult to obtain. These parameters are either given as curve fits (Tsai & Lin, 1994) or tuning diagrams (Fischer *et al.*, 1998).

Wide band excitation can also be attenuated using multiple vibration absorbers fitted to the primary structure as shown in figure 1.11. The absorbers are tuned to a range of frequencies. It is possible to increase the suppression bandwidth by increasing the number of absorbers (Igusa & Xu, 1991).

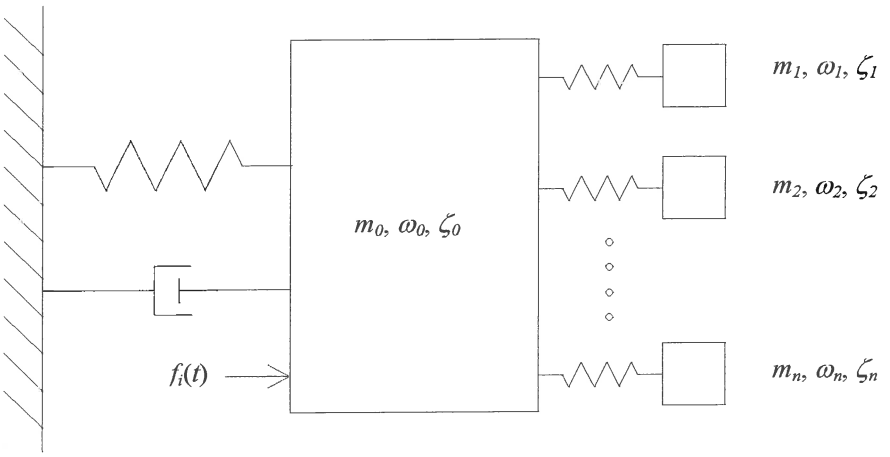

Figure 1.11 Multiple vibration absorbers in parallel

Non-linear vibration absorbers can be constructed using a non-linear stiffness element to connect the absorber to the primary mass. These absorbers have been found to increase the suppression bandwidth (Rice, 1987) and can be advantageous for sinusoidal excitation that may vary over a small frequency range. Harmonic instability can result for cases of low damping and high non-linearity.

It has also been shown that a vibration absorber can be employed to reduce the transient response of a system (Johnson, 1991). In this study the transient response was optimised so that the steepest possible decay takes place. It was found that the optimal stiffness ratio is the same as for the tuned harmonic response absorber, but that the optimal damping could be quite different.

1.4.2 Semi-active vibration absorbers

Vibration absorbers are passively tuned to match the excitation frequency. Slight variations in excitation frequency can have a significant effect on the primary system response. It is possible to decrease the sensitivity by increasing the absorber mass, but adding weight is undesirable (refer to figure 1.10). Tuning the absorber natural frequency requires that the absorber mass or stiffness be changed. O'Leary (1969) used a variable mass type absorber and reported a 1.5 Hz tuning range. Various novel tuneable stiffness designs exist. Franchek *et al.* (1995) described a coil spring with a collar that controlled the number of active coils and Margolis & Baker (1992) used the variable positioning of a fulcrum to vary the stiffness. Desanghere & Vansevenant (1991) used air pressure to adaptively tune the absorber stiffness.

It has been shown that a LR-shunted piezoceramic fixed between the primary system and the ground behaves like a mechanical vibration absorber (Agnes, 1997). Piezoelectric absorbers are tuned by changing the inductance of the RLC circuit.

1.4.3 Active vibration absorbers

It is also possible to use a positive position feedback actuator, fitted between the primary mass and the ground, to mimic a vibration absorber (Agnes, 1997). This absorber can be tuned using control system parameters. Olgac & Holm-Hansen (1993) introduced a delayed resonator where an actuator fitted between the primary and secondary masses is tuned using time delay and gain. It has been shown that the delayed resonator can reduce the primary response to zero.

1.4.4 Nodal beams and pendulums

The nodal beam concept is based on the existence of nodal points on a vibrating beam. Consider the beam response to a vertical force as shown in figure 1.12.

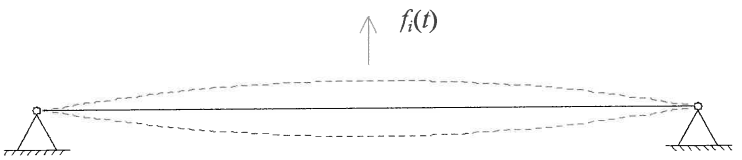

Figure 1.12. Using nodes to limit the transfer of the dynamic force

When the pinned-pinned beam is excited at its first fundamental natural frequency, two nodal points appear at the ends of the beam. Since these nodes have no motion, no force is transmitted to the ground. This property was exploited by Gaffey & Balke (1976) to produce a vibration absorber to reduce helicopter vibration. By extending the beam past the support points and adding a tuning weight to the beam's tips they were able to reduce the total weight of the absorber. The flexibility of the beam was also increased by adding a flexible joint in the middle of the beam. As soon as such a discontinuity is added the term pendulum absorber is preferred.

The Improved Rotor Isolation System (IRIS) designed by Desjardins & Hooper (1980) also used hinges and achieved 96-99% isolation during in flight testing with a weight penalty of 1.5%. The concept can be explained using figure 1.13.

At position A both the masses, the spring and inertia bar are in the neutral position. At position B the vibration of mass 1 is upward, the spring is stretched and the inertia bar is forced downward. Mass 2 remains stationary. At point D the process is reversed.

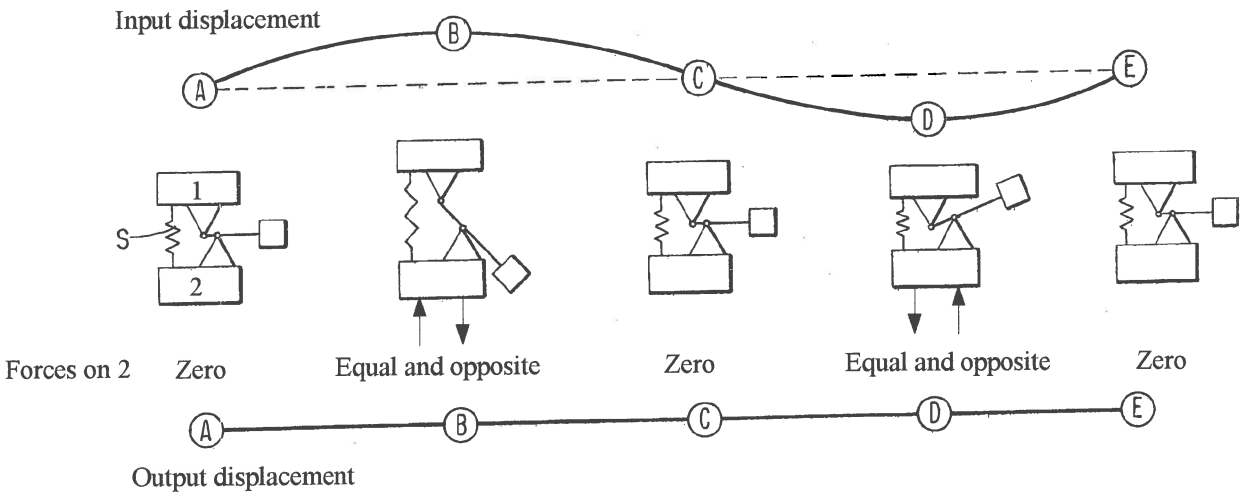

Figure 1.13 Explanation of force cancellation (Desjardins & Hooper, 1976)

It is important to note that isolation only takes place at a specific frequency. This isolation frequency can be found by analysing the equation of motion for the absorber system. A complete derivation is shown in Appendices A to C. In appendix A, a single degree of freedom system is analysed. Appendix B shows an absorber configuration added underneath a screen. Appendix C takes the effects of a flexible support into account. It is important to note which parameters influence the isolation frequency. The parameters are defined in figure 1.14 and are the two geometrical quantities, r and R, the stiffness k_1, the mass m_B and the moment of inertia of the mass m_B about its centre of gravity.

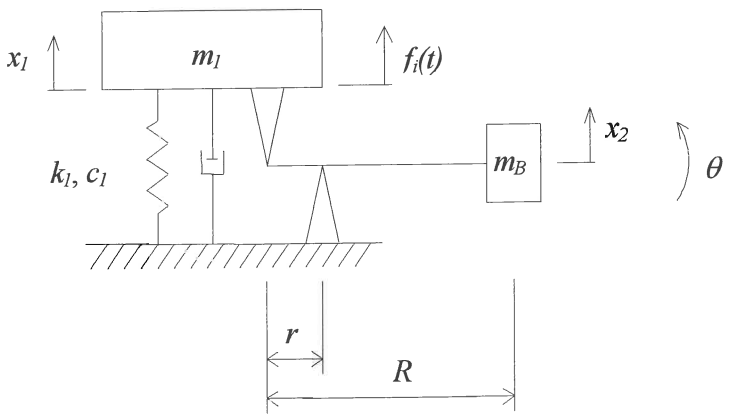

Figure 1.14 Parameters for the mechanical absorber

The complex force transmissibility is (equation A.20):

$$\frac{F_o}{F_i} = \frac{k_1 + i\omega c_1 + \omega^2\left[m_B\left(1-\frac{R}{r}\right)\frac{R}{r} - \frac{I_G}{r^2}\right]}{k_1 + i\omega c_1 - \omega^2\left[m_1 + m_B\left(1-\frac{R}{r}\right)^2 + \frac{I_G}{r^2}\right]} \tag{1.18}$$

The undamped isolation frequency is found by equating the numerator of equation 1.18 to zero:

$$\omega_a = \sqrt{\frac{k_1}{m_B\left(\frac{R}{r}-1\right)\frac{R}{r} + \frac{I_G}{r^2}}} \tag{1.19}$$

The undamped isolation frequency is independent of the system mass (m_1). This is a huge advantage for screens where the system mass may vary according to the load. Additionally the isolation frequency is a function of five parameters where the classic vibration absorber had only two tuning parameters. This gives the designer more flexibility. A comparison of non-dimensional transmissibility with and without an absorber is shown in figure 1.15. at the isolation frequency the system with an absorber's transmissibility is 33% less than for a system without an absorber. An additional advantage is the proximity to the natural frequency, which means that the spring stiffness can be increased improving the screen's stability. The force input can also be decreased while maintaining the desired acceleration.

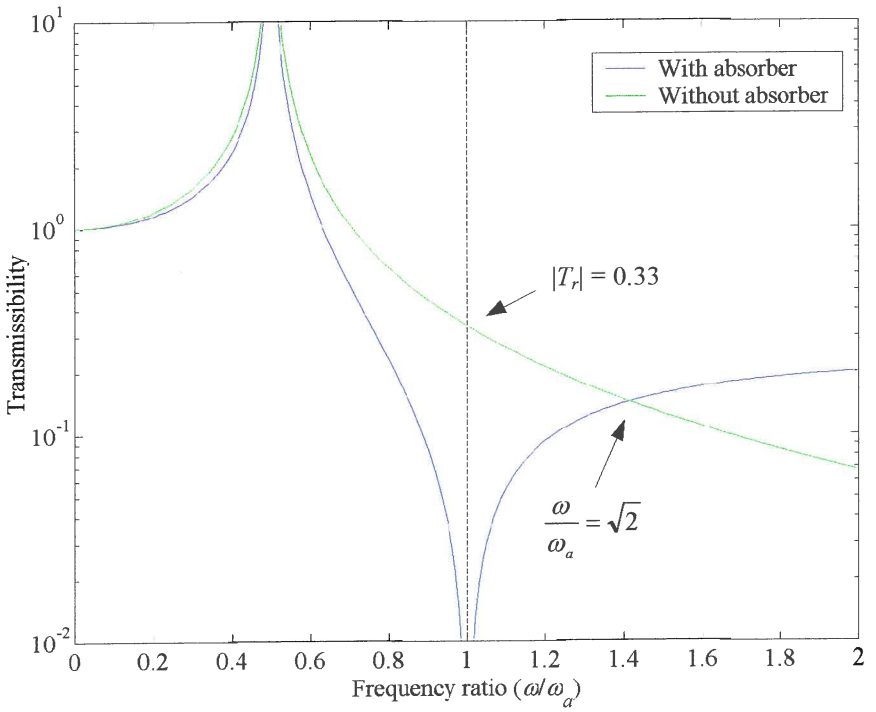

Figure 1.15 Isolator and absorber transmissibilities for systems of equal natural frequency ($\omega_a = 1$)

The practical implementation of the mathematical model is shown in figure 1.16:

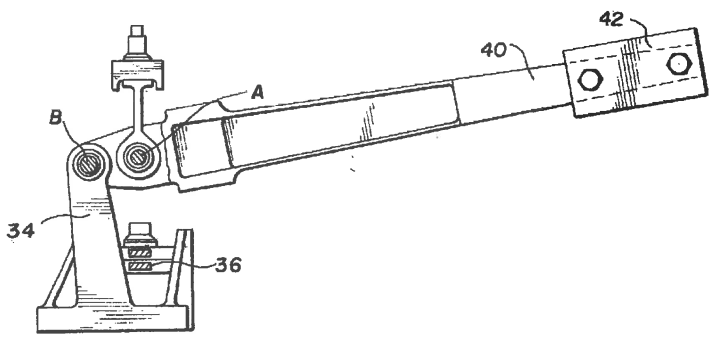

Component description	
A	Airframe pivot
B	Floor pivot
34	Anchor pad
36	Spring
40	Arm
42	Weight

Figure 1.16 IRIS for helicopter passenger floor isolator (Dejardins & Hooper, 1982)

Most of the mechanical designs have some provision for tuning after manufacture. This is usually done by moving the tip mass on the inertia bar.

This system was also improved to isolate at two frequencies by adding a spring mass system to the inertia bar as shown in figure 1.17.

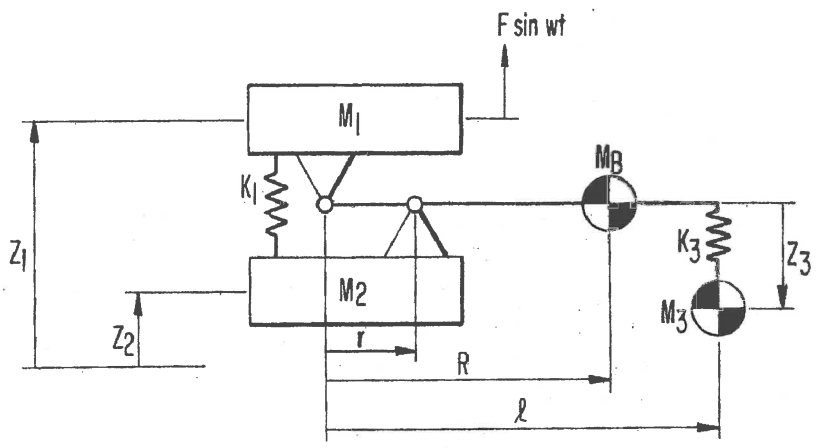

Figure 1.17 IRIS schematic for two isolation frequencies (Desjardins & Hooper, 1978)

The Dynamic Anti-resonant Vibration Isolator (DAVI) designed by Flannely (1966) operates on the same principle as the IRIS. Flannely observed that the isolation frequency could either be before or after the natural frequency of the system. Although it might seem attractive to have isolation before the natural frequency this will require a heavy absorber. Additionally, such an absorber will have a narrow bandwidth and will amplify high frequency vibrations. The DAVI was therefore designed with the isolation frequency occurring after the natural

frequency. Low isolation frequencies could be achieved with low static deflections. The importance of low damping is emphasised by figure 1.18.

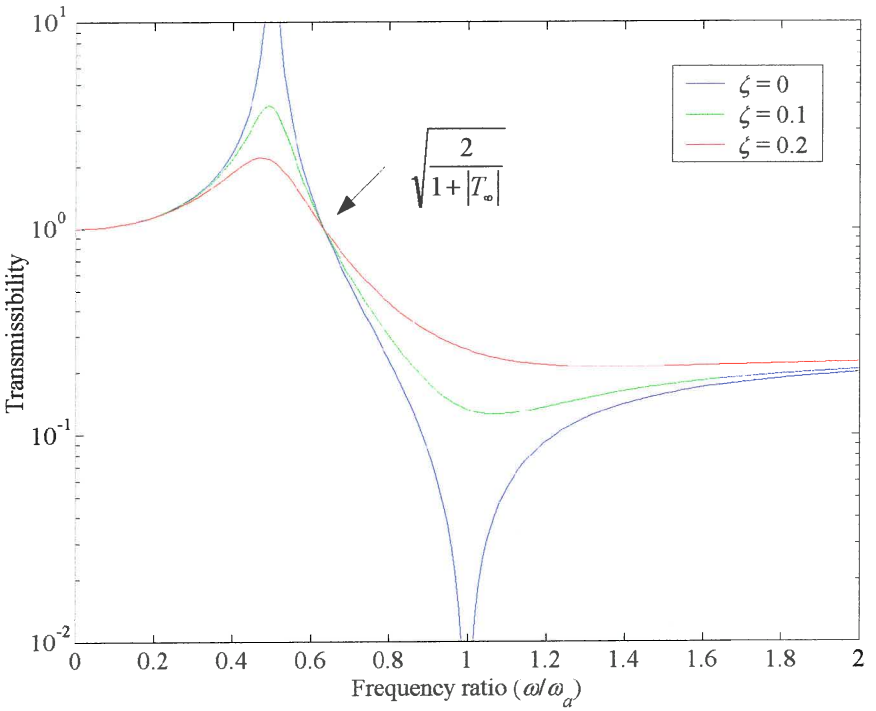

Figure 1.18 Transmissibility as a function of the damping ratio

Flannely defined the high frequency transmissibility as when the inertia terms in equation 1.18 dominates:

$$T_\infty = \frac{m_B\left(\frac{R}{r}-1\right)\frac{R}{r}+\frac{I_G}{r^2}}{m_1+m_B\left(1-\frac{R}{r}\right)^2+\frac{I_G}{r^2}} \qquad \textbf{(1.20)}$$

The high frequency transmissibility is also the ratio of the isolation to the natural frequency and will be defined such in the rest of the text. The invariant point frequency ratio ($|T_r| = 1$) is given in terms of the high frequency transmissibility:

$$\frac{\omega}{\omega_n} = \sqrt{\frac{2}{1+T_\infty}} \qquad \textbf{(1.21)}$$

For a conventional isolator this point is simply the square root of 2. It was also proved that the DAVI system would always have a response less than that of a conventional isolator having the same static deflection. The DAVI was used to isolate at 10.8 Hz. The durability of their design was proved with extensive bench and flight-testing (Rita *et al.*, 1976).

Braun (1980) published the results of the MBB Anti-Resonance Isolation System (ARIS) program. An analysis was made of different pivot bearings and it was found that elastomeric bearings provided good isolation efficiency as well as adequate radial stiffness. Braun expanded the mathematical model to include the radial and torsional stiffness and damping of the two pivots. The springs used for this design were constructed of glass fibre.

1.4.5 Hydraulic mass amplification

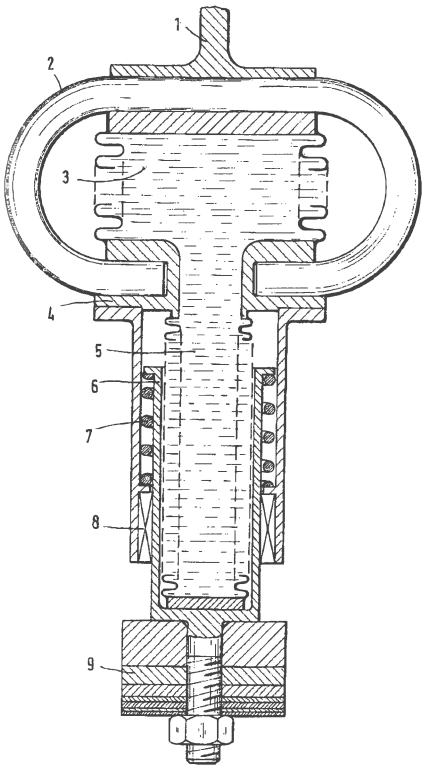

Description of elements	
1	Input force attachment
2	Glass fibre spring
3	Primary fluid chamber
4	Support
5	Secondary fluid chamber
6	Bushing
7	Spring
8	Bearing
9	Inertia mass

Figure 1.19 MBB vibration absorber (Braun, 1988)

The vibration absorber shown in figure 1.19 is essentially the same as the mechanical absorber described previously. The vibration absorber is a parallel connection of a spring and a mass with a hydraulic transmission. The absorber consists of two metal bellows and an additional glass fibre spring. The bellows form a self-containing unit and is filled with a low viscosity fluid. To minimise the flow losses it is necessary to avoid any sharp edges in the bellows system. The absorber mass is fitted to the secondary bellows and is supported by a linear bearing. The additional spring pressurises the fluid in the bellows system.

The inertia of the tuning mass causes a pressure change in the fluid chamber that acts on the vibrating mass connected to the top of the absorber and is therefore termed the force

generator. At the isolation frequency this force cancels the force imparted by the spring on the structure. The primary bellows is thick-walled in order to act as a spring. The secondary bellow is thin walled (0.25 mm) to allow large axial displacements. The isolation achieved by this design was better than 99%.

The mathematical model used was:

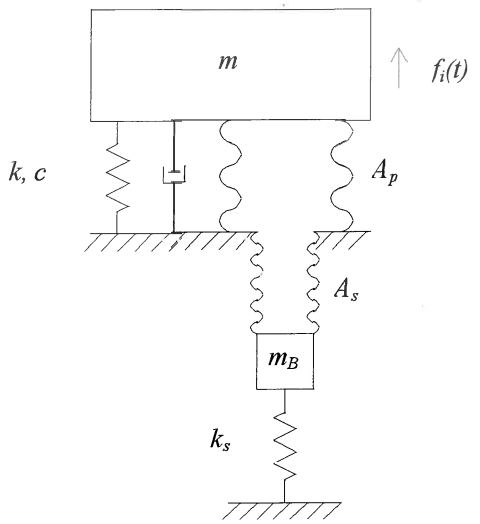

Figure 1.20 Mathematical model of the hydraulic absorber with A_p the area of the primary fluid chamber and A_s the area of the secondary fluid chamber

The undamped isolation frequency is:

$$\omega_a = \sqrt{\frac{k + k_s\left(\frac{A_p}{A_s}\right)^2}{m_B\left(\frac{A_p}{A_s} - 1\right)\left(\frac{A_p}{A_s}\right)}} \qquad \textbf{(1.22)}$$

This tuning equation differs slightly from equation 1.19 in that there is no rotary inertia present in the system and the spring k_s is amplified by the area ratio.

The advantages of this design are:

- Total symmetric arrangement of the spring and the force generator.
- Simple wear-resistant design.
- Consists of low-cost components.
- Only translational movement of the absorber mass is permitted.
- Heavily loaded pendulum bearings are not required.
- Very low damping of the spring and force generator.
- Good linearity of the isolator springs.
- Small installation space.

- Low weight.
- The force generator also allows displacement out of the isolator operating direction.
- It would be possible to add an additional spring and mass assembly for two-frequency isolation.

1.4.6 The Liquid Inertia Vibration Eliminator (LIVE)

The LIVE system was developed by Bell Helicopter Textron (Halwes, 1981). The main objective was to reduce helicopter vibrations, which contributed to crew fatigue and poor component reliability. A high-density, incompressible, low viscosity and high surface tension fluid is accelerated through a tuning port and is simultaneously used as a hydraulic fluid and an absorber mass (figure 1.21). Mercury and selenium bromide was suggested as suitable fluids. Due to relative motion between the inner and outer housing the absorber fluid is pumped through a tuning passage and generates amplified inertial forces on the inner and outer housing. At a certain frequency the inertia forces of the fluid match the spring force and the net effect is that only the damping force is transmitted. 95% isolation was achieved. The total weight penalty for the LIVE system was less than 0.75% of the helicopter gross weight. The overall size of the unit is inversely proportional to the square of the fluid density.

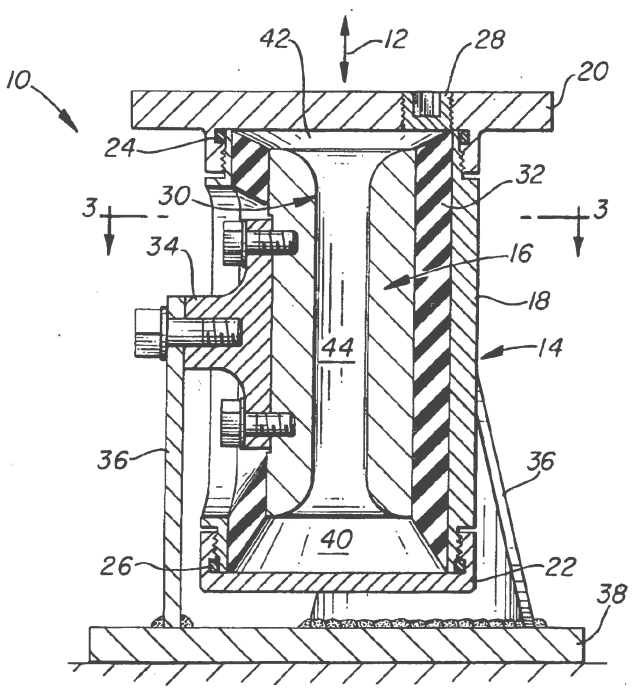

Component description	
10	Vibration isolator
12	Force direction
14	Outer housing
16	Inner housing
18	Central section
20	End section
30	Tuning cylinder
32	Elastomeric spring
38	Plate
40	Chamber
42	Chamber
44	Passage

Figure 1.21 LIVE system internal design (Halwes, 1980)

The undamped isolation frequency is:

$$\omega_a = \sqrt{\frac{k}{m_B\left(\frac{A_b}{A_a}-1\right)\left(\frac{A_b}{A_a}\right)}} \tag{1.23}$$

The advantages of this concept are:

- Reduced complexity
- Bearingless construction
- Motion safety stops inherent to the design
- Small installation envelope needed
- Linear response at high g's
- Low weight and cost
- Very low maintenance requirements

Several attempts have been made to design a semi-actively tuneable LIVE unit. Since the isolation frequency is also a function of geometric variables, there is considerably more scope for tuning than for a classic vibration absorber. Figure 1.22(a) shows an absorber with adjustable tuning port length. It is also possible to change the tuning port area by deforming a flexible member as shown in figure 1.22(b). In the same patent it is also suggested that the system damping can be decreased by adding velocity to the fluid in the tuning port. This was done using an appropriate magnetic field arrangement.

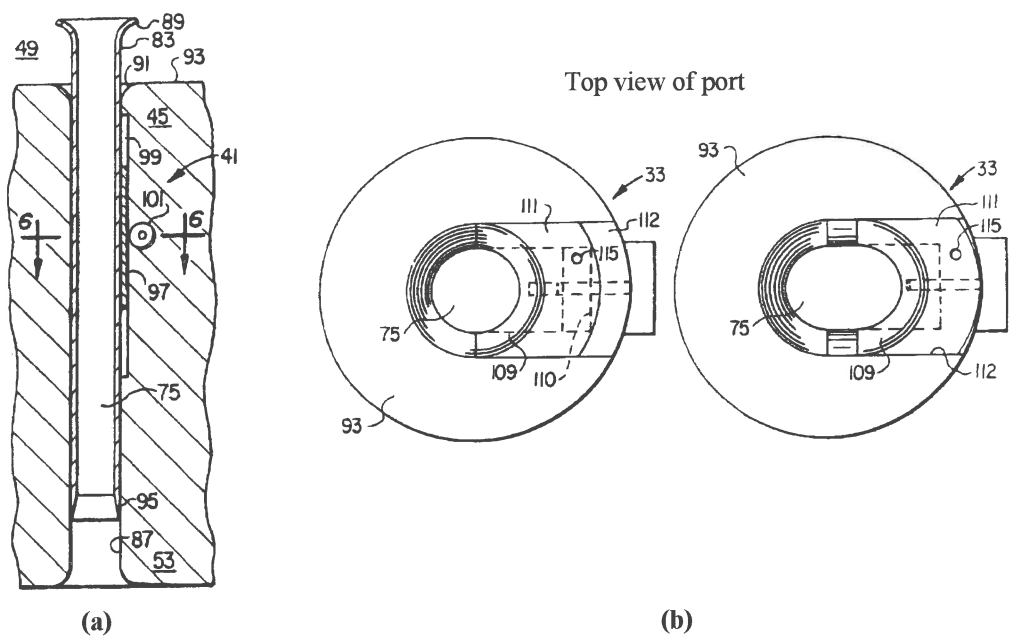

Figure 1.22 Adjustable (a) port length and (b) area (Smith & Stamps, 1998)

The fluidlastic® mount manufactured by the Lord Corporation is the only instance of a commercially available vibration absorber. Its construction was greatly simplified by keeping the port stationary and forcing the fluid through it. Furthermore it was not necessary to move the outer housing independently from the inner housing since a diaphragm was fitted at the bottom of the mount.

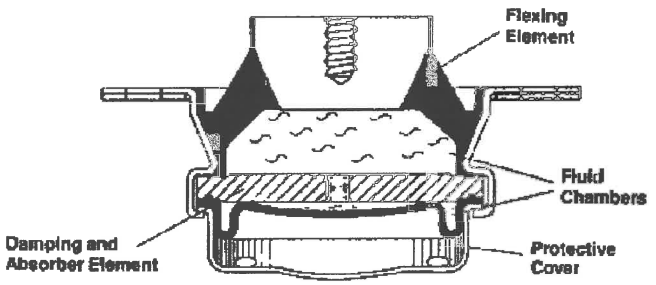

Figure 1.23 Sectional view of the fluidlastic® mount (Lord Corporation)

1.5 Objectives

The LIVE concept is the most suitable design for the attenuation of screen excitation forces. Its main advantages are the low maintenance requirements and reduced complexity. The benefit over a pendulum configuration is its linear construction without large masses vibrating through large amplitudes. The hydraulic absorber will need regular replacement due to fatigue of the metal bellows, which will make it uneconomical for this application.

The objectives of this study are to:

- Analyse the LIVE absorber using currently available techniques like finite element analysis and computational fluid dynamics.
- Design and build a LIVE type absorber. This objective's aim is to establish design guidelines and to gain experience with construction techniques specifically relating to the elastomeric spring.
- Characterise the absorber through a series of tests. The important characteristics are isolation frequency and transmissibility.
- Use the experience gained through this process to confidently predict the applicability of this absorber for a vibrating screen application.

CHAPTER 2

Mathematical model of a liquid inertia vibration absorber

2.1 Introduction

In this chapter a mathematical model of a liquid inertia vibration absorber will be developed. The absorber is similar to the LIVE concept patented by Halwes (1980) which was discussed in the previous chapter. The basic elements of the absorber are the elastomeric spring, a tuning port containing the liquid absorber mass and two liquid reservoirs. The dimensions of the reservoirs and tuning port as well as the properties of the liquid determine the response of the system. The effect of these can be found by deriving the equations of motion, which will be done in the first paragraph.

The following paragraphs will attempt to show that the damping originates from the tuning port and the elastomeric material. It will be shown that damping plays an important role in the amount of isolation that can be achieved. The complex stiffness of the elastomeric material will also be discussed.

Next the frequency response function and the transmissibility will be derived. From these the natural frequency and the frequency of isolation of the system will be determined. It will be shown which parameters will influence the frequency of isolation and the amount of isolation that can be achieved. The transmissibility will be non-dimensionalised to gain a better understanding of how optimal parameters can be found. Finally the possibility of optimising the design will be dealt with.

2.2 Equations of motion

The equations of motion will be derived for two cases. The first paragraph will deal with the basic design with square inlets. The purpose is to show how the equations are formulated and which design variables will influence the response. These equations are fairly easy to use and will be utilised for the design. Next, a more refined design using conical inlet geometry will be considered. Conical inlets will be used to reduce the amount of flow losses, but it will also influence the amount of absorber mass needed to achieve isolation at a certain frequency. The analysis of conical inlets can easily be expanded to accommodate any arbitrary inlet geometry.

2.2.1 Square inlet/outlet geometry

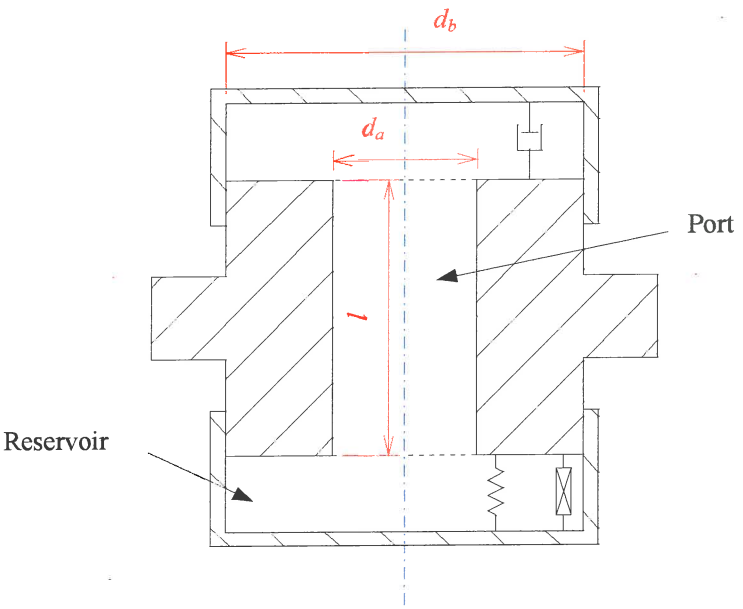

Figure 2.1 Definition of the liquid inertia system's geometry

The response of the system is governed by only 3 geometric variables (refer to figure 2.1):

- The tuning port length, l.
- The reservoir diameter, d_b. The area of the reservoir is denoted A_b.
- The port diameter, d_a. The area of the port is denoted A_a.

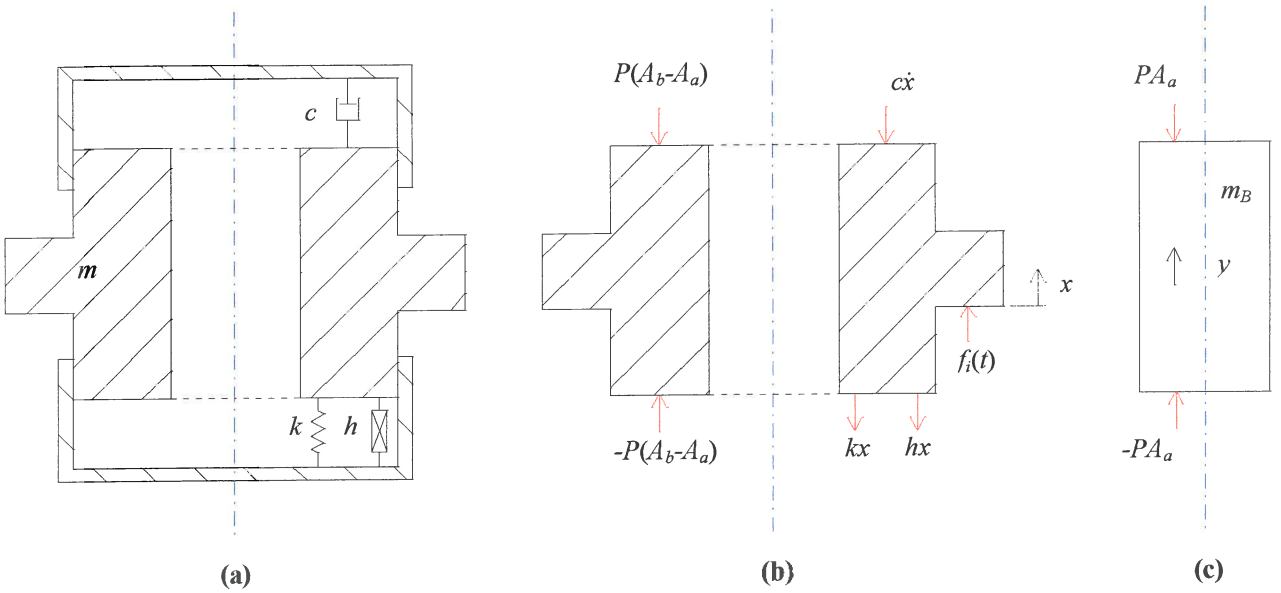

Figure 2.2 (a) Forces acting on primary system, (b) the absorber assembly, (c) forces acting on the liquid column in the tuning port

x and y denotes the displacement of the port and the liquid respectively. The relationship between $\dot{x}$ and $\dot{y}$ can be found by applying mass conservation. This relationship is called the continuity equation:

$$\begin{aligned} \dot{y}A_a &= -\dot{x}(A_b - A_a) \\ \dot{y} &= \left(1 - \frac{A_b}{A_a}\right)\dot{x} \end{aligned} \tag{2.1}$$

The force balance on the system mass (m) is:

$$m\ddot{x} = -c\dot{x} - kx - ihx - 2P(A_b - A_a) + f_i(t) \tag{2.2}$$

It is assumed that the elastomeric spring losses can be modelled using structural damping (h). The viscous damping (c) is a result of the absorber fluid losses through the tuning port.

The force balance on the absorber mass ($m_B = \rho l A_a$) is:

$$m_B\ddot{y} = -2PA_a \tag{2.3}$$

Substituting the acceleration in equation 2.3 with the conservation of mass found in equation 2.1 gives:

$$P = -\frac{m_B}{2A_a^2}(A_a - A_b)\ddot{x} \tag{2.4}$$

Using equation 2.4 the unknown pressure in equation 2.2 can be substituted to give the following single degree-of-freedom equation of motion for the system:

$$\left[m + m_B\left(1 - \frac{A_b}{A_a}\right)^2\right]\ddot{x} + c\dot{x} + k(1 + i\eta)x = f_i(t) \tag{2.5}$$

where the structural damping was written in terms of the loss factor ($h = k\eta$).

Equation 2.5 shows that the absorber mass is amplified by the area ratio and added to the system mass. The first benefit of the absorber is therefore that mass can be added to a system at relatively low cost. The second useful property of this system regards the cancellation of dynamic forces and will be shown with the derivation of the transmissibility in §2.7. Since damping plays a very important role in the amount of isolation that can be achieved, it will be discussed thoroughly.

2.2.2 Conical inlet/outlet geometry

A square inlet is very ineffective because it results in high flow losses. To reduce the amount of energy loss a smooth transition is needed. In such a port the mass and the velocity are functions of the distance from the entrance to the inlet. This paragraph will show how this effect is accounted for in the equations of motion. A formula will be derived that can be used for conical inlets, but the method can be used for any inlet geometry. The new geometry is defined in figure 2.3:

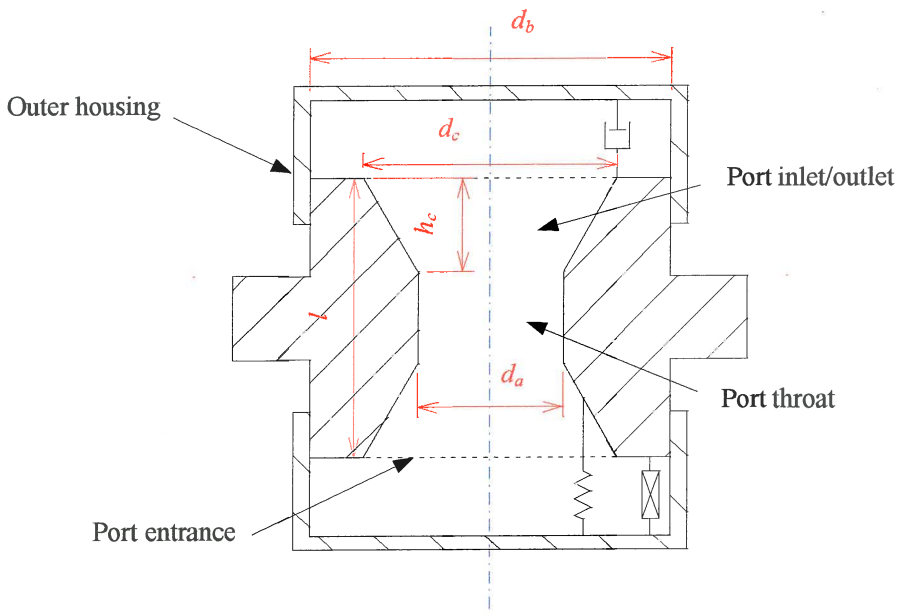

Figure 2.3 Definition of the geometry of an absorber with conical inlet/outlet

Two variables are introduced to describe the inlet geometry. They are the inlet height (h_c) and the inlet diameter (d_c). The area at the port entrance is denoted A_c.

In the previous section, the equation of motion was derived using Newton's second law of motion. For the derivation of the equation of motion in this paragraph Lagrange's equations will be used and a second degree-of-freedom (u) will be added to the system because it simplifies this analysis. Lagrange's equations are (Rao, 1990):

$$\frac{d}{dt}\left(\frac{\partial T}{\partial \dot{x}_j}\right) - \frac{\partial T}{\partial x_j} + \frac{\partial V}{\partial x_j} = Q_j^{(n)} \qquad j = 1,2,\ldots,n \qquad \textbf{(2.6)}$$

where j represents the number of degrees-of-freedom. The kinetic energy (T) is a function of mass and velocity. Both the mass and the velocity in the tuning port inlet/outlet and throat sections are functions of the geometry of the tuning port.

The following relationships are therefore needed before the kinetic energy term in Lagrange's equations can be derived:

1. The relationship between all the velocities defined by the dependent (z and y) and independent (x and u) degrees-of-freedom (figure 2.4).
2. The relationship between the inlet/outlet area and mass and the distance from the port entrance.

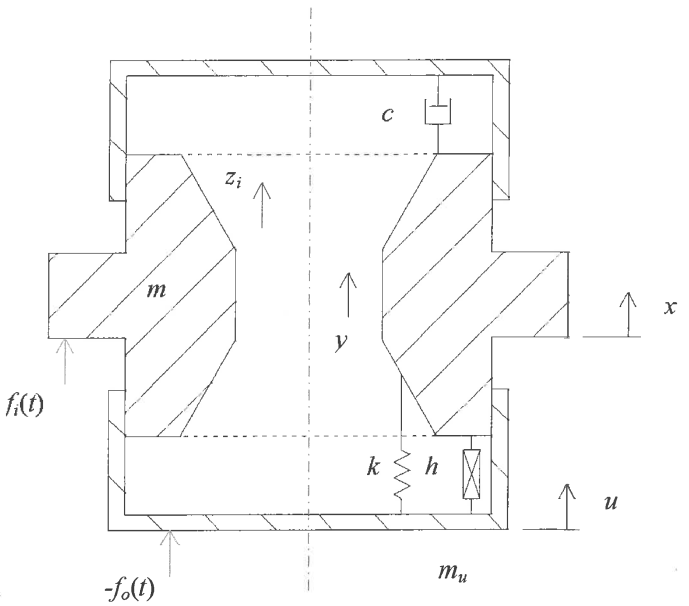

Figure 2.4 Definition of forces and displacements

The relationship between the primary system velocity ($\dot{x}$), the outer housing velocity ($\dot{u}$) and the fluid velocity in the port throat ($\dot{y}$) is given in terms of the areas:

$$-A_a\dot{y} = (A_b - A_a)\dot{x} - A_b\dot{u}$$
$$\dot{y} = \left(1 - \frac{A_b}{A_a}\right)\dot{x} + \frac{A_b}{A_a}\dot{u} \qquad (2.7)$$

The velocity in the port throat is directly related to the velocity in the inlet/outlet:

$$\dot{z} = \frac{A_a}{A_i}\dot{y} \qquad (2.8)$$

From these two equations the velocity in the inlet/outlet can be found in terms of the primary system and outer housing velocities:

$$\dot{z} = \left(\frac{A_a - A_b}{A_i}\right)\dot{x} + \frac{A_b}{A_i}\dot{u} \qquad (2.9)$$

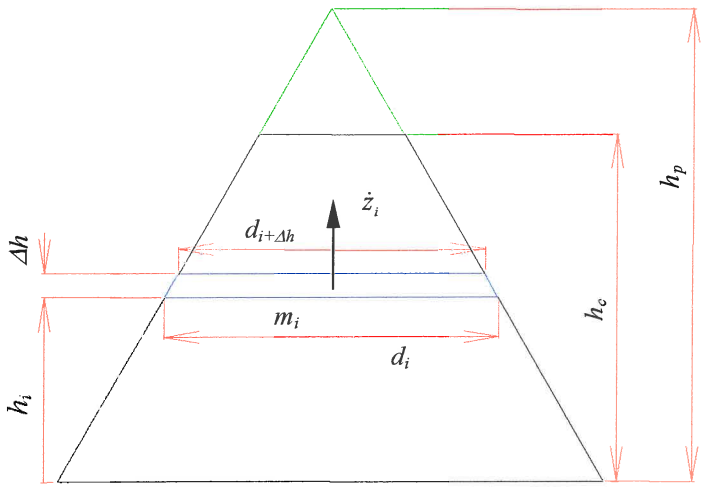

Figure 2.5 Inlet geometry definitions

The mass m_i at a distance h_i from the entrance to the port can be written in terms of the geometry and the density:

$$m_i = \frac{1}{3}\rho\frac{A_i}{(h_p - h_i)^2}\left[3\Delta h(h_p - h_i)^2 - 3\Delta h^2(h_p - h_i) + \Delta h^3\right] \tag{2.10}$$

For $\Delta h \rightarrow 0$ the higher order terms can be neglected and the equation reduces to the mass of a cylinder with height Δh:

$$m_i = \rho A_i \Delta h \tag{2.11}$$

The area is a function of the distance from the entrance to the inlet and the height of the cone defined by the inlet geometry (h_p):

$$A_i = \frac{A_c}{h_p^2}(h_p - h_i)^2 \tag{2.12}$$

The distance h_p can be expressed as a function of the basic geometric variables as follows:

$$h_p = \frac{d_c h_c}{d_c - d_a} \tag{2.13}$$

The total kinetic energy is the sum of the contribution of the primary system (m), the absorber mass in the throat of the port (m_p), the liquid in the inlet/outlet and the outer housing mass (m_u):

$$T = \frac{1}{2}\left(m\dot{x}^2 + m_p\dot{y}^2 + 2\sum m_i\dot{z}_i^2 + m_u\dot{u}^2\right) \tag{2.14}$$

After substituting the velocity values described by equation 2.7 and 2.9 the kinetic energy becomes:

$$T = \frac{1}{2}\left\{ m\dot{x} + m_p\left[\left(1-\frac{A_b}{A_a}\right)\dot{x} + \frac{A_b}{A_a}\dot{u}\right]^2 + 2\sum_{i=1}^{n} m_i\left[\left(1-\frac{A_b}{A_i}\right)\dot{x} + \frac{A_b}{A_i}\dot{u}\right]^2 + m_u\dot{u}^2 \right\} \tag{2.15}$$

From equation 2.15 the kinetic energy terms in Lagrange's equations can be derived:

$$\frac{d}{dt}\left(\frac{\partial T}{\partial \dot{x}}\right) = \left[m + m_p\left(1-\frac{A_b}{A_a}\right)^2 + 2(A_a - A_b)^2\sum_{i=1}^{n}\frac{m_i}{A_i^2}\right]\ddot{x} + \left[m_p\left(1-\frac{A_b}{A_a}\right)\frac{A_b}{A_a} + 2(A_a - A_b)A_b\sum_{i=1}^{n}\frac{m_i}{A_i^2}\right]\ddot{u} \tag{2.16}$$

$$\frac{d}{dt}\left(\frac{\partial T}{\partial \dot{u}}\right) = \left[m_p\left(1-\frac{A_b}{A_a}\right)\frac{A_b}{A_a} + 2(A_a - A_b)A_b\sum_{i=1}^{n}\frac{m_i}{A_i^2}\right]\ddot{x} + \left[m_p\left(\frac{A_b}{A_a}\right)^2 + 2A_b^2\sum_{i=1}^{n}\frac{m_i}{A_i^2} + m_u\right]\ddot{u} \tag{2.17}$$

The elastic energy is simply:

$$V = \frac{1}{2}k(x-u)^2 \tag{2.18}$$

The elastic energy terms in Lagrange's equations are:

$$\frac{\partial V}{\partial x} = kx - ku \tag{2.19}$$

$$\frac{\partial V}{\partial u} = -kx + ku \tag{2.20}$$

The damping and external forces are represented by Q_j^n. The complete equation of motion is:

$$[M]\{\ddot{x}\} + [C]\{\dot{x}\} + ([K] + i[H])\{x\} = \{f\} \tag{2.21}$$

If displacement u is set to zero then the force acting on the outer housing becomes the reaction force transmitted to the ground. The system simplifies to a single degree-of-freedom and its motion is described by the first equation in the set given by equation 2.21.

$$\left[m + m_p\left(1-\frac{A_b}{A_a}\right)^2 + 2(A_a - A_b)^2\sum_{i=1}^{n}\frac{m_i}{A_i^2}\right]\ddot{x} + c\dot{x} + k(1+i\eta)x = f_i(t) \tag{2.22}$$

This equation can be applied to any inlet geometry provided that A_i is known (m_i is dependent on A_i). If the area and the mass found in equation 2.11 and 2.12 are substituted and the sum is replaced by an integral the equation of motion becomes:

$$\left[m + \rho A_a(l-2h_c)\left(1-\frac{A_b}{A_a}\right)^2 + 2\rho\frac{A_a^2 h_p^2}{A_c}\left(1-\frac{A_b}{A_a}\right)^2\int_0^{h_c}\frac{1}{(h_p-h)^2}dh\right]\ddot{x} + c\dot{x} + k(1+i\eta)x = f_i(t) \tag{2.23}$$

Evaluating the integral leaves:

$$\left\{m+\rho A_a\left[l-2h_c+2\frac{A_a}{A_c}\left(\frac{h_p^2}{h_p-h_c}-h_p\right)\right]\left(1-\frac{A_b}{A_a}\right)^2\right\}\ddot{x}+c\dot{x}+k(1+i\eta)x=f_i(t) \qquad (2.24)$$

The force acting on the ground can be found by evaluating the second equation in the set given by equation 2.21.

$$\rho\left[l-2h_c+2\frac{A_a}{A_c}\left(\frac{h_p^2}{h_p-h_c}-h_p\right)\right]\left(1-\frac{A_b}{A_a}\right)A_b\ddot{x}-c\dot{x}-k(1+i\eta)x=-f_o(t) \qquad (2.25)$$

2.3 Viscous damping

In viscous damping, the damping force is proportional to the velocity (Rao, 1990). The forces acting on the tuning port at constant velocity is the shear force on the port wall (F_τ) and the pressure difference across the port (Δp_T). The total pressure loss consists of the pressure loss across the inlet (Δp_i), the outlet (Δp_o), and the port (Δp_w). The shear force acting in the axial direction is a function of the shear stress (τ_w) acting on the port area.

The objective of this paragraph is to find the damping coefficient as a function of the velocity of the tuning port. All the equations in the literature are however given as a function of the velocity of the liquid inside the port. The following continuity equation relates the average velocity of the fluid in the port (V) and the velocity of the port ($\dot{x}$):

$$\begin{aligned} V &= |\dot{y}| \\ &= \left(\frac{d_b^2}{d_a^2}-1\right)|\dot{x}| \end{aligned} \qquad (2.26)$$

The pressure drop across the port and the shear stress on the port wall is dependent on whether the flow is turbulent or laminar. The flow is considered to be laminar for $Re_d < 2300$. The expression for laminar shear stress is (White, 1988):

$$\begin{aligned} \tau_w^l &= \frac{\mu u_{\max}}{d_a} \\ &= \frac{2\mu V}{d_a} \end{aligned} \qquad (2.27)$$

The average velocity (V) for laminar flow is $\frac{1}{2}u_{max}$ and μ is the absolute viscosity. The expression for turbulent shear stress is (White, 1991):

$$\tau_w^t = 0.0396\rho^{3/4}V^{7/4}\mu^{1/4}d_a^{-1/4} \qquad (2.28)$$

According to White (1991) the laminar pressure drop is:

$$\Delta p_w^l = \frac{32\mu l V}{d_a^2} \tag{2.29}$$

and the turbulent pressure drop is:

$$\Delta p_w^t \approx 0.158\rho^{3/4}V^{7/4}\mu^{1/4}d_a^{-5/4} \tag{2.30}$$

The pressure drop across the inlet and the outlet is expressed in terms of loss coefficients. The relationship between the loss coefficient and the head loss is:

$$K = \frac{h_m}{V^2/2g} \tag{2.31}$$

The loss coefficient is a function of the inlet or outlet geometry. It is important to note that the port oscillates and the inlet will also act as an outlet and *vice versa*. It is therefore not advisable to design them with different geometries. The loss coefficients will be discussed using available theoretical and empirical coefficients. Since none of these exactly represent the theoretical model it will be compared with computational fluid dynamics (CFD) results. The three possibilities are:

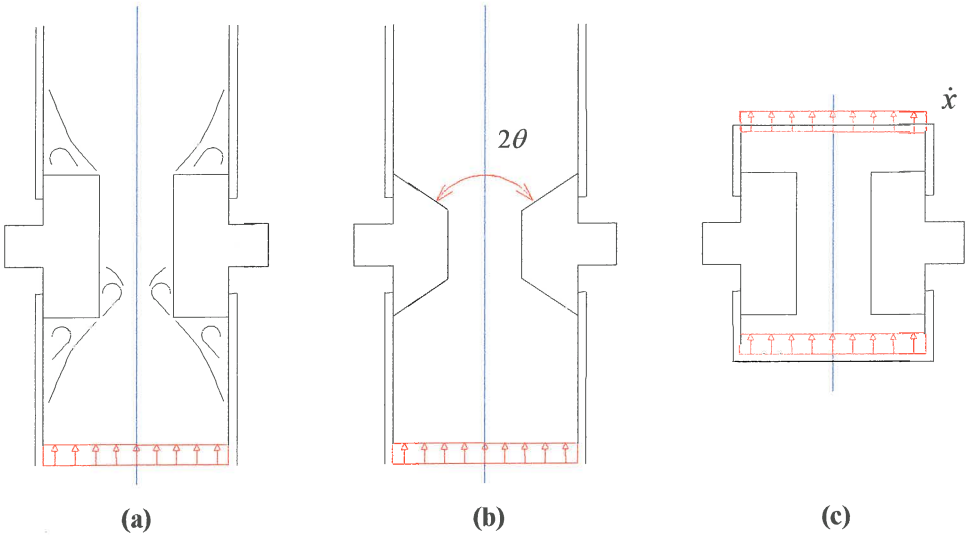

Figure 2.6 Different inlet/outlet configurations with the radially constant velocity boundary condition shown (a) infinite boundary, (b) diffuser, (c) realistic boundary

The solutions for configurations (a) and (b) have been published by White (1988). For a realistic boundary that is very close to the inlet, a solution had to be found using CFD.

2.3.1 Infinite boundary

The loss coefficient for a sudden contraction (at the inlet) is (White, 1988):

$$K_i \approx 0.42\left(1-\frac{d_a^2}{d_b^2}\right) \tag{2.32}$$

The loss coefficient for a sudden expansion (at the outlet) is expressed as:

$$K_o = \left(1-\frac{d_a^2}{d_b^2}\right)^2 \tag{2.33}$$

The head loss is related to the pressure drop by:

$$h_m = \frac{\Delta p}{\rho g} \tag{2.34}$$

The inlet pressure drop is therefore:

$$\Delta p_i \approx 0.42\left(1-\frac{d_a^2}{d_b^2}\right)\rho\frac{V^2}{2} \tag{2.35}$$

and the outlet pressure drop is:

$$\Delta p_o = \left(1-\frac{d_a^2}{d_b^2}\right)^2 \rho\frac{V^2}{2} \tag{2.36}$$

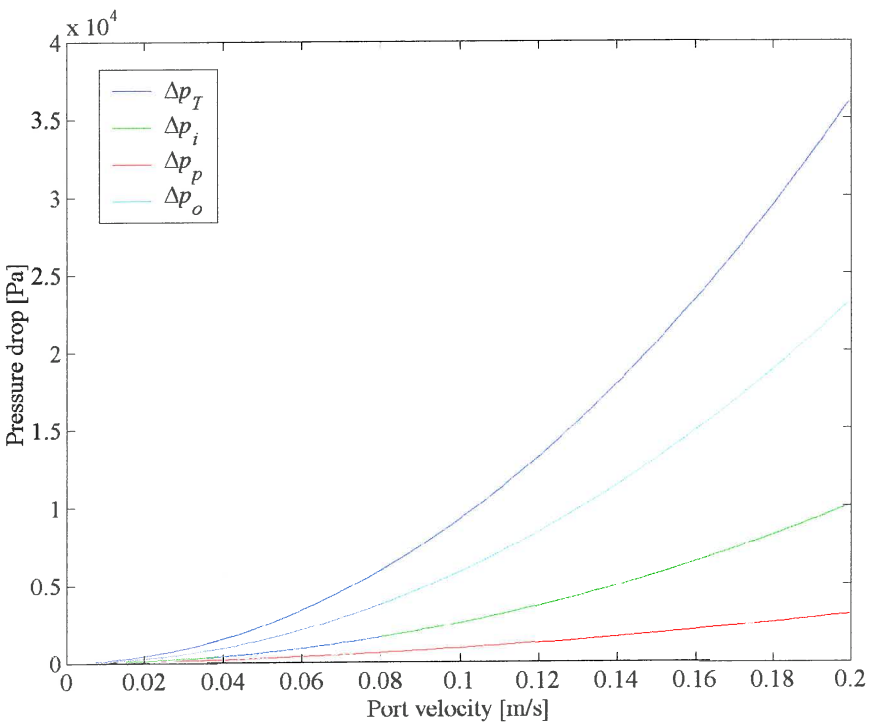

Figure 2.7 Pressure drop across the inlet, port and the outlet as a function of the port velocity ($\dot{x}$)

The force acting on the tuning port can be found in terms of the pressure difference and the shear stress on the port wall:

$$F_c = \Delta p_T (A_b - A_a) + \tau_w \pi d_a l \tag{2.37}$$

The nonlinear damping coefficient is therefore:

$$c = \frac{F_c}{\dot{x}} \tag{2.38}$$

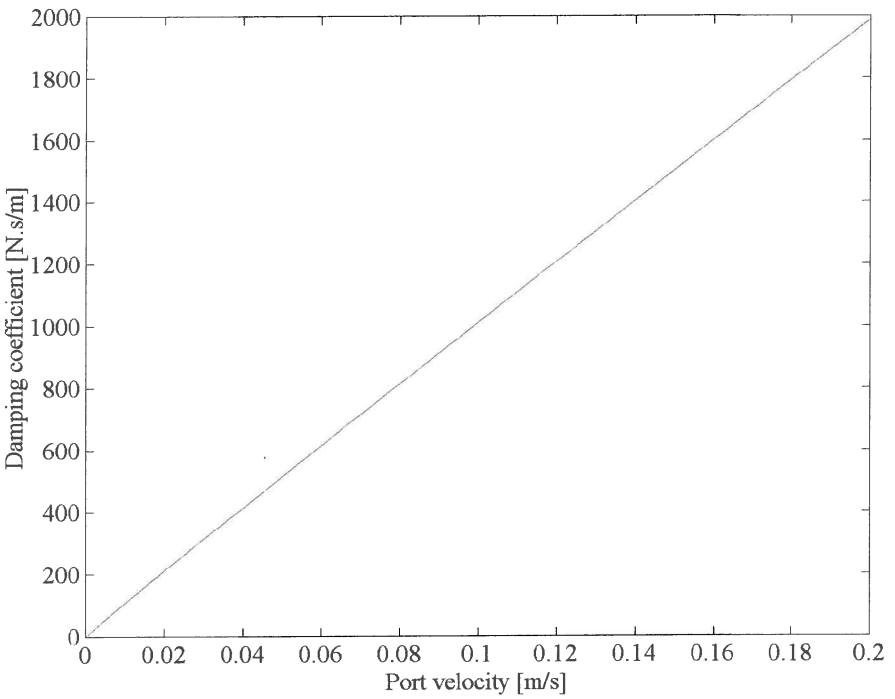

Figure 2.8 Damping as a function of the port velocity

The infinite boundary assumption does not accurately describe the flow conditions of the system. The following can however be learnt from the above analysis:

- The flow in the port will be turbulent.
- The turbulent flow loss in the port is more dependent on density than on viscosity.
- Small port diameters and large port velocities should be avoided. Large port velocities are a result of high area ratios (refer to equation 2.26).
- The inlet and outlet losses dominate the port losses.

From the above it is clear that the inlet and outlet geometry should be optimised to ensure low losses. The following paragraph will discuss how diffusers can be used in this regard.

2.3.2 Diffusers

A diffuser is a gradual conical expansion. The loss coefficient is given in terms of the pressure recovery coefficient:

$$C_p = \frac{p_2 - p_1}{\frac{1}{2}\rho V_1^2} \tag{2.39}$$

p_2 is the downstream pressure and p_1 the pressure in the port. The outlet loss coefficient is:

$$K_o = 1 - \frac{d_1^4}{d_2^4} - C_p \tag{2.40}$$

C_p values are determined experimentally. According to White (1988) the minimum value for K_o occurs at $2\theta = 5°$. For cone angles between 40° and 60° the loss becomes larger than for a sudden expansion. The inlet loss coefficient is very small as can be seen from the following experimental values:

Table 2.1 The inlet loss coefficient (White, 1988)

Diffuser angle (2θ) [deg]	Inlet loss coeffcient K_i
30	0.02
45	0.04
60	0.07

From the above analysis of diffusers it seems that diffusers can be used to reduce the amount of flow losses at the inlet and the outlet. The small angle required might make it impractical since it will require a very long port.

2.3.3 Realistic boundary

The boundary condition as shown in figure 2.6(c) is the result of the constraint put on the flow by the moving primary system. The flow next to the wall should have the same velocity as the wall. Since the boundary is very close to the inlet and outlet the losses are larger than that shown in §2.3.1. The flow through the port was analysed using STAR-CD, a commercial CFD package. The total pressure drop was calculated. The resultant force in the direction of the flow was also calculated. This includes the shear force on the port wall as well as the force resulting from the total pressure drop. The calculations were done for different inlet velocities. The inlet boundary velocity is the equal to the primary system velocity.

$$|\dot{x}| = \omega X \tag{2.41}$$

The relative pressure is calculated by the CFD program. p_i and p_o are the average pressures at the inlet and outlet respectively. The pressure loss is:

$$\Delta p_T = p_i - p_o \tag{2.42}$$

The pressure loss is shown in figure 2.9.

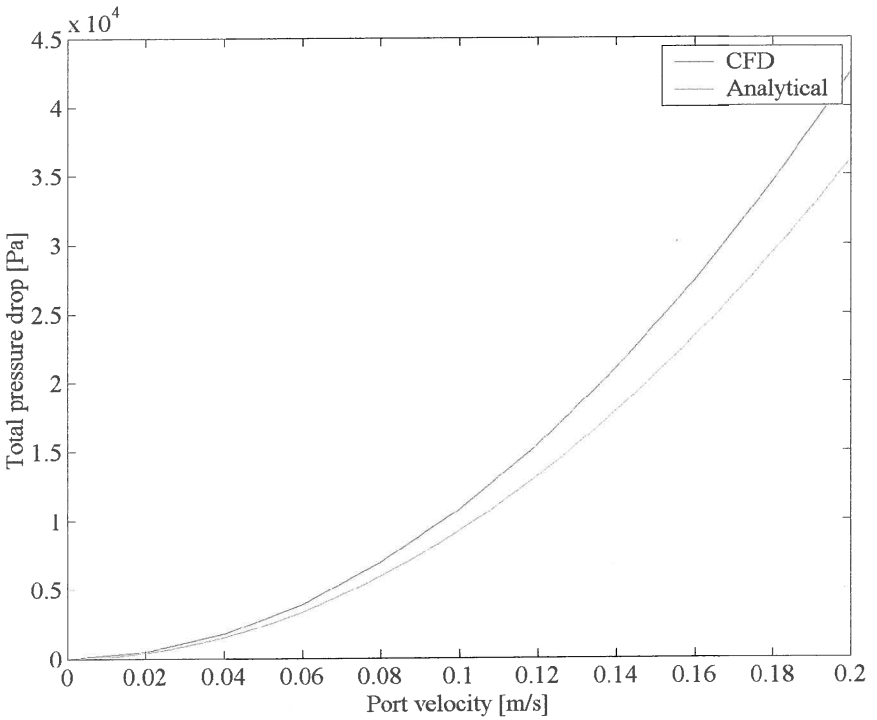

Figure 2.9 The total pressure drop across the port, as calculated using CFD (blue) and the sudden contraction and expansion analytical equations (green), as a function of port velocity

The pressure loss calculated using the two methods shows good comparison. The pressure loss calculated with the CFD method is slightly higher because of the effect the proximity of the boundary to the port entrance has on the inlet and outlet pressure loss. It seems as if the loss can be minimised by increasing the distance between the boundary and the port. This will of course affect the total height of the absorber, which will probably be limited by the available space and economics.

The damping coefficient is shown in figure 2.10. The coefficient is a linear function of frequency.

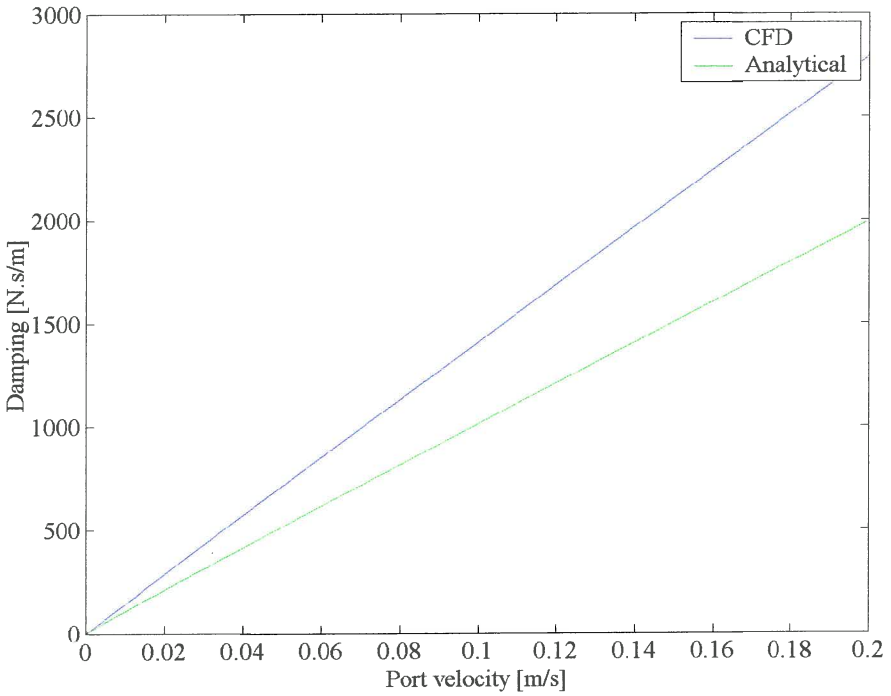

Figure 2.10 The damping coefficient, as calculated using CFD and the sudden contraction and expansion analytical equations, as a function of port velocity

2.4 Material damping

When materials are deformed, energy is absorbed and dissipated by the material. The material damping is given in terms of the loss factor. The loss factor is defined as the ratio of the loss and storage moduli (Garibaldi *et al.*, 1996):

$$\eta = \tan(\theta) = \frac{\text{Loss modulus } (E'')}{\text{Storage modulus } (E')} \tag{2.43}$$

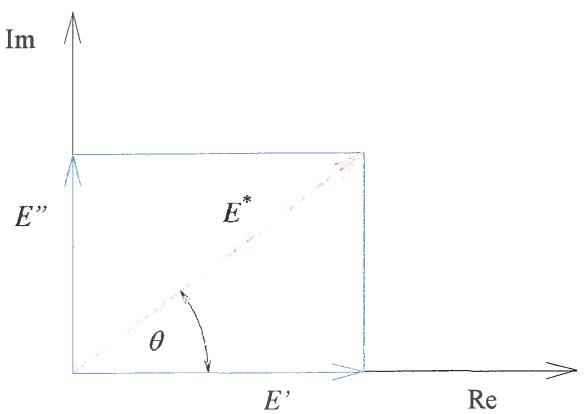

Figure 2.11 The definition of the loss factor

The loss factor must be measured experimentally and published values do exist for various kinds of elastomers (Nashif *et al.*, 1985).

2.5 Stiffness

The stiffness (k) is a function of the real part of the complex modulus in figure 2.11, and the geometry:

$$E^* = E' + iE'' \tag{2.44}$$

The stiffness of elastomeric compounds is a function of the strain rate and therefore of frequency (Davey *et al.*, 1964). For the purposes of this chapter the stiffness will assumed to be constant.

2.6 Frequency response function

Equation 2.5 can be transformed to the frequency domain by substituting the harmonic response and its derivatives, which results from harmonic excitation:

$$x(t) = Xe^{i\omega t} \tag{2.45}$$

$$\dot{x}(t) = i\omega Xe^{i\omega t} \tag{2.46}$$

$$\ddot{x}(t) = -\omega^2 Xe^{i\omega t} \tag{2.47}$$

$$f_i(t) = F_i e^{i\omega t} \tag{2.48}$$

$$\frac{X}{F_i} = \frac{1}{k(1+i\eta)+i\omega c-\omega^2\left[m+m_B\left(1-\frac{A_b}{A_a}\right)^2\right]} \tag{2.49}$$

The undamped natural frequency of this system is:

$$\omega_n = \sqrt{\frac{k}{m+m_B\left(1-\frac{A_b}{A_a}\right)^2}} \tag{2.50}$$

The normalised response and phase angle are:

$$\frac{X}{\delta_{st}} = \frac{1}{\left\{\left[1-\left(\frac{\omega}{\omega_n}\right)^2\right]^2 + \left[2\zeta\frac{\omega}{\omega_n}+\eta\right]^2\right\}^{\frac{1}{2}}} \tag{2.51}$$

$$\phi = \tan^{-1}\left\{\frac{2\zeta\frac{\omega}{\omega_n}}{1-\left(\frac{\omega}{\omega_n}\right)^2}\right\} \tag{2.52}$$

The ratio of the natural frequency of the system with (ω_n) and without (ω_n') an absorber is:

$$G_n = \frac{\omega_n}{\omega_n'} = \sqrt{\frac{m}{m+m_B\left(1-\frac{A_b}{A_a}\right)^2}} \tag{2.53}$$

Figure 2.12 shows the effect of the absorber on the system response for a certain frequency ratio (G_n). As mass is added to the system with the vibration absorber the natural frequency decreases. G_n is of course always less than one.

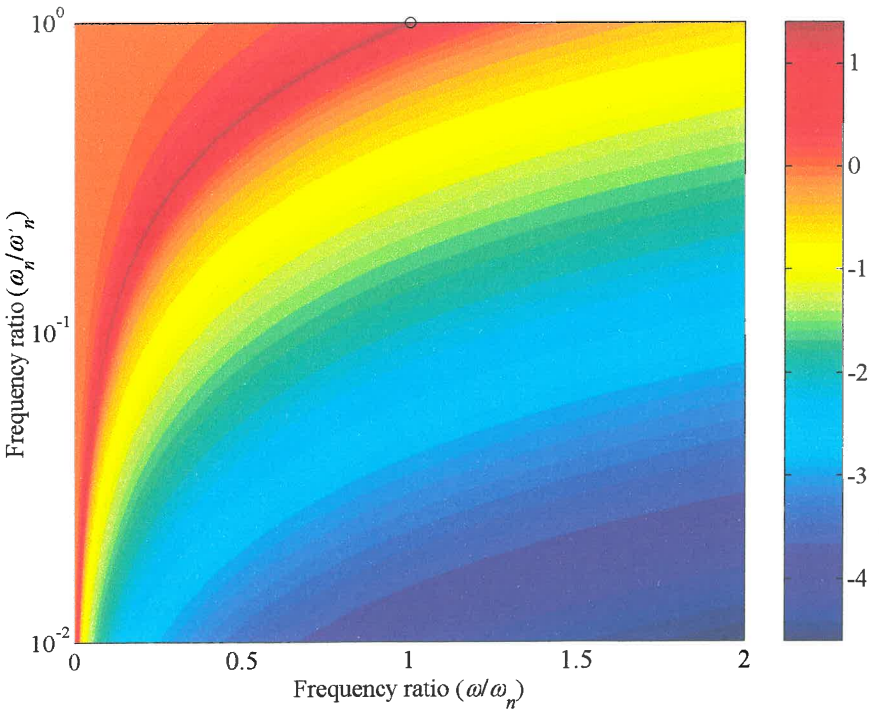

Figure 2.12 The log response of the system ($\log|X/\delta_{st}|$) as a function of the frequency ratio indicates the shift in natural frequency as mass is added to the system with $\zeta = 0.01$ and $\eta = 0.01$

2.6.1 FRF of a system with a conical inlet/outlet geometry

The FRF for a system with a conical inlet/outlet is:

$$\frac{X}{F_i} = \frac{1}{k(1+i\eta)+i\omega c-\omega^2\left\{m+\rho A_a\left[l-2h_c+2\frac{A_a}{A_c}\left(\frac{h_p^2}{h_p-h_c}-h_p\right)\right]\left[1-\frac{A_b}{A_a}\right]^2\right\}} \tag{2.54}$$

The inlet reduces the effective absorber mass. If the absorber mass terms in equation 2.54 is compared to that in equation 2.5 the following results:

$$M_r = \frac{l-2h_c+2\frac{A_a}{A_c}\left(\frac{h_p^2}{h_p-h_c}-h_p\right)}{l} \tag{2.55}$$

Equation 2.55 is plotted in figure 2.13 to illustrate the effect of the inlet dimensions (h_c and d_c) on the absorber mass ratio. The effective absorber mass can be significantly reduced with the addition of conical inlet/outlet.

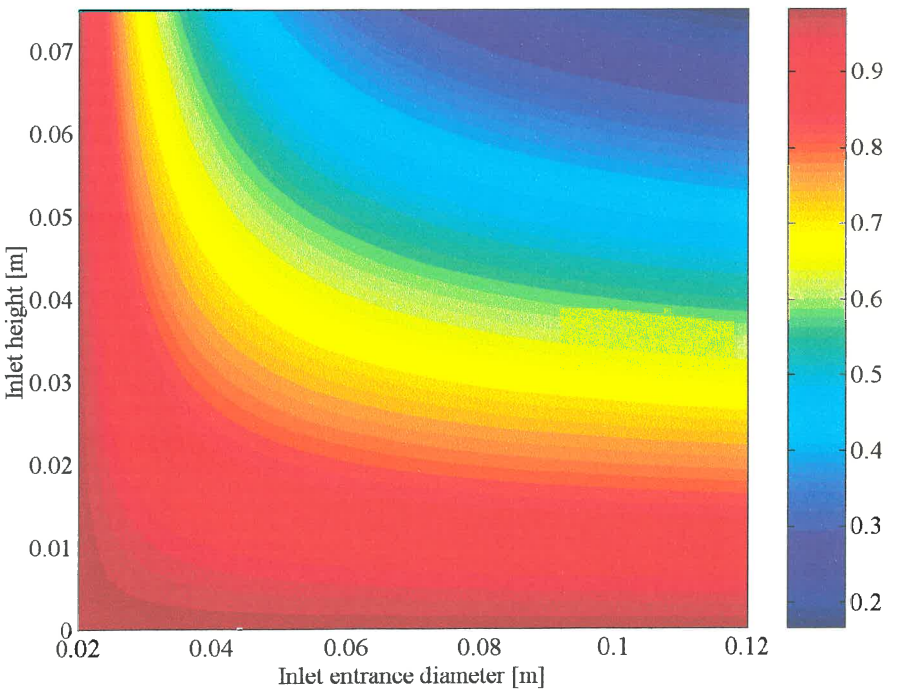

Figure 2.13 Absorber mass ratio as a function of inlet diameter (d_c) and height (h_c)

2.7 Transmissibility

The transmissibility is defined as the force amplitude ratio of the force transmitted to the ground (F_o) and the applied force (F_i).

The applied force can be derived from equation 2.49:

$$F_i = \left\{ k(1+i\eta) + i\omega c - \omega^2 \left[m + m_B \left(1 - \frac{A_b}{A_a} \right)^2 \right] \right\} X \tag{2.56}$$

The force resulting from the pressure difference in the reservoirs is (figure 2.2):

$$F_p = 2PA_b \tag{2.57}$$

The peak pressure is (equation 2.4):

$$P = \frac{m_B}{2A_a} \left(1 - \frac{A_b}{A_a} \right) \omega^2 X \tag{2.58}$$

The pressure in equation 2.57 can now be eliminated:

$$F_p = m_B \left(1 - \frac{A_b}{A_a} \right) \frac{A_b}{A_a} \omega^2 X \tag{2.59}$$

The force acting on the ground is a combination of the pressure, the spring stiffness and structural damping as well as the viscous damping. The reaction force on the ground is therefore:

$$F_o = \left[k(1+i\eta) + i\omega c + \omega^2 m_B \left(1 - \frac{A_b}{A_a} \right) \frac{A_b}{A_a} \right] X \tag{2.60}$$

The transmissibility is given by eliminating X in equations 2.56 and 2.60:

$$\frac{F_o}{F_i} = \frac{k(1+i\eta) + i\omega c + \omega^2 m_B \left(1 - \frac{A_b}{A_a} \right) \frac{A_b}{A_a}}{k(1+i\eta) + i\omega c - \omega^2 \left[m + m_B \left(1 - \frac{A_b}{A_a} \right)^2 \right]} \tag{2.61}$$

The objective of the absorber is to minimise the force transmitted to the ground. This can be achieved by choosing the parameters in equation 2.61 correctly. The following paragraphs will show how this is accomplished.

2.7.1 Undamped frequency of isolation

The transmitted force in equation 2.60 can be rearranged in real and imaginary parts:

$$F_o = \left[k + \omega^2 m_B \left(1 - \frac{A_b}{A_a} \right) \frac{A_b}{A_a} + i(\omega c + k\eta) \right] X \tag{2.62}$$

The real part of equation 2.62 can be zero for a specific frequency. This frequency is called the isolation frequency and is:

$$\omega_a = \sqrt{\frac{-k}{m_B \left(1 - \frac{A_b}{A_a} \right) \frac{A_b}{A_a}}} \tag{2.63}$$

In the literature this frequency is often termed the anti-resonant frequency. Equation 2.63 is exactly the same as that found by Halwes (1980). Halwes derived this frequency for an undamped two degree-of-freedom system and defined the transmissibility in terms of displacements. Since anti-resonance for an undamped system is defined as a point of no response to excitation (Maia *et al.*, 1998) and since the absorber discussed here does not aim to do that, the term isolation frequency will be used.

It is important to note that isolation frequency is independent of the system mass. This is an extremely attractive property since a changing system mass, as may be the case for a screen carrying different loads, will not affect the isolation frequency. The imaginary part can never be zero. Ensuring the lowest possible structural and viscous damping can however minimise the force transmitted to the ground.

2.7.2 Damped frequency of maximum and minimum transmissibility

The frequency of minimum transmissibility (isolation) for the damped case is more difficult to obtain. In this case the force transmitted to the ground is not zero at the isolation frequency, but equal to the damping force. Increasing the value of the denominator in equation 2.61 can now be used to minimise the transmissibility. The frequency of isolation can be found by differentiating the absolute value of the transmissibility with respect to frequency:

$$\frac{\partial}{\partial \omega} \left\{ \frac{\left(k + \omega^2 m_B \left(1 - \frac{A_b}{A_a} \right) \frac{A_b}{A_a} \right)^2 + (\omega c + k\eta)^2}{\left(k - \omega^2 \left[m + m_B \left(1 - \frac{A_b}{A_a} \right)^2 \right] \right)^2 + (\omega c + k\eta)^2} \right\}^{\frac{1}{2}} = 0 \tag{2.64}$$

By rewriting this equation and assigning the numerator $f(\omega)$ and the denominator $g(\omega)$ it can be differentiated as follows:

$$\frac{\partial}{\partial\omega}\left(\frac{F_o}{F_i}\right)=\frac{\partial}{\partial\omega}\left(\left\{\frac{f(\omega)}{g(\omega)}\right\}^{\frac{1}{2}}\right)=\frac{1}{2}\left(\frac{f(\omega)}{g(\omega)}\right)^{-\frac{1}{2}}\frac{f'(\omega)g(\omega)-f(\omega)g'(\omega)}{[g(\omega)]^2}=0$$

with

$$\begin{aligned}
f(\omega)&=\left(k+\omega^2 m_B\left(1-\frac{A_b}{A_a}\right)\frac{A_b}{A_a}\right)^2+(\omega c+k\eta)^2\\
f'(\omega)&=4\omega m_B\left(k+\omega^2 m_B\left(1-\frac{A_b}{A_a}\right)\frac{A_b}{A_a}\right)\left(1-\frac{A_b}{A_a}\right)\frac{A_b}{A_a}+2c(\omega c+k\eta)\\
g(\omega)&=\left(k-\omega^2\left[m+m_B\left(1-\frac{A_b}{A_a}\right)^2\right]\right)^2+(\omega c+k\eta)^2\\
g'(\omega)&=4\omega\left(k-\omega^2\left[m+m_B\left(1-\frac{A_b}{A_a}\right)^2\right]\right)\left[m+m_B\left(1-\frac{A_b}{A_a}\right)^2\right]+2c(\omega c+k\eta)
\end{aligned}\qquad \textbf{(2.65)}$$

This leads to one of the following:

$$\left(\frac{f(\omega)}{g(\omega)}\right)^{-\frac{1}{2}}=0 \qquad \textbf{(2.66)}$$

or

$$f'(\omega)g(\omega)-f(\omega)g'(\omega)=0$$

The first term can never be zero. The second term yields five roots of which one is zero, two are negative and two positive. The positive roots correspond to the frequencies of maximum and minimum transmissibility. The importance of this analysis is that the isolation frequency is no longer independent of the system mass. It is also dependent on damping, which could lead to considerable design difficulties. For the undamped case it was possible to choose a stiffness coefficient, absorber mass and port area and then calculate the reservoir area for the frequency that needs to be isolated. This method is no longer possible due to the complexity of equation 2.61. A possible solution is to solve the equation numerically.

2.7.3 Non-dimensional transmissibility

By substituting the variables in equation 2.61 with the definitions in equations 1.5 to 1.7 the non-dimensional transmissibility can now be written in terms of the undamped resonance and isolation frequencies:

$$|T_r| = \left\{ \frac{\left[1-\left(\frac{\omega}{\omega_a}\right)^2\right]^2 + \left[2\zeta\frac{\omega}{\omega_n}+\eta\right]^2}{\left[1-\left(\frac{\omega}{\omega_n}\right)^2\right]^2 + \left[2\zeta\frac{\omega}{\omega_n}+\eta\right]^2} \right\}^{\frac{1}{2}} \tag{2.67}$$

The phase angle is:

$$\phi = \tan^{-1}\left\{\frac{2\zeta\frac{\omega}{\omega_n}+\eta}{1-\left(\frac{\omega}{\omega_a}\right)^2}\right\} - \tan^{-1}\left\{\frac{2\zeta\frac{\omega}{\omega_n}+\eta}{1-\left(\frac{\omega}{\omega_n}\right)^2}\right\} \tag{2.68}$$

By choosing $\omega_a = 1$ and $\omega_n = 0.5$ the following figures could be plotted showing the influence of viscous and structural damping. The figures clearly indicate the importance of low damping for good isolation.

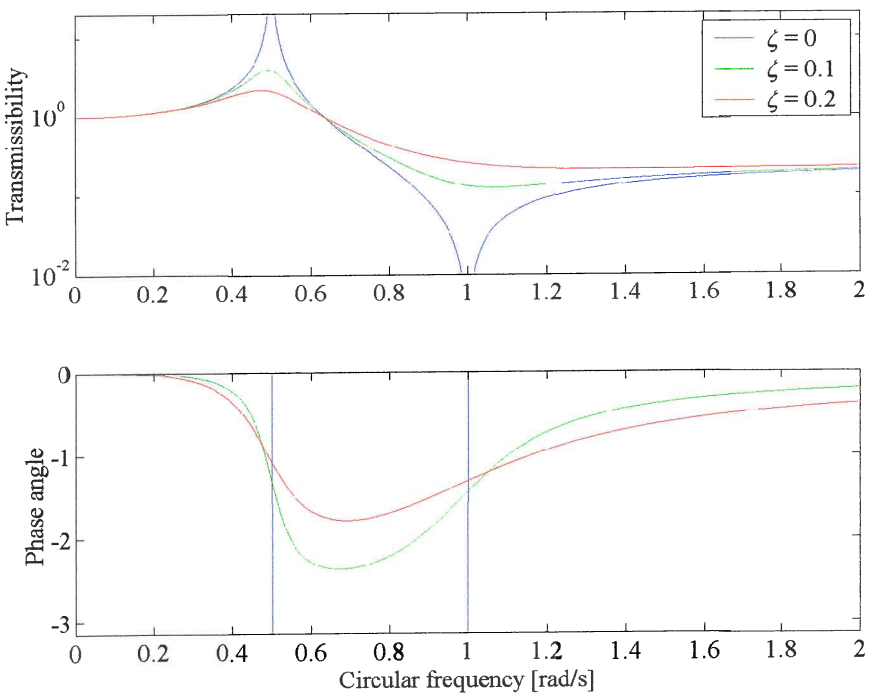

Figure 2.14 Transmissibility as a function of damping ratio with $\omega_n = 0.5$ and $\omega_a = 1$

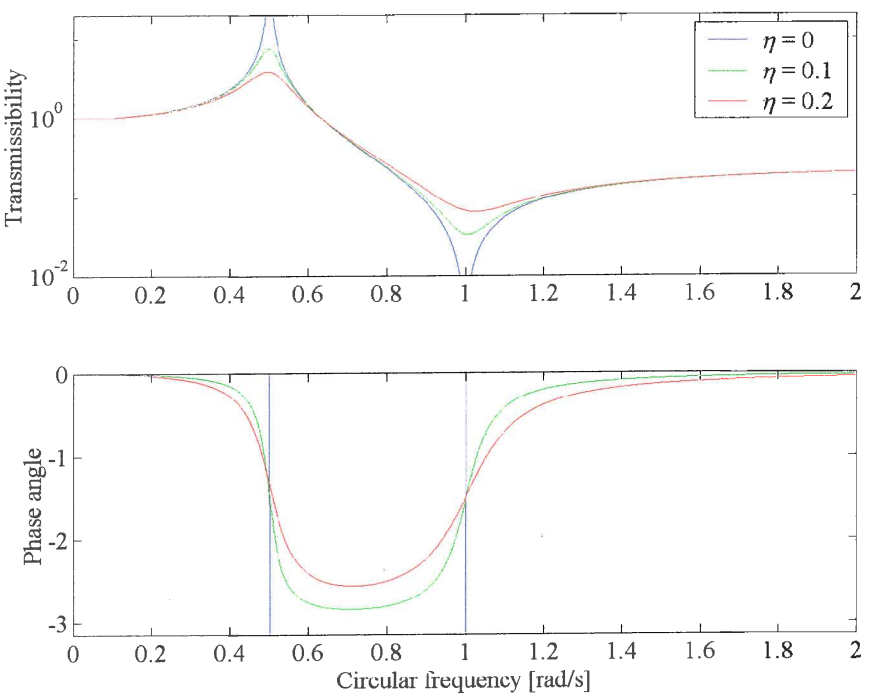

Figure 2.15 Transmissibility as a function of loss factor with $\omega_n = 0.5$ and $\omega_a = 1$

It is also important to study the effect of the frequency ratio on the amount of isolation achieved. The frequency ratio is defined as:

$$G_a = \frac{\omega_n}{\omega_a} = \sqrt{\frac{m_B\left(\frac{A_b}{A_a} - 1\right)\frac{A_b}{A_a}}{m + m_B\left(\frac{A_b}{A_a} - 1\right)^2}} \tag{2.69}$$

Figure 2.16 shows two regions of isolation at the chosen isolation frequency $\omega_a = 1$. For a frequency ratio less than one the frequency of maximum transmissibility appears before the isolation frequency. It is not feasible to design in the region where the frequency ratio is more than one. This will require a very high absorber mass (m_B) and a high area ratio. Additionally the amount of isolation will be small, the bandwidth rather narrow and high frequencies will be amplified. If the system mass is small in comparison with the absorber mass equation 2.69 reduces to:

$$G_a = \sqrt{\frac{\frac{A_b}{A_a}}{\frac{A_b}{A_a} - 1}} \tag{2.70}$$

Equation 2.70 is always greater than one for area ratios larger than one. This shows that the system mass must be large in comparison with the absorber mass to achieve good isolation.

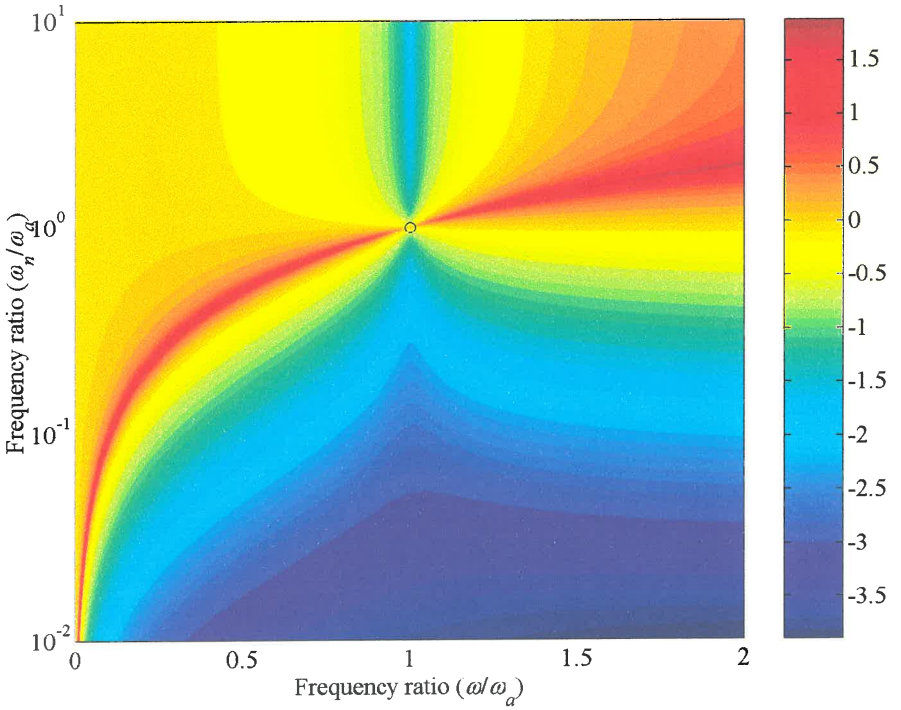

Figure 2.16 Log transmissibility ($\log|T_r|$) as a function frequency ratio (G_a) and circular frequency (ω/ω_a) with $\zeta = 0.01$ and $\eta = 0.01$ showing the isolation frequency $\omega_a = 1$

It is useful to compare the transmissibility before and after the addition of the absorber. The transmissibility without an absorber is:

$$|T_r| = \left\{ \frac{1 + \left[2\zeta \frac{\omega}{\omega_n} + \eta \right]^2}{\left[1 - \left(\frac{\omega}{\omega_n} \right)^2 \right]^2 + \left[2\zeta \frac{\omega}{\omega_n} + \eta \right]^2} \right\}^{\frac{1}{2}} \tag{2.71}$$

The corresponding phase angle is:

$$\phi = \tan^{-1}\left\{ 2\zeta \frac{\omega}{\omega_n} + \eta \right\} - \tan^{-1}\left\{ \frac{2\zeta \frac{\omega}{\omega_n} + \eta}{1 - \left(\frac{\omega}{\omega_n} \right)^2} \right\} \tag{2.72}$$

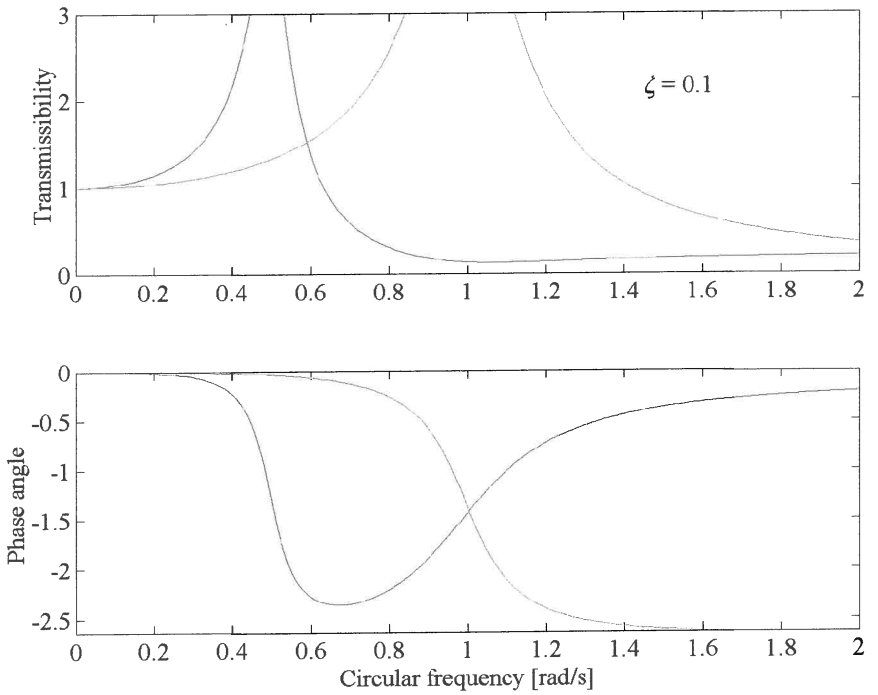

Figure 2.17 Comparison of transmissibilities with (blue) and without (green) an absorber

Figure 2.17 shows how a resonant frequency can be moved with the addition of a vibration absorber.

2.7.4 Transmissibility of system with a conical inlet/outlet geometry

As in the previous paragraphs the transmissibility is defined in terms of the applied and transmitted forces. The applied and transmitted forces defined by equations 2.24 and 2.25 can be transformed to the frequency domain using the assumed harmonic excitation and response. The result is:

$$\frac{F_o}{F_i} = \frac{k(1+i\eta)+i\omega c+\omega^2\rho\left[l-2h_c+2\frac{A_a}{A_c}\left(\frac{h_p^2}{h_p-h_c}-h_p\right)\right]\left(1-\frac{A_b}{A_a}\right)A_b}{k(1+i\eta)+i\omega c-\omega^2\left\{m+\rho A_a\left[l-2h_c+2\frac{A_a}{A_c}\left(\frac{h_p^2}{h_p-h_c}-h_p\right)\right]\left(1-\frac{A_b}{A_a}\right)^2\right\}} \tag{2.73}$$

The undamped isolation frequency is:

$$\omega_a' = \sqrt{\frac{k}{\rho\left[l-2h_c+2\frac{A_a}{A_c}\left(\frac{h_p^2}{h_p-h_c}-h_p\right)\right]\left(1-\frac{A_b}{A_a}\right)A_b}} \tag{2.74}$$

The ratio of isolation frequencies before (ω_a) and after (ω'_a) the addition of the conical inlets is:

$$\frac{\omega'_a}{\omega_a} = \sqrt{\frac{l}{l - 2h_c + 2\frac{A_a}{A_c}\left(\frac{h_p^2}{h_p - h_c} - h_p\right)}} \tag{2.75}$$

This equation shows that the conical inlet's effect can be represented by a change in length of the tuning port. The denominator in equation 2.75 is always less than the numerator. The isolation frequency of a port fitted with conical inlet/outlet will therefore always be more than for an absorber with a square inlet/outlet.

2.8 Conclusion

The LIVE absorber has rather unique properties that require careful analysis for successful design. This chapter showed that:

- An absorber will decrease the natural frequency of a system by adding mass to the system.
- Damping will have a serious detrimental effect on the achievable transmissibility. It can be controlled with diligent choice of elastomeric compound and inlet/outlet geometry.
- Changes to the inlet/outlet geometry will increase the isolation frequency.
- The ideal absorber will be designed with the natural frequency occurring as far as possible before the isolation frequency.

The next chapter will show how this analysis will be used to design an experimental absorber for evaluation.

CHAPTER 3

Design of an experimental vibration absorber

3.1 Introduction

This chapter will document the proposed design methodology for a LIVE type vibration absorber. The main objective of the absorber is to isolate at the excitation frequency. Equation 2.63 shows that the isolation frequency is a function of many variables and several sets of these will isolate at the design frequency. Some sets will give better isolation than others will, and this can be used to reduce the number of possible solutions. Even after this criterion has been satisfied several possible solutions still exist. The particular application will also have additional specific demands regarding size, weight, static deflection and others, which will be used to choose the optimal solution.

Two design methods will be discussed. The first is an iterative design approach, which is rather tedious, but this method will be used to explain the design process and will give some insight into the problem. The second method uses constrained optimisation. This method is more efficient and can be used to do several designs in order to study the effect each variable has on the transmissibility and isolation frequency.

Using these methods an experimental absorber was designed. This absorber was manufactured and extensively tested to verify this design methodology as well as to get practical experience with some of the manufacturing and design difficulties. The design difficulties mainly originated from the requirement that the port must be able to move axially in a cylinder with closed ends. This necessitated connection through the side of the outer cylinder, which proved difficult to manufacture.

Two important aspects of the design are the spring rate of the elastomeric spring and the damping caused by the liquid. The available methods to estimate the spring's stiffness will be discussed. The damping constant was calculated using computational fluid dynamics and the result will be reported.

The chapter will start with the final design showing its parts and explaining the variables that will influence its performance.

3.2 The experimental absorber

This paragraph will highlight some of the practical aspects of the absorber's design. It will introduce the parts and list their requirements. It will also show which dimensions will influence its performance. Finally the choice of absorber liquid will be justified.

3.2.1 Absorber parts

The absorber consists of a port that can move axially relative to a concentric cylinder (sleeve). The port is connected to the sleeve with a polyurethane spring, which is cast in this position and is rigidly fixed to the port and the sleeve. To facilitate the axial movement the port and the sleeve must be connected to the opposite ends of the absorber. The port is connected via a connector block, connector cylinder and lid to the top load cell. The sleeve is connected using the bottom plug. The plugs form reservoirs of fluid that will be accelerated through the port when relative axial movement between the port and sleeve occurs. Additional detail relating to the design can be found in appendix F.

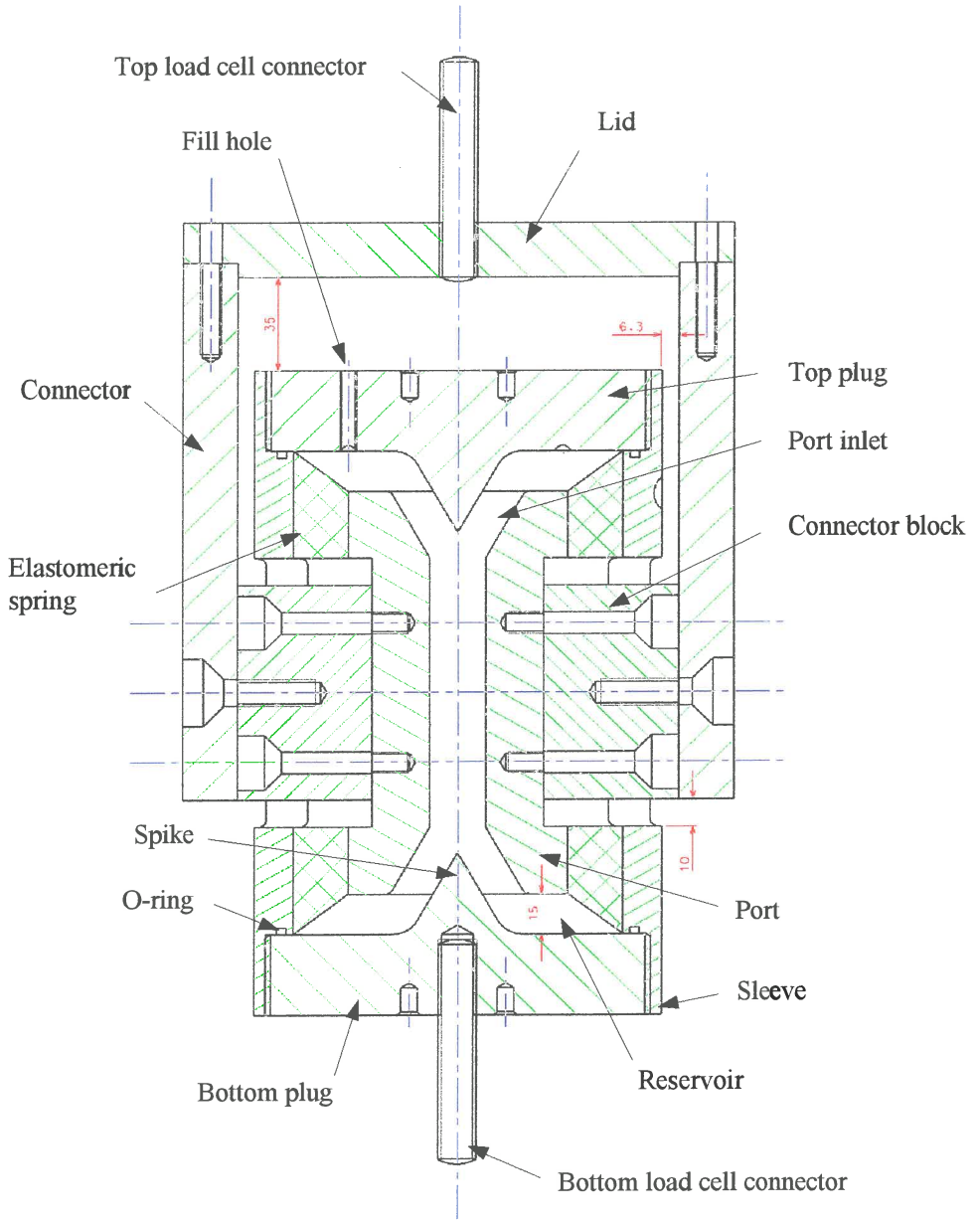

Figure 3.1 Absorber assembly showing clearances and parts

The connection of the port with the top load cell was the most difficult part of the design. The purpose of the connection is to transfer the force from the actuator at the bottom to the fixed load cell at the top. The connection had to:

- transfer a buckling moment from the actuator to the load cell,
- be free from play in the axial direction, and
- have high axial stiffness compared to the elastomeric spring so as not to have an influence on the absorbers performance.

The connector blocks transfer the buckling moment from the connector to the port. These blocks were curved on their outer side and thus could not rotate in the connector, which had the same curvature. The block was fitted to the connector using a M16 flat head socket screw and was fixed to the port using two M8 flat head socket screws. This was done to prevent rotation as the interface between the block and the port is flat. The lid was fitted to the connector using 6 M8 allencap screws. The lid was fixed to the load cell with a M14×2 threaded rod. It is of extreme importance that there should be no free play in the axial direction since this will have a negative impact on the absorber's performance. The play was minimised by using two sets of screws to fit the connector to the port via the connector block. Flat head socket screws were used to ensure a tight fit on the seat surface.

The absorber was designed for a maximum of 10 mm axial displacement, which is more than would be needed but will make it possible to fit very soft springs in future tests. The 6.3 mm gap between the connector and the sleeve should accommodate any radial misalignment between the two load cell connection points.

In the top plug a M6 fill hole was used to add the absorber fluid. At the bottom of this plug a groove was machined to facilitate the escape of air from inside the reservoir. It is important that there should be no trapped air in the reservoir because this will negate the all-important conservation of mass between the reservoir and the port. Both the plugs were fitted with 6 mm holes which were used to tighten the plug on the 3 mm O-ring.

3.2.2 Design variables

The basic design variables are shown in figure 3.2. Decisions made about each of these will influence the absorber performance. The required isolation frequency and transmissibility determined the values of some of these variables. The size of the side entrances is influenced by the clearance required between the connector block and the sleeve as well as the size of the screws used, the distance required between them to transfer the moment and the size of the curved surface on the outer side. The size of the side entrance, the port outer diameter and

the reservoir height will in turn influence the spring stiffness. The dimensions of the spike, and the inlet entrance will influence the viscous damping.

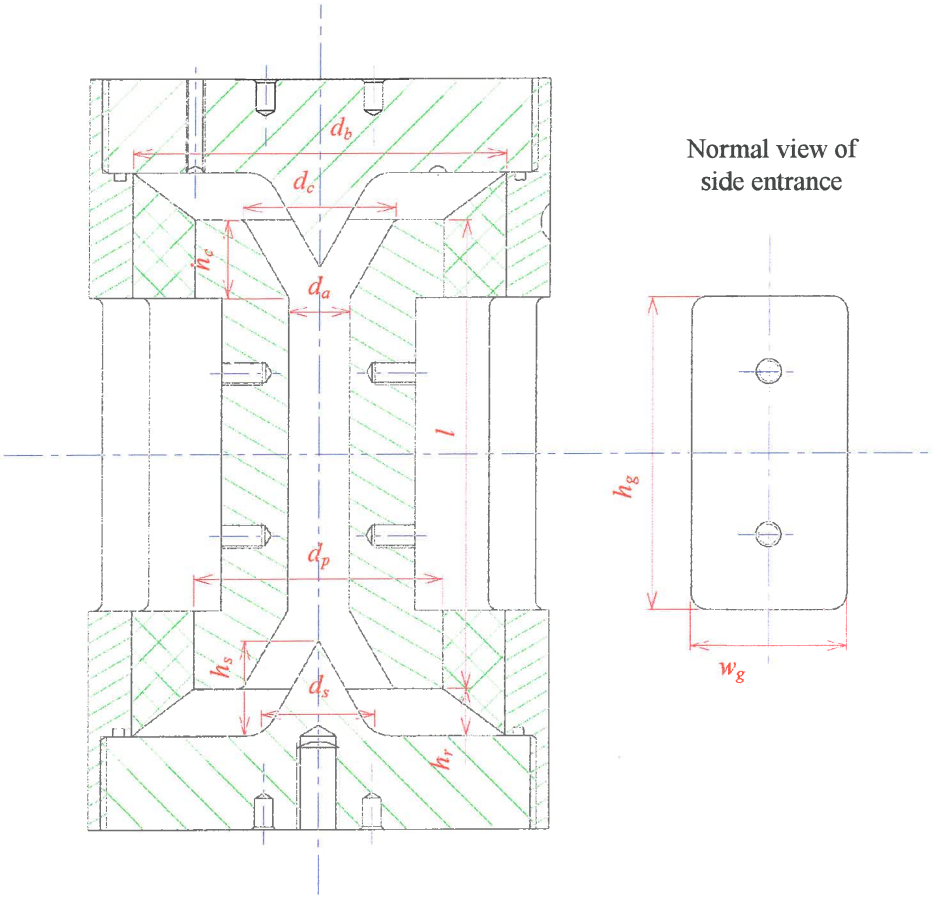

Figure 3.2 Basic design variables

Table 3.1 Basic design variables

Variable	
Port length	l
Port inner diameter	d_a
Port outer diameter	d_p
Reservoir diameter	d_b
Inlet height	h_c
Inlet entrance diameter	d_c
Spike height	h_s
Spike base diameter	d_s
Reservoir height	h_r
Gap height	h_g
Gap width	w_g

3.2.3 Absorber liquid

This absorber was designed to use water as the absorber liquid. Halwes (1980) stated that the absorber size will be inversely proportional to the square of the density of the absorber liquid. High-density liquids will therefore result in smaller absorbers. If this design was done using mercury the reservoir diameter would have been less than half of the absorber using water. The following properties are however required of the absorber liquid:

- High density
- Low-toxicity
- Liquid at expected working temperature (-10 to 50 °C)
- Low viscosity (low damping)
- Non-corrosive (elastomers, steel)
- Non-abrasive (elastomers, steel)
- Inexpensive
- Available

Table 3.2 Summary of liquid properties at 25°C

Liquid		ρ [kg/m^3]	μ [N.s/m^2]	T_m [°C]	T_b [°C]	Hazard rating*
Water	H_2O	998	1.00×10^{-3}	0	100	0
Bromine	Br_2	3113	0.91×10^{-3}	-7	59	4
Bromoform	$CHBr_3$	2894		N/A	150	3
Carbon tetrachloride	CCl_4	1590	0.97×10^{-3}	-23	76	3
Lead tetrachloride	$PbCl_4$	3174		-15	105	
LST		2954				
Mercury	Hg	13550	1.56×10^{-3}	-38	356	4
Phosphorous tribromide	PBr_3	2846		-40	173	3
Selenium bromide	Se_2Br_2	3597			227	
Selenium monochloride	Se_2Cl_2	2764		-85	130	
Tetrabromoacetylene	$Br_2CHCHBr_2$	2954		0	135	2
Thionyl bromide	$SOBr_2$	2675		-52	138	
Thiophosphorylbromidechloride	$PSBr_2Cl$	2475		-60	95	
Tindibromidedichloride	$SnBr_2Cl_2$	2814		-20	65	

* Baker SAF-T-DATA™ health rating, 0 = no hazard, 4 = extreme hazard.

Most heavy liquids are too hazardous to consider as possible absorber fluids. The only liquid that will have a significant impact on absorber size is mercury. However, the benefit of using mercury will be offset by the cost involved in ensuring that it doesn't find its way into the environment. Mercury will also result in higher damping than water because the turbulent shear stress is a function of density and viscosity. Water with a corrosion inhibitor additive is recommended for a screen where the size of the absorber is not as critical.

3.3 Design methodology

The isolation frequency is the most important quantity in the design process. In chapter 2 the tuning equation was derived giving the relationship between the five variables and the isolation frequency. The simplified equation is:

$$\omega_a = \sqrt{\frac{k}{\rho l\left(\frac{A_b}{A_a}-1\right)A_b}} \tag{3.1}$$

At first glance it appears obvious to simply choose four of the variables and calculate the remaining one using equation 3.1. However, this approach neglects the effect that the choice of parameters will have on a damped system's transmissibility and the absorber's size. The transmissibility can be written in terms of the five variables as follows (from equation 2.61):

$$\frac{F_o}{F_i} = \frac{k(1+i\eta)+i\omega c+\omega^2\rho l\left(1-\frac{A_b}{A_a}\right)A_b}{k(1+i\eta)+i\omega c-\omega^2\left[m+\rho l A_a\left(1-\frac{A_b}{A_a}\right)^2\right]} \tag{3.2}$$

It can be assumed that a set of optimal parameters exist that will minimise the transmissibility at the frequency of isolation while also satisfying certain size constraints. It seems therefore that the design of the absorber lends itself to an optimisation approach. However, it was found that the optimisation design method does not lead to significant insight. To address this shortcoming an iterative design method will be discussed first. This design will be done for an application with an operating frequency of 50 Hz. Although this is not a common screen operating frequency it will be sufficient for the validation of the mathematical model. It will also simplify the design and can be accommodated by the available hydraulic actuator.

3.3.1 Iterative design approach

As noted before, the specific application will fix the isolation frequency and thus by choosing any four parameters the remaining one can be calculated using equation 3.1. The analysis can be simplified by reducing the number of variables available for tuning from five to two, which is achieved by introducing the absorber mass into equation 3.1:

$$m_B = \rho l A_a \tag{3.3}$$

The absorber mass is written as a function of area ratio, isolation frequency and stiffness:

$$m_B = \frac{k}{\omega_a^2\left(\frac{A_b}{A_a}-1\right)\frac{A_b}{A_a}} \tag{3.4}$$

A second criterion must also be satisfied namely low transmissibility. The transmissibility is written in non-dimensional form so as to simplify accounting for the effect of damping:

$$|T_r| = \left\{ \frac{\left[1-\left(\frac{\omega}{\omega_a}\right)^2\right]^2 + \left[2\zeta\frac{\omega}{\omega_n}+\eta\right]^2}{\left[1-\left(\frac{\omega}{\omega_n}\right)^2\right]^2 + \left[2\zeta\frac{\omega}{\omega_n}+\eta\right]^2} \right\}^{\frac{1}{2}} \tag{3.5}$$

From the analysis in chapter 2 we know that the natural frequency must be small compared to the isolation frequency. Figure 3.3 reiterates this by showing a region of low transmissibility for a system with low stiffness. Another important feature of the figure is the infeasible design region below the red area. In this area the natural frequency is higher than the isolation frequency resulting in high frequency amplification.

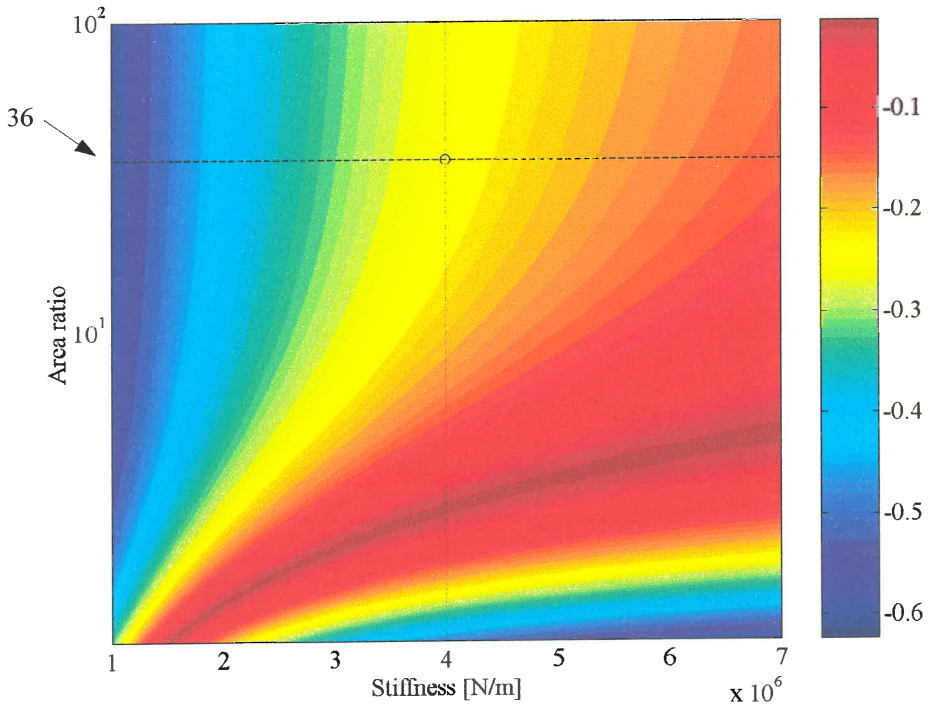

Figure 3.3 The min(log$|T_r|$) as a function of area ratio and stiffness for $f_a = 50$ Hz and with $m = 15$ kg, $\rho = 1000$ kg/m^3, $\eta = 0.1$ and $\zeta = 0.1$

From figure 3.3 it is clear that a high area ratio and low stiffness will minimise the transmissibility. There are, however, constraints on the area ratio and the stiffness. Most practical applications can only accommodate a certain amount of static deflection. This deflection will therefore be the lower bound of the stiffness. The elastomeric material properties and the space available for installation also influence the stiffness. Polyurethane was chosen as the preferred material because of its low loss factor and ease of manufacture.

Although the polyurethane was available in hardnesses ranging from 35 to 90 Shore A, they all will result in a rather stiff spring. After some calculations were done regarding the available shear modulus of elasticity and some reasonable geometries, 4 MN/m was chosen as the design stiffness. This choice fixed the vertical stiffness line as shown on figure 3.3.

Furthermore a high area ratio will result in either a small port diameter or a large reservoir diameter. The port diameter is constrained by the viscous damping. Equation 2.28 shows that the damping is a function of port diameter. High area ratios will also increase the inlet and outlet losses as well as the port velocity. The port reservoir diameter was chosen as 120 mm which makes the absorber bulky but manageable. Figure 3.3 shows that the gain in transmissibility decreases rapidly at high area ratios. For this reason as well as the increase in damping the area ratio was fixed at 36.

The length of the port is constrained by the buckling moment that needs to be transferred across the absorber when it is in compression.

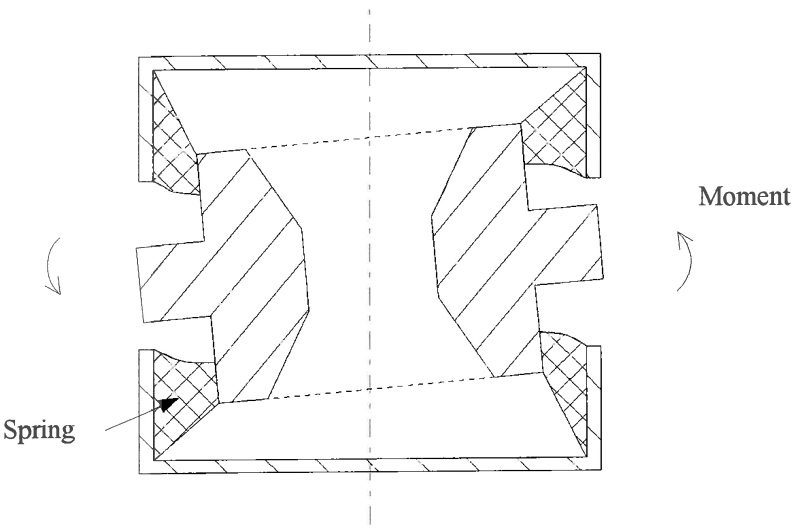

Figure 3.4 Schematic explanation of the necessity to transfer the buckling moment

To transfer the buckling moment a certain thickness, length and modulus of elasticity is required of the elastomeric spring. The thickness is governed by the outer diameter of the port since the reservoir diameter is fixed by the overall size constraint. This diameter is also influenced by the required axial stiffness of the spring as well as the attachment method. A reasonable design approach would be to specify a minimum ratio of port length to port inner diameter. This will leave the rather complex specification of a port outer diameter to be determined by the required axial stiffness. The following slenderness ratio was recommended:

$$\frac{l}{d_a} \geq 6 \qquad \textbf{(3.6)}$$

The only other property that will influence the design is the density of the absorber liquid. From the above analysis it is clear that the size of the absorber will be influenced significantly by the density. If the density is increased the area ratio can be decreased which will result in a smaller absorber. The variables discussed above are summarised in the following table.

Table 3.3 Design variables

Design variable		Value
Stiffness [MN/m]	k	4
Area ratio	A_r	36
Undamped isolation frequency [Hz]	f_a	50
Reservoir diameter [mm]	d_b	120
Density [kg/m^3]	ρ	1000

Using these design variables the remaining unknowns in equation 3.1 can be calculated.

Table 3.4 Design results

Unknowns	From		Value
Port diameter [mm]	From area ratio	d_a	20
Absorber mass [kg]	From tuning equation 3.4	m_B	4.02×10^{-2}
Volume [m^3]	From absorber mass and equation 3.3	$\frac{\pi}{4}d_a^2 l_{\min}$	4.02×10^{-5}
Port length [mm]	Port volume	l_{min}	102
Slenderness ratio	Test in length conforms to equation 3.6	l_{min}/d_a	6.4

The designer must also take into account the shift that occurs in the isolation frequency due to damping. Assuming that the design will have a loss factor and a viscous damping ratio both of 0.1, the transmissibility curve can be calculated. From this curve the final results for the absorber's physical properties can be found and these are shown in table 3.5.

Table 3.5 Designed absorber's physical properties $\zeta = 0.1$, $\eta = 0.1$

Property	Design	Minimum
Transmissibility	0.70	0.57
Isolation frequency [Hz]	50	56.96

It is important to note that since the port length was calculated using the undamped isolation frequency of 50 Hz, the damped minimum only occurred at 56.96 Hz. This resulted in a less than optimal design as can be seen from figure 3.5. However, the length calculated in this way is useful since it represents a minimum port length. A simple search for the minimum

transmissibility can now be done by increasing the port length, starting at the calculated minimum value. This is shown in figure 3.6.

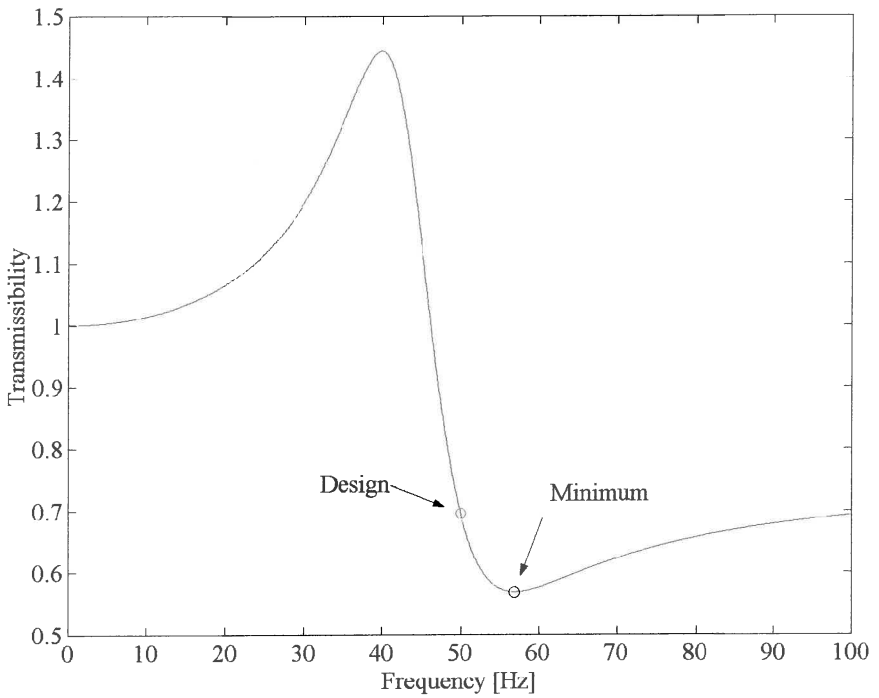

Figure 3.5 Minimum transmissibility search with $m = 15$ kg, $\zeta = 0.1$ and $\eta = 0.1$

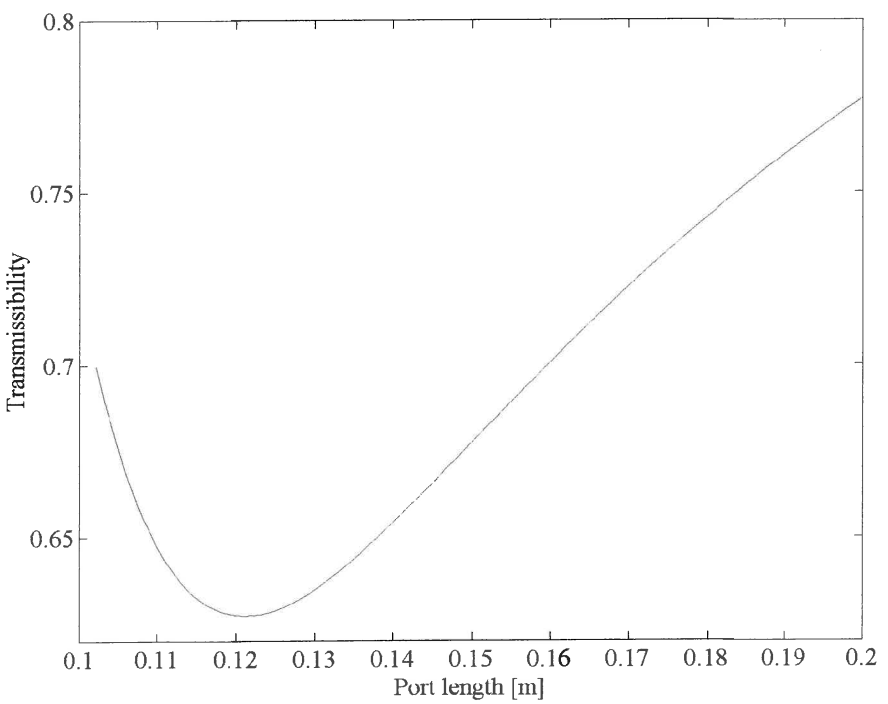

Figure 3.6 Minimum transmissibility search with $m = 15$ kg, $\zeta = 0.1$ and $\eta = 0.1$

This procedure resulted in the transmissibility plot shown in figure 3.7. The original design is shown in blue and the new design in green. The isolation frequency cannot be decreased without increasing the transmissibility.

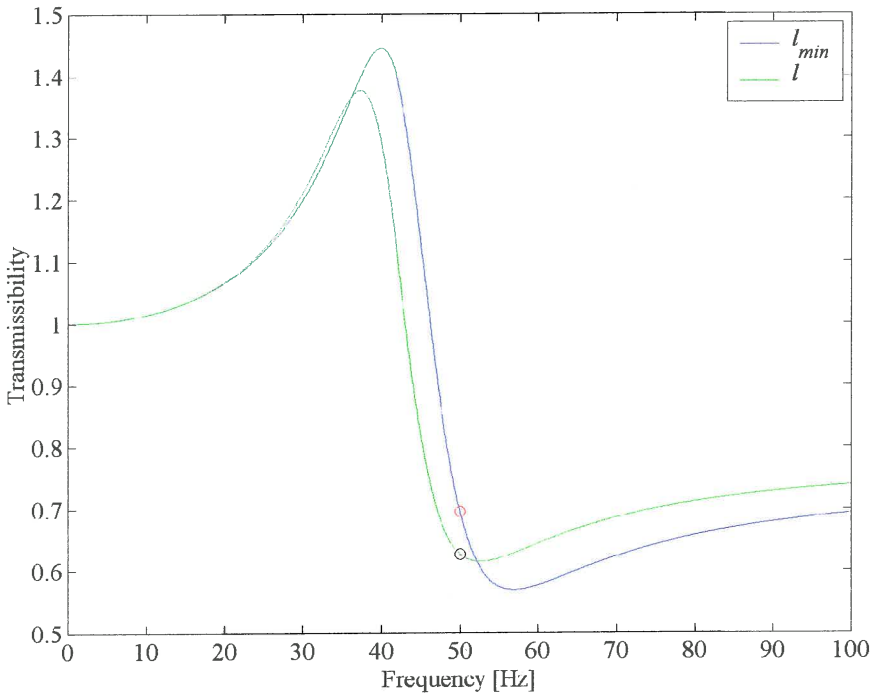

Figure 3.7 Ideal transmissibility for isolation at 50 Hz (green) and the transmissibility curve of the design done using the undamped isolation frequency (blue) with $m = 15$ kg, $\zeta = 0.1$ and $\eta = 0.1$

The optimal port length was 121 mm and the transmissibility for this design 0.63, which is significantly better than the first design. It is important to note that the minimum on this curve is not the optimal transmissibility either. This design will be sensitive to changes in excitation frequency and it could therefore be beneficial to sacrifice transmissibility for bandwidth by lengthening the port further.

The addition of the conical port inlet/outlet must still be taken into account. The effect of the addition is to increase the isolation frequency. Increasing the port length will counteract this increase. The isolation frequency ratio given by equation 2.75 will be used to calculate the port length, which will result in the same isolation frequency as an absorber with a square inlet/outlet. The required ratio between the isolation frequency of a port with and without an absorber is 1 and the equation can therefore be re-written as follows:

$$l' = l + 2h_c - 2\frac{A_a}{A_c}\left(\frac{h_p^2}{h_p - h_c} - h_p\right) \tag{3.7}$$

The inlet geometry and its effect on the port length are summarised in Table 3.6.

Table 3.6 Port length adjustment

Design variable [mm]		Value
Original port length	l	121.0
Inlet height	h_c	25.0
Inlet entrance diameter	d_c	48.9
Port diameter	d_a	20.0
Port cone height	h_p	42.3
Adjusted port length	l'	150.5

The lengthening of the port will result in slightly higher viscous damping.

At the beginning of the design it was assumed that a 4 MN/m spring could be moulded in the available space. This should now be verified using the approach that will be discussed later in §3.4. If these calculations prove that it is impossible to achieve the desired stiffness the design must be attempted using the same procedure with a new stiffness.

3.3.2 Optimisation approach

Using optimisation to solve this problem simplifies the design process. Given a set of constraints the transmissibility is minimised at a specific frequency. The results are exactly the same as in the previous section, but the process is more efficient, especially if several designs are needed.

The variables are listed table 3.7.

Table 3.7 Variables and constraints

Design variable		Optimisation variable	Bound
Stiffness [MN/m]	k	x_1	≥ 4
Reservoir diameter [mm]	d_b	x_2	≤ 120
Port diameter [mm]	d_a	x_3	≥ 20

All the variables are of course physical properties and cannot be less than zero.

The objective function and the constraints are:

$$f(\bar{x}) = \left| \frac{x_1(1+i\eta)+i\omega_a 2\zeta\sqrt{x_1\left[m+\frac{\pi}{4}\rho x_4 x_2^2\left(1-\frac{x_3^2}{x_2^2}\right)^2\right]}+\frac{\pi}{4}\omega_a^2\rho x_4 x_3^2\left(1-\frac{x_3^2}{x_2^2}\right)}{x_1(1+i\eta)+i\omega_a 2\zeta\sqrt{x_1\left[m+\frac{\pi}{4}\rho x_4 x_2^2\left(1-\frac{x_3^2}{x_2^2}\right)^2\right]}-\omega_a^2\left[m+\frac{\pi}{4}\rho x_4 x_2^2\left(1-\frac{x_3^2}{x_2^2}\right)^2\right]} \right|$$

subject to

(3.8)

$$g_1(\bar{x}) = -x_1 + k^{\min} \le 0$$
$$g_2(\bar{x}) = x_2 - d_b^{\max} \le 0$$
$$g_3(\bar{x}) = -x_3 + d_a^{\min} \le 0$$
$$g_4(\bar{x}) = \sqrt{\frac{x_1}{m+\frac{\pi}{4}\rho x_4 x_2^2\left(1-\frac{x_3^2}{x_2^2}\right)^2}} - \omega_a \le 0$$

The objective function was found by substituting the viscous damping in terms of the damping ratio and critical damping. The first three constraints are the same as were discussed in §3.3.1. The last constraint ensures that the design is in the feasible region where the natural frequency is smaller that the design isolation frequency. Without this constraint the solution can get stuck at a local minimum which is larger than the global minimum.

Table 3.8 Optimisation variables

Design variable		Optimisation variable	Optimum
Stiffness [MN/m]	k	x_1	4
Reservoir diameter [mm]	d_b	x_2	120
Port diameter [mm]	d_a	x_3	20
Port length [mm]	l	x_4	121

The MATLAB constrained optimisation algorithm `fmincon.m` was used for the optimisation. At the optimum design point the stiffness was at the minimum and the area ratio at the maximum allowed by the constraints. This confirms the previous analysis. The resulting transmissibility plot is the same as shown in figure 3.7. The problem must not be over-constrained by adding a maximum bound on the port length. This constraint will not allow the algorithm to find the minimum. Equation 3.7 can now be used to calculate the port length that will offset the port inlet/outlet geometry.

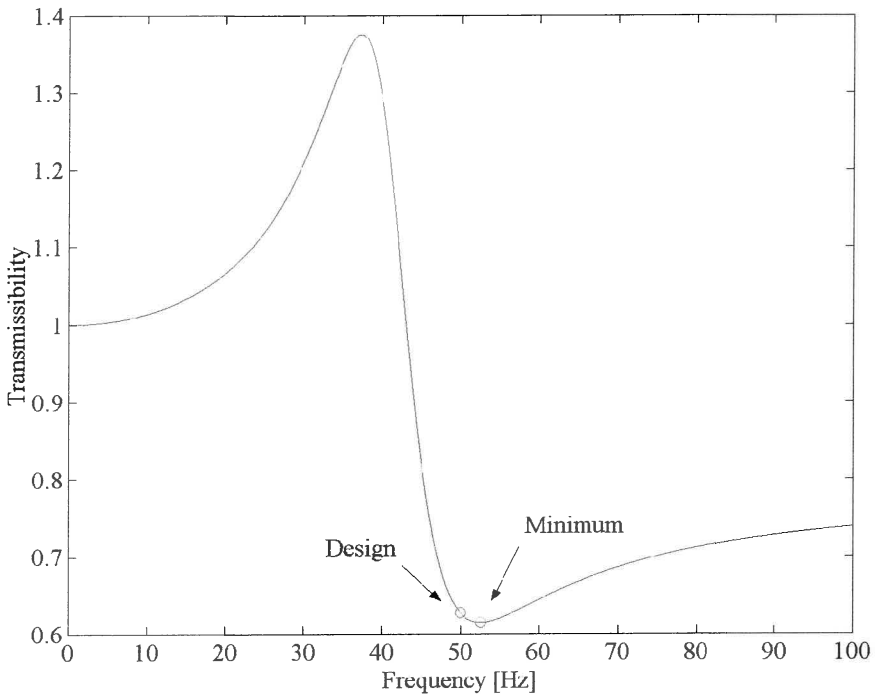

Figure 3.8. Ideal transmissibility curve for isolation at 50 Hz with $m = 15$ kg, $\zeta = 0.1$ and $\eta = 0.1$

If it is deemed that it will be more beneficial to locate the minimum transmissibility to coincide with the isolation frequency the approach suggested in chapter §2.7.2 can be used. The absolute value of the transmissibility was differentiated to give an expression for the curve's minimum and maximum frequency. It was found that the minimum corresponds to the second root of a rather complex polynomial. This equation cannot be solved analytically and a numerical search procedure had to be used. The MATLAB function `fsolve.m` was used to minimise the absolute value of the difference between the second root and the isolation frequency. This function uses a least-squares method to find the optimal length that will minimise the objective function. This procedure resulted in a design with a slightly longer port length and higher transmissibility than was found previously. The results are summarised in table 3.9.

Table 3.9 Port length and transmissibility

Search result		Value
Port length [mm]	l	135
Transmissibility	$\lvert T_r \rvert$	0.64

This port length can also be adjusted so that the inlet/outlet geometry can be taken into account using equation 3.7.

3.4 Calculation of the spring stiffness

The stiffness is a function of the material and the geometry. The material properties will be discussed first. In the following paragraphs the geometry will be analysed through successive refinements. The spring will first be estimated as a hollow cylinder, then as a cylinder with tapered ends and lastly the effect of the side entrances will be taken into account.

3.4.1 Material properties

Polyurethane will behave non-linearly at large strains. This behaviour is called hyperelasticity. In order to decide if non-linear behaviour is present, the normal strain must be calculated. The shear and normal strains are given by equation 3.9 and 3.10 (Gere & Tomoshenko, 1991):

$$\gamma = \text{atan}\left(\frac{x}{t}\right) \tag{3.9}$$

$$\varepsilon^2 + 2\varepsilon - \sin\gamma = 0 \tag{3.10}$$

Where x is the deflection and t the thickness of the rubber. The following table summarises the shear strain results for a 20 mm thick spring.

Table 3.10 Summary of strain for different deflections

Description	Deflection [mm]	Shear strain	Normal strain
Normal operating	1	0.050	0.0247
Operating maximum	5	0.245	0.1147
Design maximum	10	0.460	0.2030

The static properties of 55-Shore A polyurethane are published by the manufacturer at the three strains shown in table 3.11.

Table 3.11 Published modulus of elasticity vs strain

Modulus of elasticity [MPa]	Strain
1.4	1
3.4	5
6.9	10

The modulus of elasticity at a strain of 0.05 caused by a deflection of 1 mm is estimated as 0.975 MPa. The shear modulus is related to the modulus of elasticity:

$$G = \frac{E}{2(1+\nu)} \tag{3.11}$$

The Poisson's ratio for incompressible materials is 0.5 and the shear modulus is consequently one third of the modulus of elasticity.

The dynamic properties of polyurethane are described by the complex modulus of elasticity as shown in equation 2.44. There are several factors that can influence the dynamic properties relating to the material, load etc. (Garibaldi & Onah, 1996). The most important are the following:

- Temperature. This is the most important factor.
- Frequency. The modulus of elasticity will increase with frequency.
- Strain. If the strains are large the material behaviour is non-linear and the complex modulus will represent an average value.

The value of the complex dynamic modulus of elasticity is not published by the manufacturer and was obtained from tests done at the University of Pretoria. E^* and η was measured as a function of frequency only.

These tests were done with a 40 mm cube that was bonded on two opposite ends. The correct relation between modulus of elasticity and shear modulus for this configuration is given by equation 3.12 (Nashif *et al.*, 1985):

$$E_c = 3G\kappa_T \tag{3.12}$$

$$\kappa_T = 1 + \beta\left(\frac{S}{S'}\right)^2 \tag{3.13}$$

κ_T is known as the shape factor. β is a non-dimensional constant equal to 2 for an unfilled and 1.5 for a filled elastomer. Filler is added to natural rubber to change its properties. Since this is not applicable to polyurethane both values were tested and the shape factor proved to be insensitive to this parameter. S is the cross sectional area (40×40) and S' (40×40×4) the nonload-carrying area. The relation between E and G is therefore slightly less than suggested by equation 3.11. For all the calculations involving data from these tests it will be assumed that the relation is 0.3.

Measurements were done using a 60 Shore A specimen up to an excitation of 30 Hz, at room temperature and at various strains. From these measurements it is estimated that the storage modulus (E') stabilises at around 9 MPa. The static property was calculated as 1.07 MPa at a normal strain of 0.05 using the published data. For the 55 Shore A sample the static modulus of elasticity was calculated as 0.975 MPa at the same strain. Using the ratio of static moduli and the measured storage modulus of the 60 Shore A sample the storage modulus was estimated as 8.2 MPa. Using the relationship found in equation 3.12 the shear storage modulus can be calculated and is 2.73 MPa.

3.4.2 Hollow cylinder

The first approximation is a plate of which the height and width are equal to the average height and circumference of a hollow cylinder. The average height of the plate is taken as half the sum of the inner surface height (l) and the outer surface height ($l + 2h_r$):

$$\bar{h} = l + h_r \tag{3.14}$$

The width of an equivalent plate is:

$$w = \pi\left(\frac{d_p + d_b}{2}\right) = \pi\bar{d} \tag{3.15}$$

The shear stiffness of the equivalent plate is therefore (Gere & Timoshenko, 1991):

$$k = \frac{GA}{t} = \frac{G\bar{h}\pi\bar{d}}{t} \tag{3.16}$$

where t is the spring thickness and is equal to ½(d_b - d_p). Equation 3.13 can only be applied to small strains. Summing the stiffness of rectangular flat sheets in series can approximate the spring shown in figure 3.9.

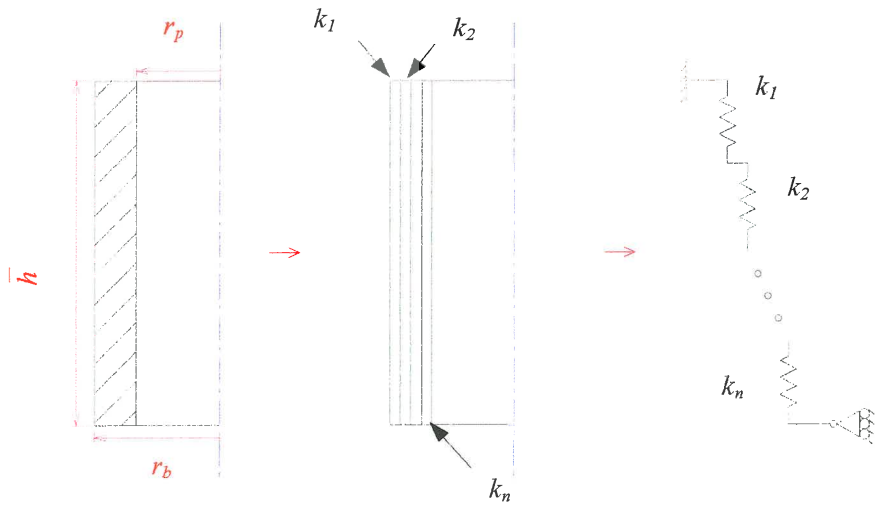

Figure 3.9 Approximation of the total spring stiffness

The total stiffness can be calculated by summation of the springs as shown in equation 3.17.

$$\frac{1}{k} = \sum_{i=1}^{n} \frac{1}{k_i} \tag{3.17}$$

k_i is defined by equation 3.16.

By substituting equation 3.16 and taking the sum of an infinite number of springs between r_p ($\frac{1}{2}d_p$) and r_b ($\frac{1}{2}d_b$) the following integral can be derived

$$\begin{aligned}\frac{1}{k} &= \int_{r_p}^{r_b} \frac{1}{2\pi G r \bar{h}} dr \\ &= \frac{1}{2\pi G \bar{h}} \int_{r_p}^{r_b} \frac{1}{r} dr \\ &= \frac{1}{2\pi G \bar{h}} \ln|r| \Big|_{r_p}^{r_b} \\ &= \frac{1}{2\pi G \bar{h}} [\ln(r_b) - \ln(r_p)]\end{aligned} \tag{3.18}$$

The stiffness for a hollow cylinder is therefore:

$$k = \frac{2\pi G \bar{h}}{\ln\left(\frac{r_b}{r_p}\right)} \tag{3.19}$$

The following formula takes the effect of combined bending and shear into account (Davey & Payne, 1964):

$$k = \frac{\bar{h} G}{\frac{1}{Q_1} + \frac{r_b^2}{\bar{h}^2 Q_2}} \tag{3.20}$$

Q_1 and Q_2 is defined as:

$$Q_1 = \frac{2\pi}{\ln\left(\frac{r_b}{r_p}\right)} \tag{3.21}$$

$$Q_2 = \frac{16\pi \left(\frac{r_b}{r_p}\right)^2 \left[\left(\frac{r_b}{r_p}\right)^2 - 1\right]}{3\left\{\left[\left(\frac{r_b}{r_p}\right)^2 - 1\right]^2 - 4\left(\frac{r_b}{r_p}\right)^2 \left[\ln\left(\frac{r_b}{r_p}\right)\right]^2\right\}} \tag{3.22}$$

Q_2 represents the bending and if this term is zero, the equation simplifies to equation 3.19.

The geometry was also analysed using finite elements. ABAQUS recommends that hybrid elements be used for an analysis involving incompressible materials. Higher order axi-symmetric elements gave the best results. The inner surface was displaced by 1 mm axially while any displacement normal to the surface was constrained. The outer surface was fully constrained. The reaction force on the outer surface was calculated by summation of all the constrained node reaction forces in the axial direction on this surface.

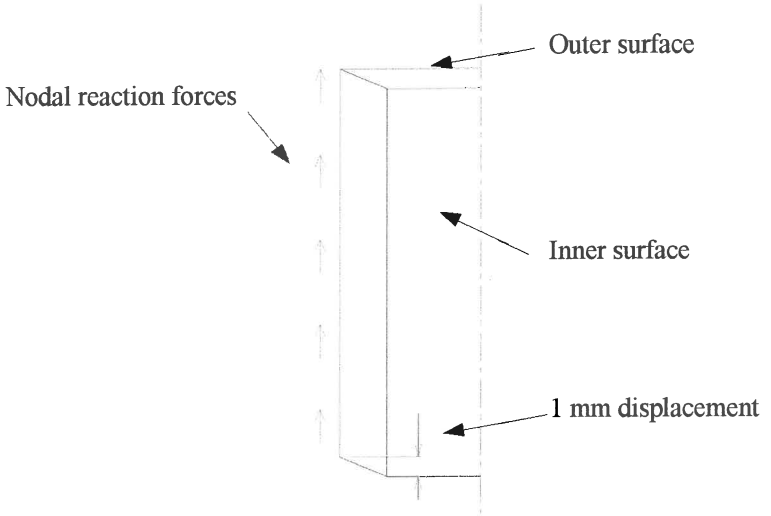

Figure 3.10 Schematic of the axi-symmetric finite element model (swept through 90°)

Several mesh refinements gave similar results and the best estimate is shown in table 3.12. Since the stiffness is a linear function of the shear modulus it will be more useful to report the results in terms of a stiffness coefficient. This coefficient can be used for any material, but only this specific geometry.

Table 3.12 Stiffness coefficients for a hollow cylinder

Method	Equation	Geometric stiffness (k/G)
Equivalent plate	3.16	2.592
Hollow cylinder	3.19	2.557
Hollow cylinder with bending	3.20	2.548
FEM estimate		2.492

3.4.3 Cylinder with tapered ends

If the tapered ends of the cylinder are taken into account the following equation should be used (Davey & Payne, 1964):

$$k = \frac{2\pi G\left[(l+2h_r)r_p - lr_b\right]}{(r_b - r_p)\left[\ln\left((l+2h_r)r_p\right) - \ln(lr_b)\right]} \qquad (3.23)$$

This equation is compared to the finite element model of a spring with tapered ends in table 3.13.

Table 3.13 Tapered cylinder results

Method	Equation	Geometric stiffness (k/G)
Tapered hollow cylinder	3.23	2.534
FE estimate		2.522

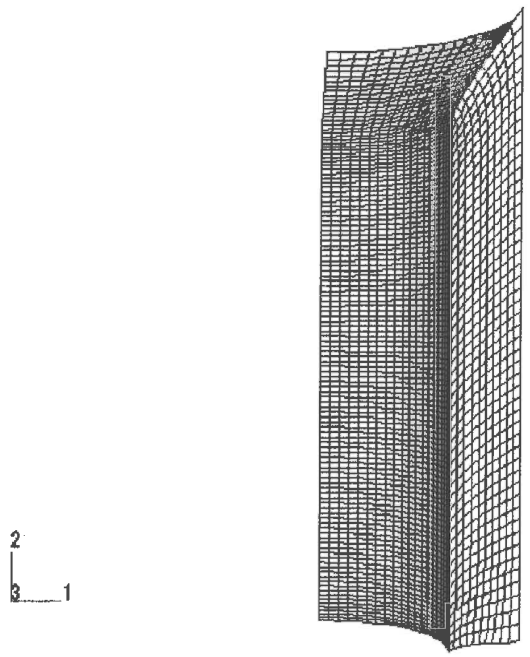

Figure 3.11 Exaggerated deformation and mesh of the spring with tapered ends (swept through 90°)

The results show that the average height and circumference assumption slightly overestimated the spring stiffness. The finite element model showed no mesh size or element type dependency.

3.4.4 Exact geometry

The previous analysis showed that the tapered ends do not have a large effect on the stiffness. It might therefore be possible to ignore their effect during the design especially if the ratio between the port length and reservoir height is large. The side entrances will, however, have a major impact due to its size. The spring can theoretically be divided into four springs that act in parallel as shown in figure 3.12.

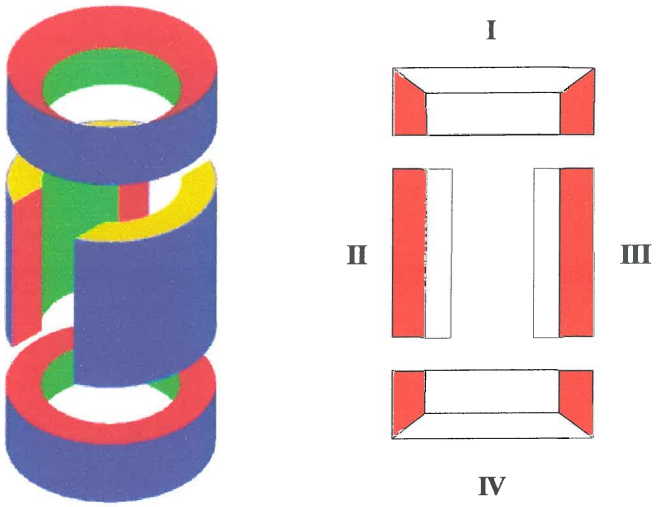

Figure 3.12 Subdivision of the absorber spring

The springs will be numbered from I to IV. It is obvious from the symmetry of the model that the stiffness of spring I and II is equal to that of spring III and IV. The total stiffness is therefore:

$$k = 2(k_I + k_{II}) \tag{3.24}$$

The section dimensions of spring I are shown in figure 3.13.

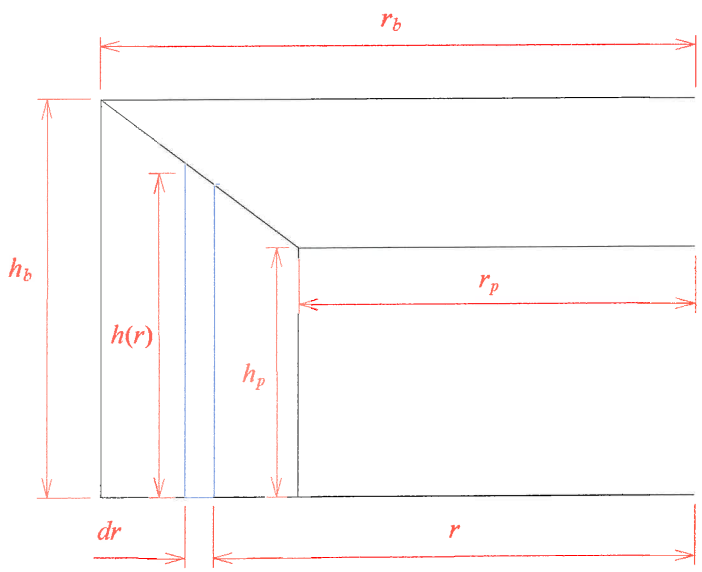

Figure 3.13 Section dimensions for spring I

The total stiffness of the shape in figure 3.13 can be found through the summation of rectangular sheets of infinitesimal thickness according to the rule for summation of springs in series. The height of the sheet is a function of the radius and is given by equation 3.25:

$$h(r) = \frac{r - r_p}{r_b - r_p}\left(h_b - h_p\right) + h_p \tag{3.25}$$

The width of the sheet is $2\pi r$. The stiffness of the sheet is given by equation 3.26:

$$dk = \frac{GA}{dr} = \frac{2\pi Gr\left[\frac{r - r_p}{r_b - r_p}\left(h_b - h_p\right) + h_p\right]}{dr} \tag{3.26}$$

The inverse of the stiffness of spring I can now be calculated by evaluating the following integral:

$$\frac{1}{k_I} = \int_{r_r}^{r_b} \frac{1}{2\pi Gr\left[\frac{r - r_p}{r_b - r_p}\left(h_b - h_p\right) + h_p\right]} dr \tag{3.27}$$

This integral will be evaluated numerically.

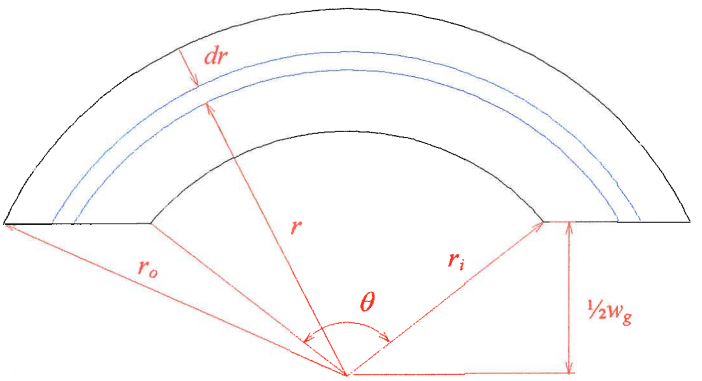

Figure 3.14 Section dimensions of spring II

The spring has height h_g. The inverse of the stiffness is:

$$\frac{1}{k_{II}} = \int_{r_r}^{r_b} \frac{dr}{2Grh_g \operatorname{acos}\left(\frac{w_g}{2r}\right)} = \frac{1}{2Gh_g}\int_{r_r}^{r_b} \frac{1}{r \operatorname{acos}\left(\frac{w_g}{2r}\right)} dr \tag{3.28}$$

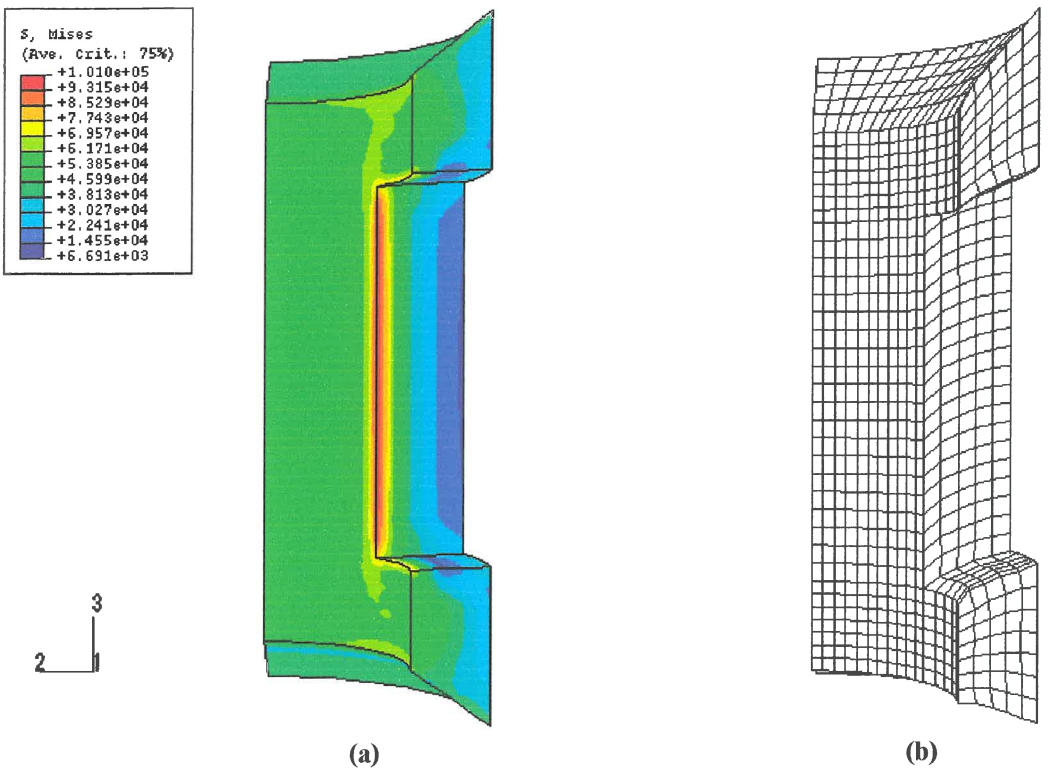

Figure 3.15 (a) Von Mises stress contours and (b) exaggerated deformation for a ¼ section of the absorber spring

For the finite element approximation 3D brick elements were used. In this case it was possible to simplify the analysis by only modelling ¼ of the absorber spring. Various element types and mesh sizes gave similar results. The von Mises stress contours show that care should be taken with the entrance design to ensure minimal stress concentration.

The results of the finite element model estimate and the integration of the geometry are shown in table 3.14. As expected the side entrances have a major effect on the resulting geometric stiffness if compared to the result in table 3.13. The exact geometry integration is very close to the finite element result and it is therefore recommended that this method be used for the calculation of the spring stiffness for design purposes.

Table 3.14 Exact geometry

Method	Equation	Geometric stiffness (k/G)
Exact geometry integration	3.24	1.985
FE estimate		1.921

For the estimate of the shear modulus made in §3.4.1 (2.37 MPa) the spring stiffness will be 4.55 MN/m which is close enough to the assumed value of 4 MN/m.

3.4.5 Casting of the polyurethane spring

The elastomeric spring was cast by fitting polypropylene moulds on the ends of the sleeve and in the side entrances as shown in figure 3.16. All the areas where the polyurethane should stick to the surface were treated with an adhesive. The rest of the port, sleeve and moulds were treated with a release agent. The moulds also had to ensure the proper alignment of the port and the sleeve. This was achieved by machining a locating pin on the ends of the plug moulds. The entrance moulds were screwed onto the port to ensure that the port does not rotate about its centre axis. This alignment is important to ensure that the centrelines of the two load cell connection points coincide. The moulds also prevented the polyurethane from leaking into the port during casting. The entrance moulds were machined slightly smaller than the entrances. The resulting gap was filled with putty. A riser was machined into the top mould to accommodate the shrinkage that occurs as a result of polymerisation.

The polyurethane was supplied as a three component casting system consisting of resin base, isocyanate and 1,4-butane diol. These three compounds are mixed in a specific ratio that will determine its mechanical properties. The mixture is castable for ±15 min. During this time it is important to limit the formation of bubbles, which will become inclusions in the spring after it is cast. Centrifugal force is used to drive the bubbles to the surface of the mixture.

The mould assembly was evenly heated to about 40°C in an oven to accelerate the chemical reaction. After it has been cast the top entrance mould was bolted in place to ensure that all the polyurethane was driven from the interface with the port. The spring cured within 2 days.

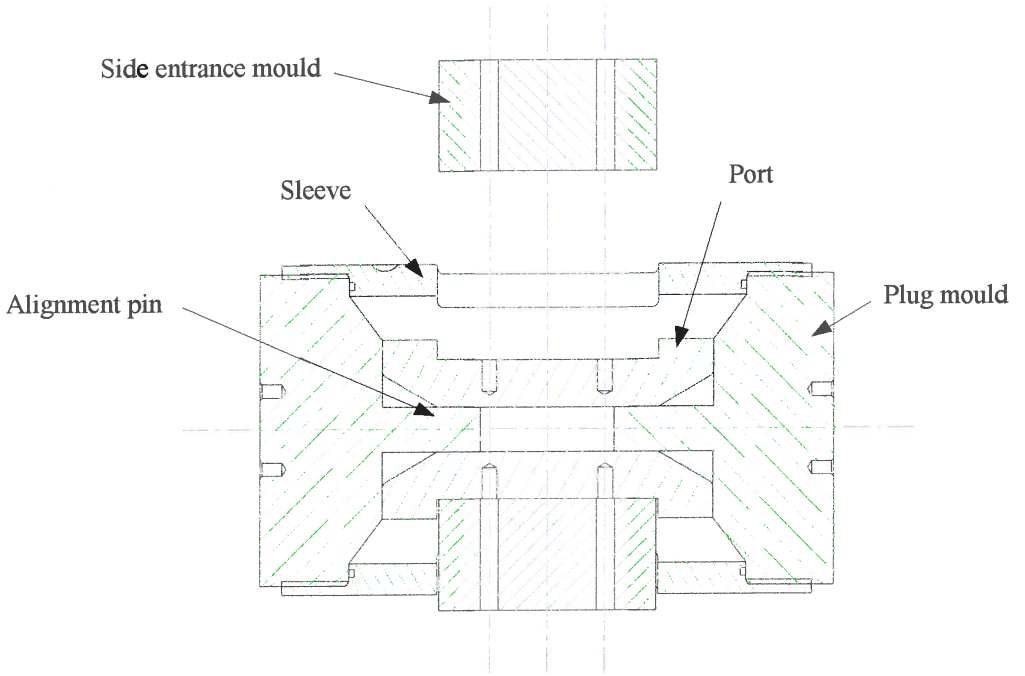

Figure 3.16 Mould assembly for the casting of the polyurethane spring

3.5 Calculation of the viscous damping

The viscous damping is calculated as described in chapter 2. For this design the geometry differs from the theoretical case and this will affect the damping significantly. Since the method was explained in detail in chapter 2 this paragraph will focus on the improvement obtained with the use of the new geometry. Appendix E contains more detailed results from this analysis as well as description of the methods used. The mesh is shown in figure 3.17.

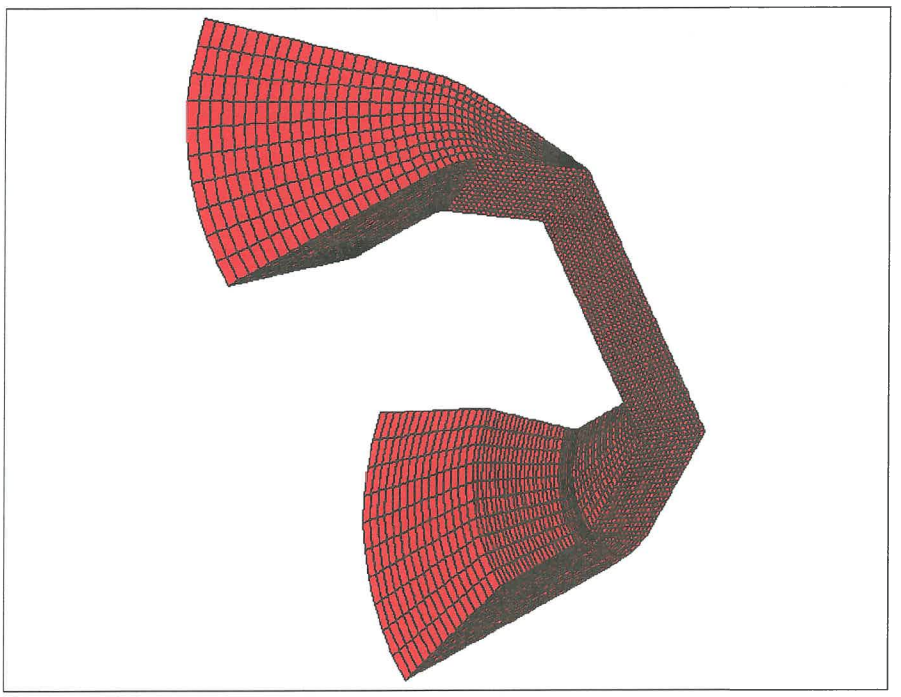

Figure 3.17 3D grid for 1/8th of the flow region

A comparison between the results for a square and a conical inlet/outlet at a port velocity of 0.2 m/s is shown in table 3.15.

Table 3.15 Comparison at a port velocity of 0.2 m/s

	Theoretical value / Design value
Inlet pressure drop	4.5
Outlet pressure drop	1.9
Total pressure drop	2.7
Viscous damping	5.1

The inlet pressure drop was the main contributor to the 5.1 times reduction in viscous damping. This is a significant improvement and it can probably be reduced further using optimisation techniques. However, an optimised port inlet/outlet might be expensive to manufacture.

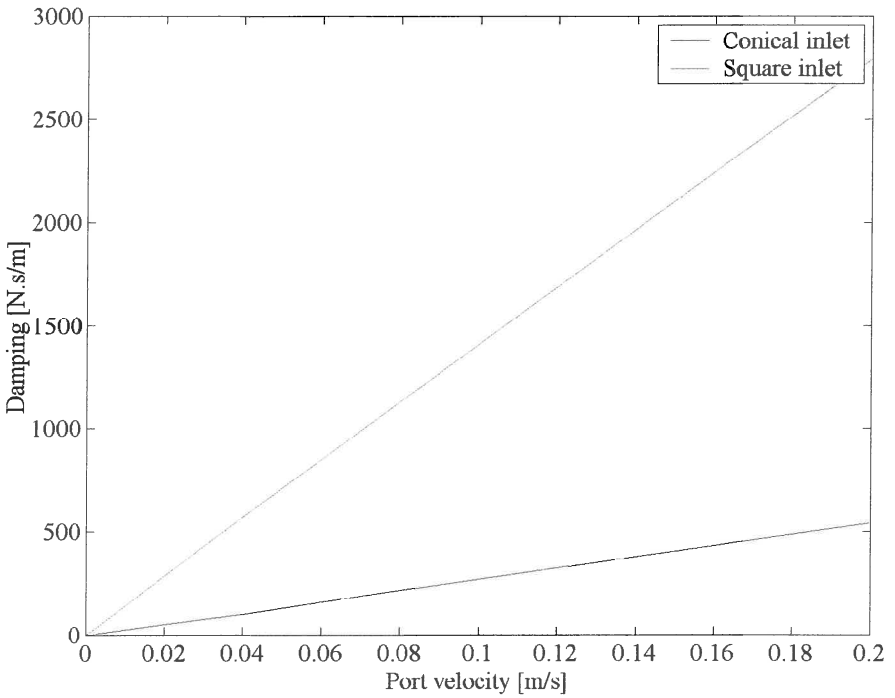

Figure 3.18 Viscous damping (c) as a function of port velocity ($\dot{x}$)

3.6 Conclusion

It is possible to find the optimal geometry of a damped LIVE type absorber for a desired frequency of isolation taking into account the various practical requirements. The port length must be adjusted to account for the addition of conical inlets/outlets. The spring stiffness should be calculated to ensure that it is viable with the chosen elastomeric material. If this proves impossible the outer port diameter can be modified. The port inlet/outlet geometry must be optimised to ensure the lowest possible viscous damping.

CHAPTER 4

Testing the experimental absorber

4.1 Introduction

This chapter will document all the methods used for characterising the experimental vibration absorber. It will also report the most important experimental results.

The properties of the elastomeric spring are of extreme importance, since they are difficult to calculate during the design and have a big influence on the value of the isolation frequency. The first part of the chapter will therefore address techniques for the measurement of the stiffness and the loss factor. The first few methods used constant frequency excitation. From the data, the relaxation of the spring could be calculated. The second method employed sine sweep excitation. This method gave the properties as a function of frequency. Lastly, the transmissibility was calculated. From these measurements, the system properties could be extracted.

Two separate tests were done with the experimental absorber. The first test was with a 55 Shore A spring and the second with a 35 Shore A spring. The second spring was fitted to reduce the stiffness and thereby the isolation frequency.

A schematic of the test set-up is shown in figure 4.1. The load cells were used to measure the transmissibility. The LVDT and the top load cell were used to calculate the spring stiffness and loss factor. The actuator was set in displacement control for all tests to ensure that the specimen is not subjected to large displacements that could damage the spring.

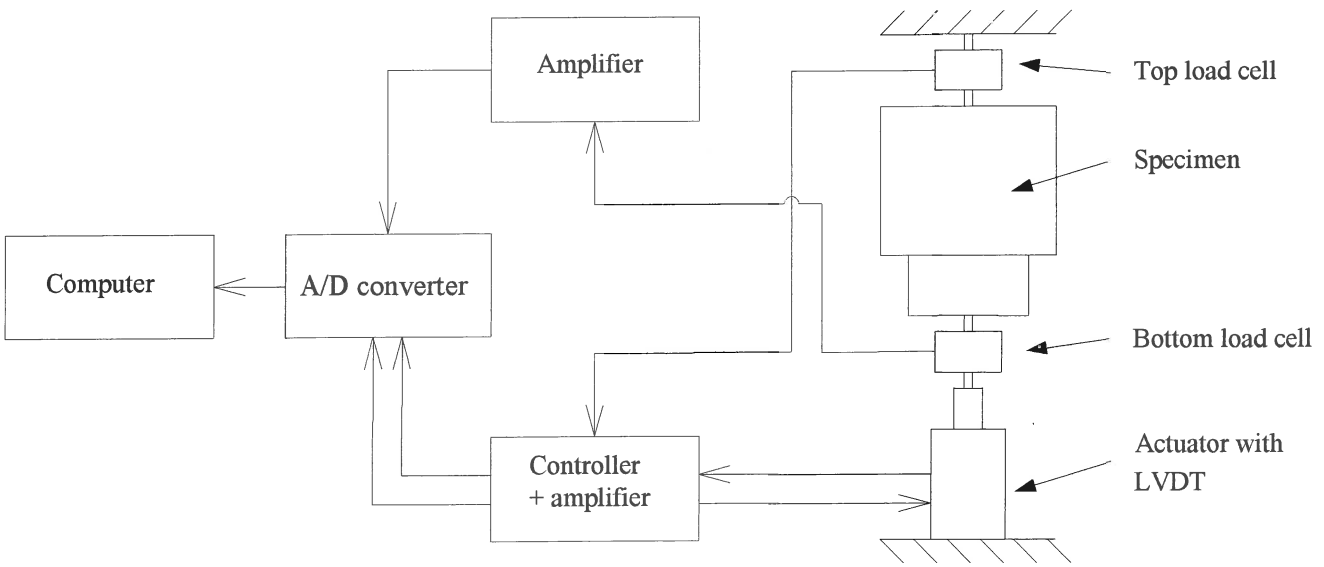

Figure 4.1 Schematic of the test set-up

The hydraulic actuator's controller was also used to amplify the signal from the top load cell and the LVDT. A second amplifier was needed for the bottom load cell. A CDAS analogue to digital converter was used to digitise the signal. The CDAS filter was set well above the excitation frequency. A Pentium computer with QanTIM software was used to generate the sine sweep signals. The constant frequency excitation signals were generated by the Schenk controller.

4.2 Constant frequency excitation

Constant frequency excitation was used to study how the properties of the elastomeric spring changed as a function of time. Data was gathered at 1-minute intervals, each for 1 second at a sampling frequency of 500 Hz. The total time of excitation was at least 1½ hours. These tests were done at 5 Hz intervals from 5 to 40 Hz.

The stiffness and loss factor will be reported. Three methods were used to estimate the parameters:

1. Hysteresis loop method. This method calculates the viscous damping from the intersection of the loop with the force axis.
2. Sine curve fit method. This method fitted sine curves to the data and used the resulting equations to calculate the parameters. This method is essentially a more refined approach to the first method since all the measured data is used, while only two data points per cycle were used for the first method.
3. Hysteresis loop area method. This method calculates the loss factor from the area of the hysteresis loop.

The stiffness and loss factor are time dependent properties. Relaxation in stiffness occurs and this could have a major influence on the absorber's performance. It is assumed that the properties will decay exponentially until a stable value is reached. An exponential decay function was fitted to the data to extract the initial and stable values.

It is necessary to condition the data before use by:

1. De-trending the data by subtracting the average offset.
2. Filtering the data using a low pass digital filter with a cut off frequency set at 1.5 times the excitation frequency to reduce the influence of high frequency noise.
3. Calibrating the data with the appropriate factors.

4.2.1 Hysteresis loop equation method

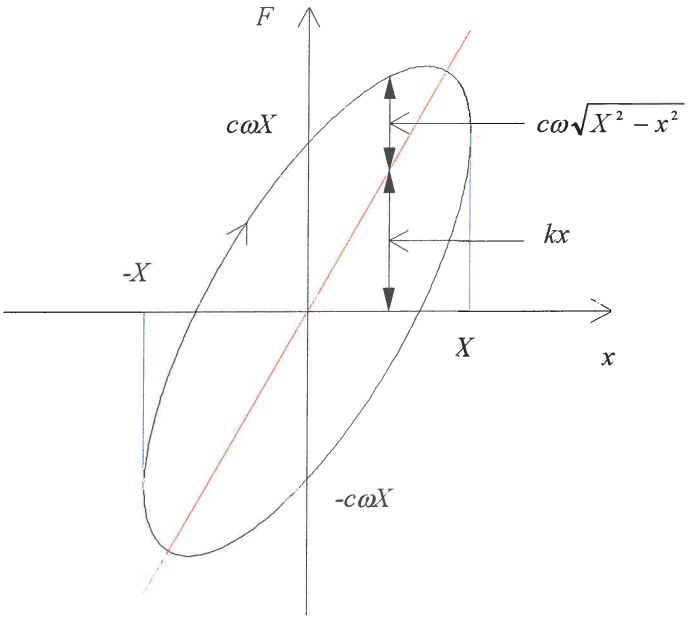

Figure 4.2 Hysteresis loop

The viscous hysteresis loop is described by Rao (1990):

$$f(t) = kx \pm c\omega\sqrt{X^2 - x^2} \tag{4.1}$$

in which x is:

$$x(t) = X \sin \omega t \tag{4.2}$$

From equation 4.1 it can be seen that the force at maximum displacement is given by:

$$f_{x=X} = kX \tag{4.3}$$

The force at zero displacement is given by:

$$f_{x=0} = \pm c\omega X \tag{4.4}$$

Equation 4.2 was implemented as shown below:

$$\sum_{i=1}^{n} |f_i|_{x=0} = c\omega \sum_{i=1}^{n} |X_i| \tag{4.5}$$

where n is the number of displacement peaks and troughs in the data set. X_i is the maximum and minimum displacement of the i-th peak or trough identified from the displacement time data. The extrema are identified from a change in the sign of the slope (figure 4.3).

The example in figure 4.3 shows the peaks identified at 15 Hz excitation. The number of peaks and troughs identified (n) varied between 29 and 30 for 15 Hz because there were not always 15 complete waves due to the excitation frequency that drifted slightly.

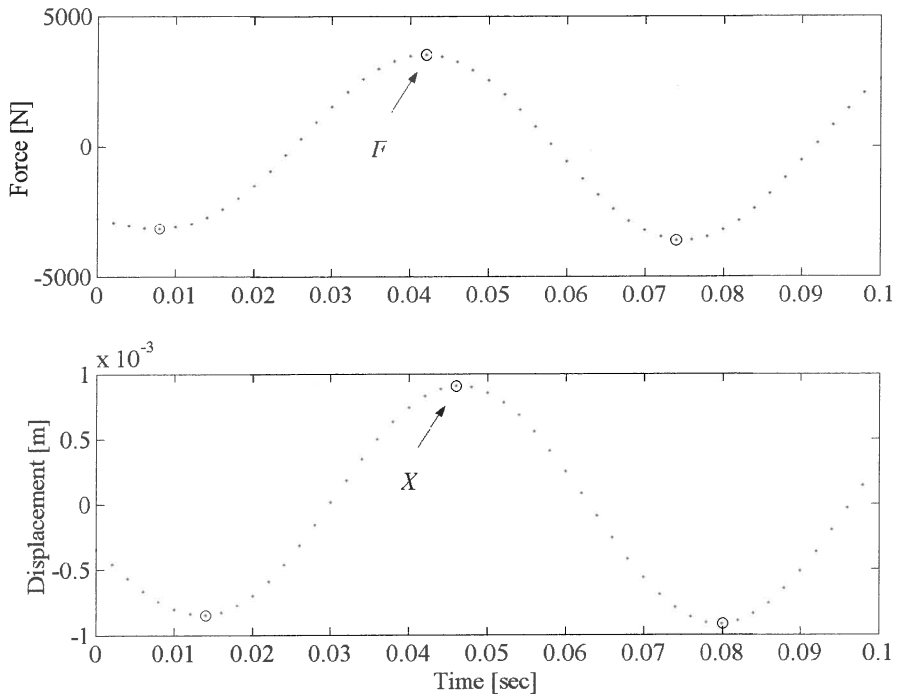

Figure 4.3 Peaks and troughs identified from the time data

f_i at $x = 0$ was determined by finding two data points between which the sign of the displacement changed. The exact time was then calculated through linear interpolation:

$$t_{x=0} = \frac{-x_k}{x_{k+1} - x_k}(t_{k+1} - t_k) + t_k \qquad \textbf{(4.6)}$$

The force at $x = 0$ could now be computed using this time point and the force time data:

$$f_{x=0} = \frac{t_{x=0} - t_k}{t_{k+1} - t_k}(f_{k+1} - f_k) + f_k \qquad \textbf{(4.7)}$$

The force and displacement data was captured simultaneously.

In equation 4.5 the excitation frequency was calculated by determining the frequency of maximum energy of a power spectral density calculation (PSD) of the displacement time data. The resolution of the PSD is 1 Hz. Figure 4.4 shows the PSD and illustrates the implementation of the low pass digital filter with a cut-off frequency of 1.5 times the excitation frequency.

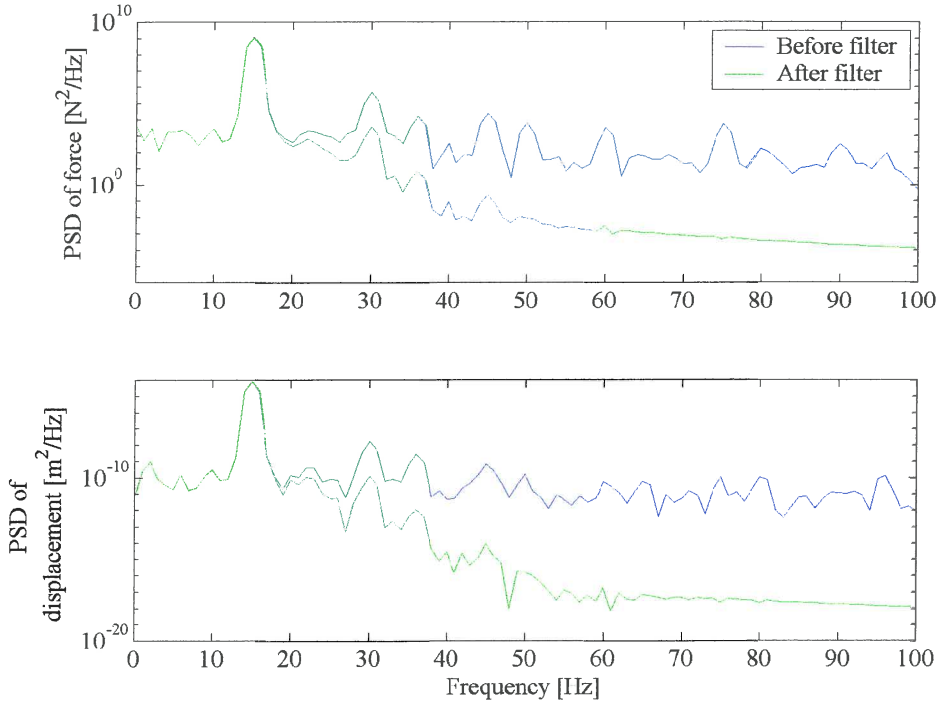

Figure 4.4 PSD of force and displacement data clearly showing the excitation frequency at 15 Hz as well as the effect of the low pass filter with a cut-off frequency at 22.5 Hz

c can be calculated using:

$$c = \frac{\sum_{i=1}^{n} |f_i|_{x=0}}{\omega \sum_{i=1}^{n} |X_i|} \tag{4.8}$$

The stiffness coefficient can be calculated by dividing the force at maximum displacement by the maximum displacement as follows:

$$k = \frac{\sum_{i=1}^{n} |f_i|_{x=X}}{\sum_{i=1}^{n} |X_i|} \tag{4.9}$$

The force at maximum displacement was found using the time at which the maximum displacement occurred as shown in figure 4.5. These values were averaged as shown in equation 4.9. The hysteretic damping can be calculated using:

$$h = c\omega \tag{4.10}$$

The loss factor is:

$$\eta = \frac{h}{k} \tag{4.11}$$

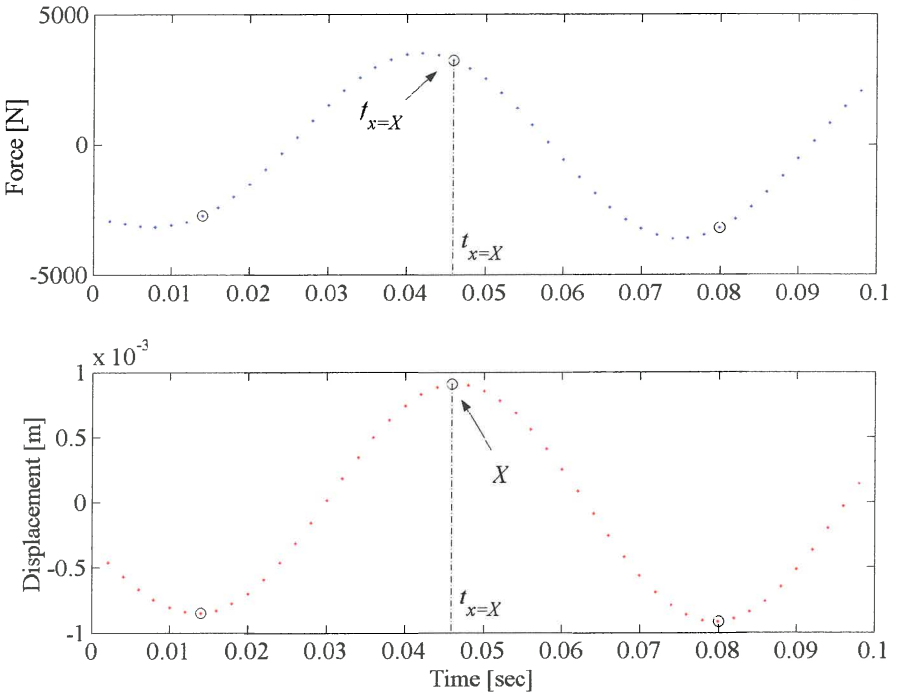

Figure 4.5 The force at maximum displacement ($x = X$)

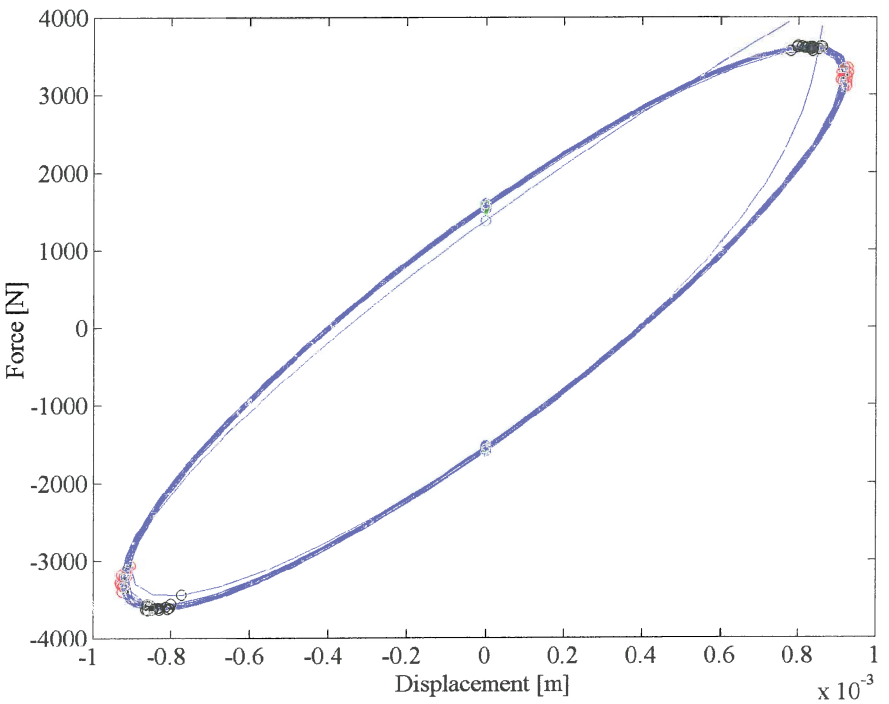

Figure 4.6 A typical hysteresis plot at 15 Hz excitation showing the force at minimum and maximum displacement (red), the minimum and maximum force (black) and the force at zero displacement (green) for each wave

4.2.2 Sine curve fit method

This method attempted to fit a sine curve through the data using an optimisation algorithm. The sine curve is described by the amplitude (A), the excitation frequency (ω) and the phase angle (ϕ):

$$y = A\sin(\omega t + \phi) \tag{4.12}$$

The objective function is:

$$f(\bar{x}) = \sum_{i=1}^{m}(x_1 \sin(x_2 t_i + x_3) - y_i)^2 \tag{4.13}$$

where $m = f_s \Delta t$ is the total number of data points (y_i) measured. This was done twice for each set of data, once for the force data and once for the displacement data. The MATLAB `fminsearch.m` algorithm was used. This algorithm uses an unconstrained Nelder-Mead type simplex search method. The initial values for the amplitude and frequency were taken from the results of previous method (§4.2.1) and the phase angle was chosen as zero. It was found that convergence was not always achieved and in such cases it was remedied by restarting the optimisation using a random phase angle in the interval [-2π,2π].

The convergence criteria where:

- a positive amplitude (A),
- the value of the objective function must be less than an acceptable value (which was found through trial and error), and
- the difference between the current and a previous value for the objective function should be less than 1×10^{-5}.

The fitted parameters for the displacement are shown in equation 4.14.

$$x(t) = A_x \sin(\omega_x t + \phi_x) \tag{4.14}$$

The fitted parameters for the force are shown in equation 4.15.

$$f(t) = A_f \sin(\omega_f t + \phi_f) \tag{4.15}$$

The time at which the displacement is zero can now be calculated from the fitted parameters:

$$t_{x=0} = -\frac{\phi_x}{\omega_x} \tag{4.16}$$

The force at zero displacement is therefore:

$$f_{x=0} = A_f \sin\left(-\omega_f \frac{\phi_x}{\omega_x} + \phi_f\right) \tag{4.17}$$

The force at maximum displacement can be found by adding a quarter of the period to the time at zero displacement:

$$f_{x=X} = A_f \sin\left[\omega_f\left(-\frac{\phi_x}{\omega_x}+\frac{\pi}{2\omega_x}\right)+\phi_f\right] \tag{4.18}$$

The damping can now be calculated with ω taken as the average of two fitted values:

$$c = \frac{f_{x=0}}{\omega A_x} \tag{4.19}$$

The stiffness is:

$$k = \frac{f_{x=X}}{A_x} \tag{4.20}$$

The values of h and η can be found from equation 4.10 and 4.11.

It is also possible to find the loss factor (η) from the difference in the phase angle between the two signals:

$$\eta = \tan(\phi_f - \phi_x) \tag{4.21}$$

4.2.3 Hysteresis loop area method

The hysteresis loop area method estimates the energy loss per cycle. The area of the loop is equal to the amount of energy dissipated. The area is calculated using the trapezium method. The area of the loop is:

$$Area = \frac{1}{n}\sum_{i=1}^{m}\frac{f_{i+1}+f_i}{x_{i+1}-x_i} \tag{4.22}$$

n is the number of complete loops found. m is the total number of sampling points for n loops. The energy loss is related to the hysteretic damping by:

$$\Delta W = \pi h X^2 \tag{4.23}$$

The hysteretic damping is:

$$h = \frac{Area}{\pi X^2} \tag{4.24}$$

The loss factor (η) can be found using equation 4.11

4.2.4 Relaxation

The properties of the polyurethane changes with time. The initial values are denoted k_0 and η_0 and the stable values k_∞ and η_∞. It is assumed that it will decay exponentially from the initial value until a stable value is reached:

$$k(t) = k_0 e^{-dt} + k_\infty \tag{4.25}$$

A non-linear least-squares data fitting procedure using the Gauss-Newton method (`nlinfit.m`) in the MATLAB statistics toolbox was used to fit the model described by equation 4.26 to the observed data. A good fit was not always obtained.

$$y = \beta_1 e^{-\beta_2 t} + \beta_3 \tag{4.26}$$

This method also returned the residuals and the Jacobian, which can be used to find the confidence interval with the function `nlpredci.m`. Figure 4.7 shows a typical good fit of stiffness.

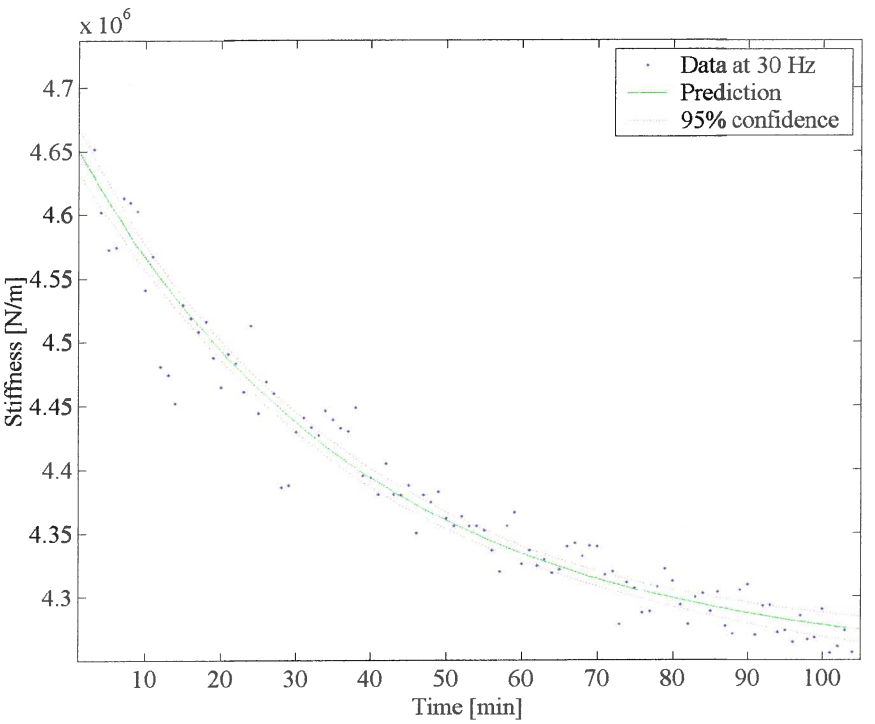

Figure 4.7 The stiffness (k) as a function of time

4.3 Sine sweep excitation

The sine sweep is a sinusoidal command signal, the frequency of which is varied slowly but continuously through the range of interest (Ewins, 1995). It is necessary to check that the progress through the frequency range is slow enough that steady-state conditions are attained before measurements are made. If excessive sweep rates are used the measured FRF is distorted. One way of checking the suitability of a sweep rate is to make two measurements, one sweeping up and another sweeping down. If the same curve is obtained then there is a possibility, though not a certainty, that the sweep rate is not excessive.

It is possible to prescribe an optimum sweep rate for a given structure. In theory any sweep rate is too fast to guarantee that the full steady-state response level will be attained, but in practice it is possible to attain a condition very close to this desired state. ISO 7626 suggest the following maximum sweep rates.

$$S_{\max} < 54 f_r^2 \eta_r^2 \quad \text{or} \quad S_{\max} < 216 f_r^2 \zeta_r^2 \tag{4.27}$$

For the experimental test set-up a worst case would be:

- $f_r = 20$ Hz
- $\eta_r = 0.2$

The maximum sweep rate would therefore be 864 Hz/min. For the desired 70 Hz sine sweep should therefore not be completed in less than 4.86 seconds.

4.3.1 Transfer function estimate of the stiffness and loss factor

The amplitude of the displacement and the force transmitted to the top load cell were used to calculate the stiffness and the loss factor:

$$\frac{F_o}{X} = k(1 + i\eta) \tag{4.28}$$

The transfer function between the force and the displacement is an estimate of the amplitude ratio:

$$\frac{F_o}{X} = \frac{S_{f_o f_o}(\omega)}{S_{f_o x}(i\omega)} \tag{4.29}$$

The transfer function is estimated in MATLAB with the `tfe.m` function using Welch's averaged periodogram method.

The stiffness is:

$$k_s(\omega) = \mathrm{Re}\left(\frac{F_o}{X}\right) \tag{4.30}$$

The loss factor is calculated as follows:

$$\eta_s(\omega) = \frac{\mathrm{Im}\left(\frac{F_o}{X}\right)}{k_s(\omega)} \tag{4.31}$$

The displacement signal was modified to compensate for the control system's inability to provide the required amplitude at higher frequencies and to reduce the response at resonance. This was done through trial and error. The best response was obtained using the amplitude shown in figure 4.8.

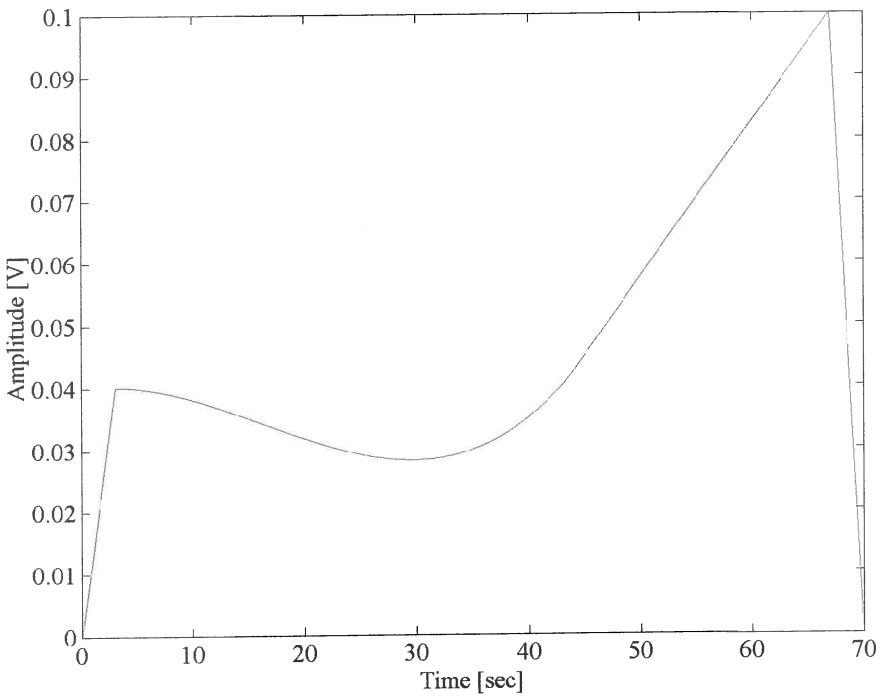

Figure 4.8 Modified time signal amplitude

A typical moving average envelope of the displacement for a 70-second sine sweep is shown in figure 4.9.

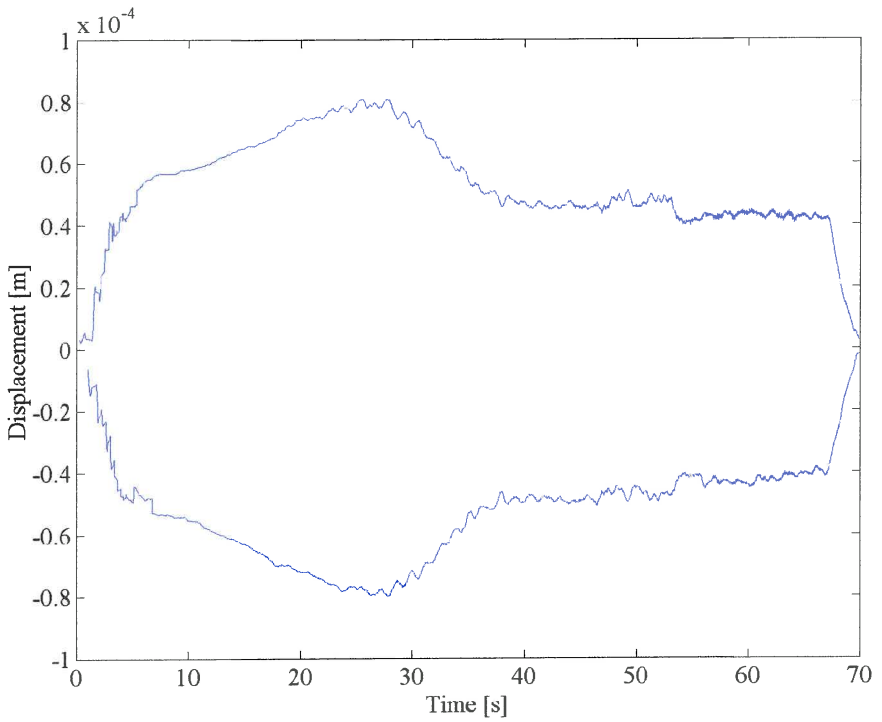

Figure 4.9 Actual measured displacement envelope (20 point moving average)

4.3.2 Transmissibility

The transmissibility was calculated using the transfer function estimate as was done in equation 4.29.

$$\frac{F_o}{F_i} = \frac{S_{f_o f_o}(\omega)}{S_{f_o f_i}(i\omega)} \tag{4.32}$$

This was done for an absorber filled with liquid as well as for an unfilled absorber which, highlighted the change in system's response. For the filled absorber the system characteristics can be extracted from the measured transmissibility data by finding the parameters that best represents the transmissibility curve with an optimisation procedure. Fitting all the parameters at once proved impossible. However, the system's mass (m), geometry and absorber fluid density was known and only the stiffness, loss factor and viscous damping needed to be calculated. The loss factor was estimated as 0.1 from previous tests to further simplify the analysis. The stiffness is a linear function of frequency for the frequency range of interest:

$$k(\omega) = k_1\omega + k_2 \tag{4.33}$$

In chapter 2 the viscous damping was found to be a linear function of frequency which must be zero when the port velocity is zero:

$$c(\omega) = c_1 \omega \tag{4.34}$$

The model of the transmissibility used for the curve fit is therefore:

$$T_r = \frac{(x_1\omega + x_2)(1+i\eta) + i\omega^2 x_3 + \omega^2 m_B \left(1 - \frac{A_b}{A_a}\right)\frac{A_b}{A_a}}{(x_1\omega + x_2)(1+i\eta) + i\omega^2 x_3 - \omega^2 \left[m + m_B\left(1 - \frac{A_b}{A_a}\right)^2\right]} \tag{4.35}$$

MATLAB does not specifically allow for complex optimisation and therefore the absolute value and phase angle of the transmissibility was used to define the objective function as a multiple objective optimisation problem. The square of the difference in the absolute value and phase angle at each measurement point is compared and the sum of the differences is minimised.

$$f(\bar{x}) = w_1 \sum_{i=1}^{n} \left(|(T_r)_i| - |(T_r^m)_i| \right)^2 + w_2 \sum_{i=1}^{n} \left(\angle(T_r)_i - \angle(T_r^m)_i \right)^2$$

subject to

$$g_i(\bar{x}) = -x_i \le 0 \qquad i = 1,2,3 \tag{4.36}$$

where T_r^m is the measured data, n the number of sampling points used and w_1 and w_2 weight assigned to the objectives. The values of all the variables had to be greater than zero since they are physical properties. It is not necessary to include all the sampling points for the optimisation, especially data at low frequencies where the measurements can be inaccurate. It is recommended that most of the points measured close to the maximum transmissibility and isolation are included.

The weights were chosen through trial and error and it was found that the contribution of both these functions were of the same order. Visual inspection of the fit is recommended to ensure that both the absolute value and phase angle are fitted successfully.

The constrained non-linear optimisation algorithm `fmincon.m` was used to minimise the objective function.

4. Results

4.4.1 Stiffness

The relaxation data for the hysteresis loop equation and the sine curve fit are compared in figure 4.10. Both methods showed some scatter, but the trend is clear.

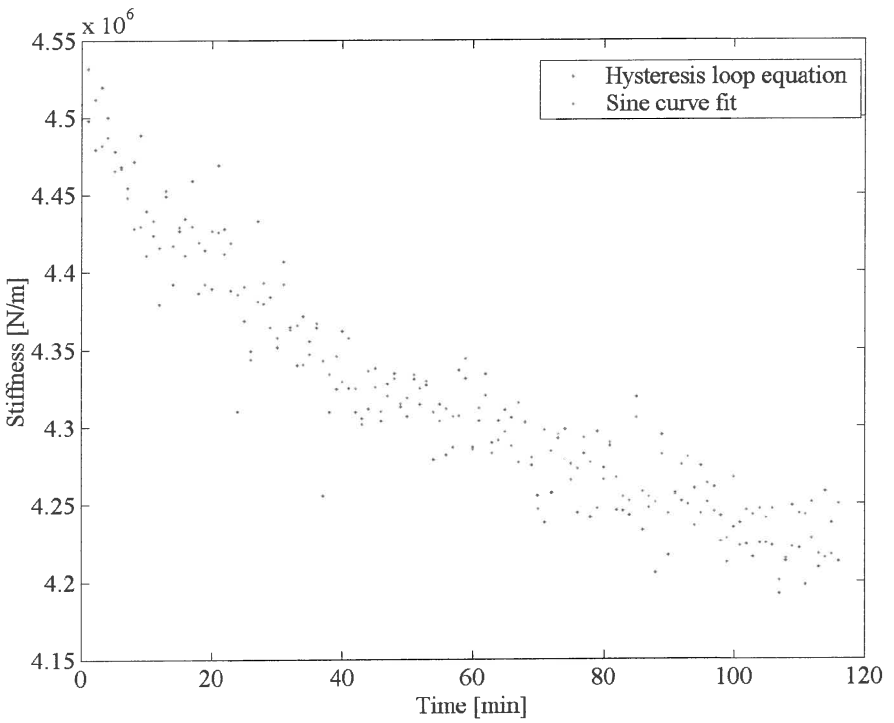

Figure 4.10 Stiffness compared (35 Hz)

In figure 4.7 an example of a relaxation curve fit was shown. Not all these curve fits were successful due to excessive scatter in the data (refer to appendix G). An average of the successful fits were used to determine the initial and stable values for the stiffness at the measured frequencies. The amount of relaxation that occurred was between 1 and 9%. This drift in stiffness will result in a change in the isolation frequency. In practice, some form of compensation will be necessary. These values are shown in figure 4.11 together with the stiffness determined from the sine sweep.

Table 4.1 Comparison of straight-line curve fits in figure 4.11 (55 Shore A spring)

Stiffness		Slope [$\times 10^3$]	Ordinate [$\times 10^6$]
Initial stiffness	k_0	8.88	2.74
Stable stiffness	k_∞	7.97	2.69
Sine sweep	k_s	11.36	2.48

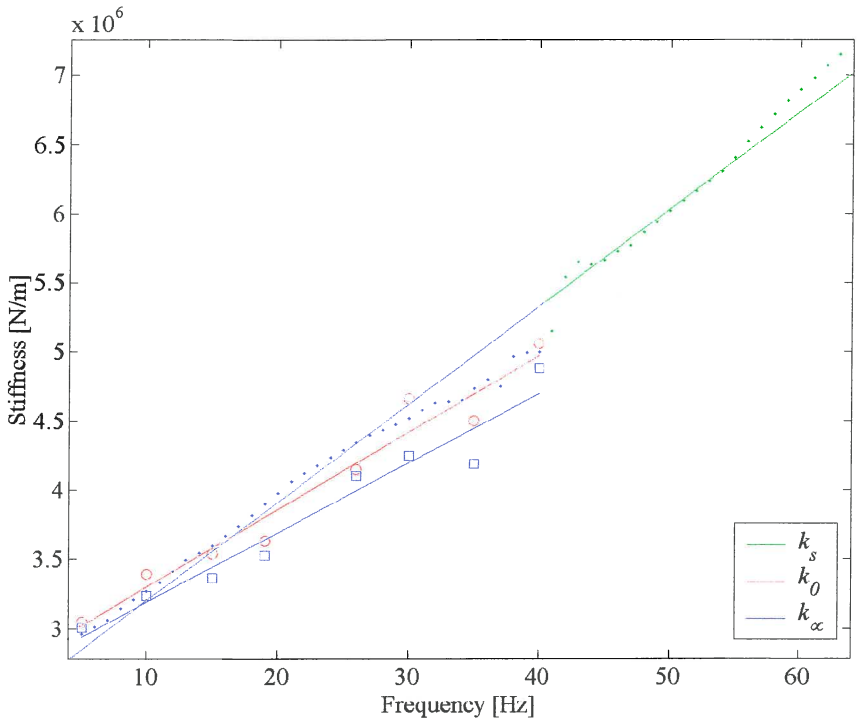

Figure 4.11 The stiffness of the 55 Shore A spring calculated with the sine sweep method (green) and the initial (red) and stable (blue) stiffness calculated with the constant frequency excitation method

The results of the two methods differ slightly. The sine sweep and initial stiffness data below 40 Hz showed excellent correlation. The sine sweep method at the 1 Hz per second sweep rate is therefore deemed to be adequate for the calculation of the initial spring stiffness.

The relaxation test was very time consuming and was not repeated for the 35 Shore A spring. Instead 10 seconds of time data was sampled at 1000 Hz from 10 to 55 Hz and was used to calculate the stiffness using the constant frequency excitation methods. The transient run-up and run-down sections of the data were ignored and only the steady state portion was used for the calculation. The curve fits are compared in figure 4.12. The spring was approximately 40% softer than the 55 Shore A spring at 0 Hz while the slope was ±20% less. 35 Shore A is the softest polyurethane that was available and this represents the lowest stiffness value achievable using this material and geometry.

Table 4.2 Comparison of straight-line curve fits in figure 4.12 (35 Shore A spring)

Stiffness		Slope [$\times 10^3$]	Ordinate [$\times 10^6$]
Initial stiffness	k_0	7.29	1.62
Sine sweep	k_s	6.74	1.72

The static stiffness of the 35 Shore A spring was 1.28×10^6 N/m

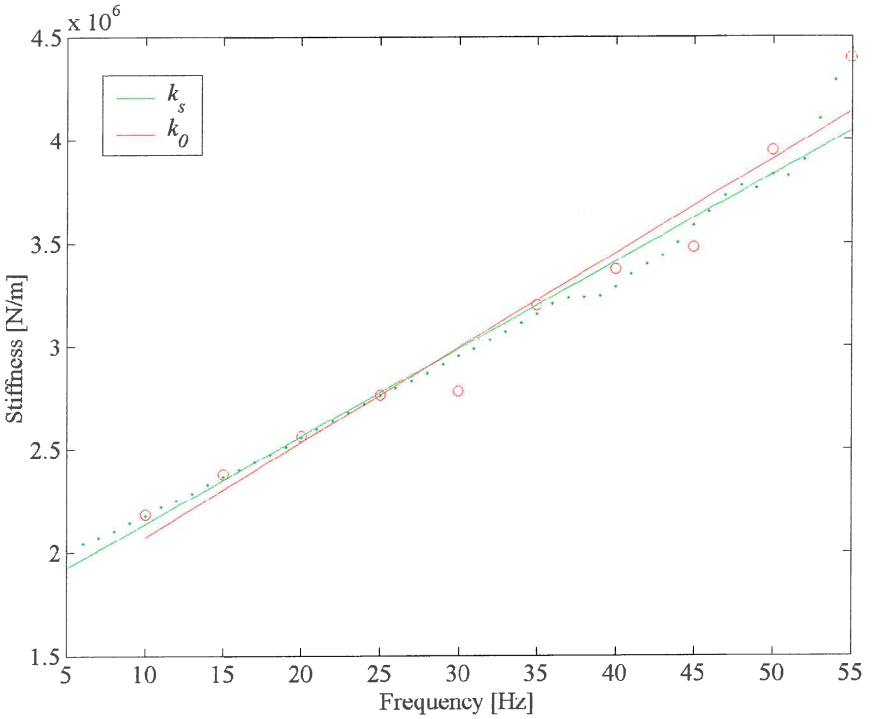

Figure 4.12 The stiffness of the 35 Shore A spring calculated with the sine sweep method (green) and the initial stiffness calculated with the constant frequency excitation method (red)

4.4.2 Loss factor

The results for the loss factor were less successful than for stiffness. Although the methods showed good agreement, admittedly with some scatter, it was generally higher than expected (figure 4.13). It is concluded that the phase angle measurement did not accurately represent the material but was influenced by the absorber assembly. A 40 mm cube of the same material was tested (figure 4.14) and the loss factor was closer to the 0.1 that was expected from published values by DuPont for Hylene®PPDI (a similar polyurethane) and the 60 shore A results measured at the University of Pretoria. The tests did show that the loss factor was not a function of frequency. The loss factor did also not show any relaxation as the stiffness did as can be seen in figure 4.15 which shows a typical curve fit.

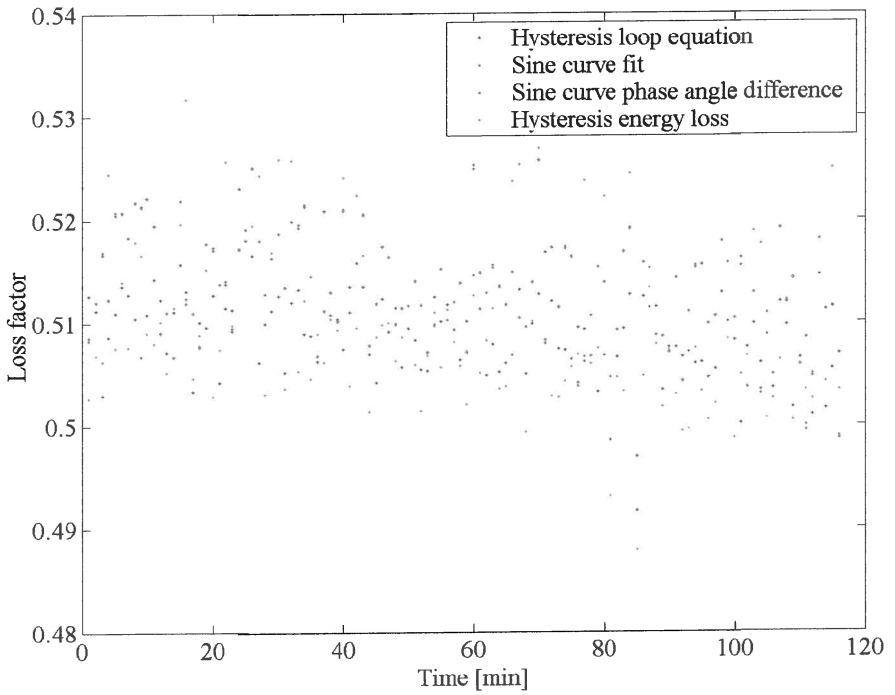

Figure 4.13 Comparison of the loss factor using four methods (35 Hz)

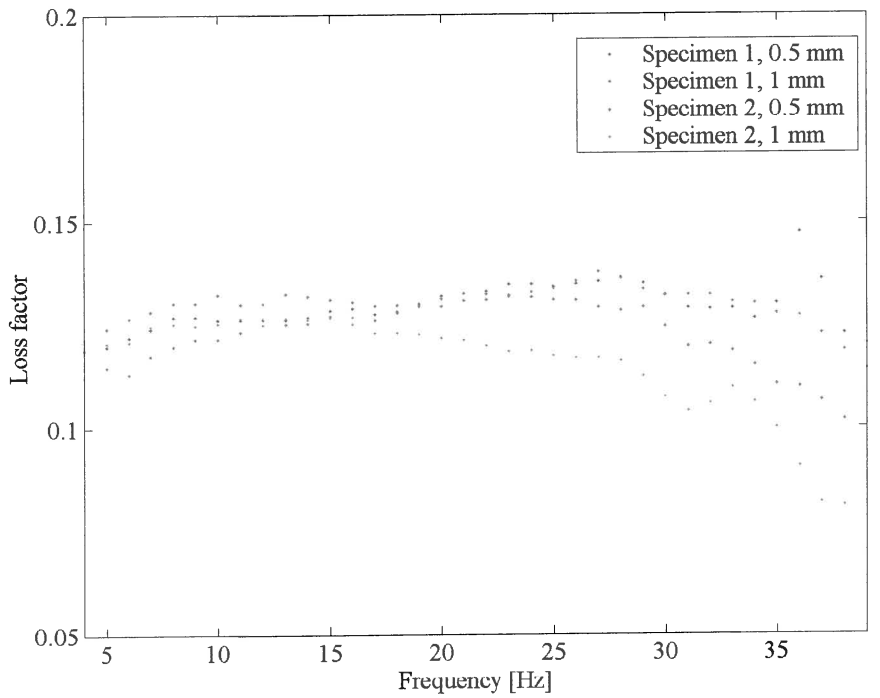

Figure 4.14 The loss factor for 2 cubic specimens at 0.5 mm and 1 mm displacements

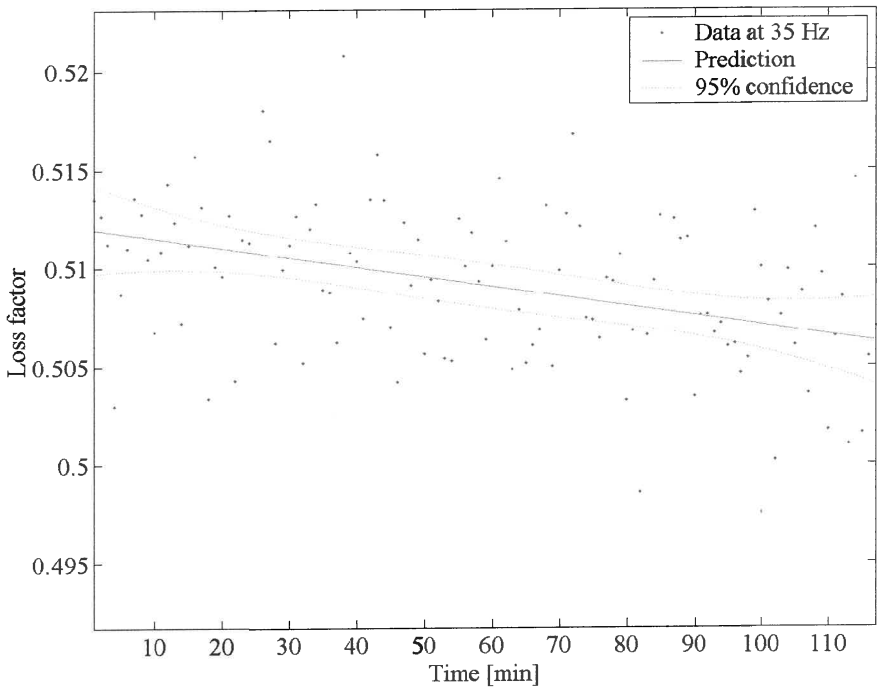

Figure 4.15 An unsuccessful curve fit of the loss factor for the absorber

4.4.3 Transmissibility

The transmissibility was measured with and without the absorber fluid to highlight the dramatic reduction in the force transmitted (figures 4.16 and 4.17). As expected the 35 Shore A spring had better isolation and a lower isolation frequency. The characteristics are shown in table 4.3

Table 4.3 Absorber characteristics

Spring hardness [Shore A]		Frequency [Hz]	$\lvert T_r \rvert$
55	Maximum response	39	2.07
	Isolation	49	0.45
35	Maximum response	33	1.77
	Isolation	42	0.16

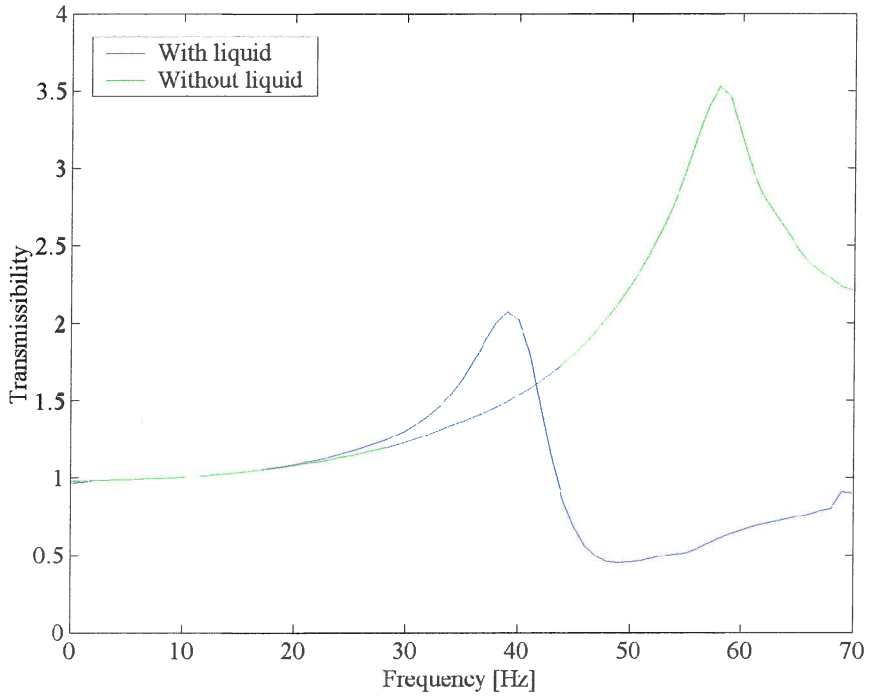

Figure 4.16 Comparison of the transmissibility for the 55 Shore A spring before and after the addition of the absorber liquid

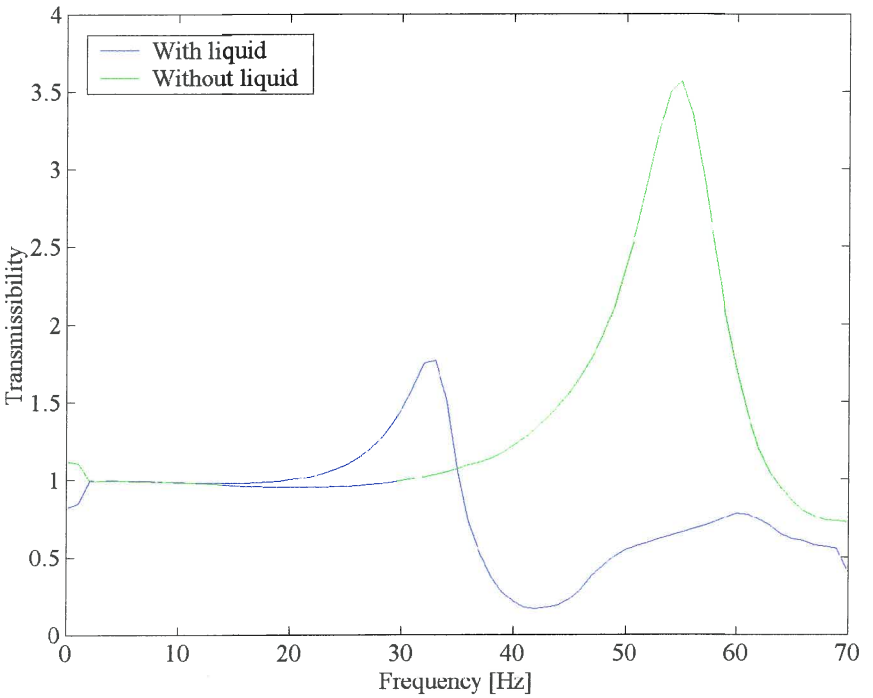

Figure 4.17 Comparison of the transmissibility for the 35 Shore A spring before and after the addition of the absorber liquid

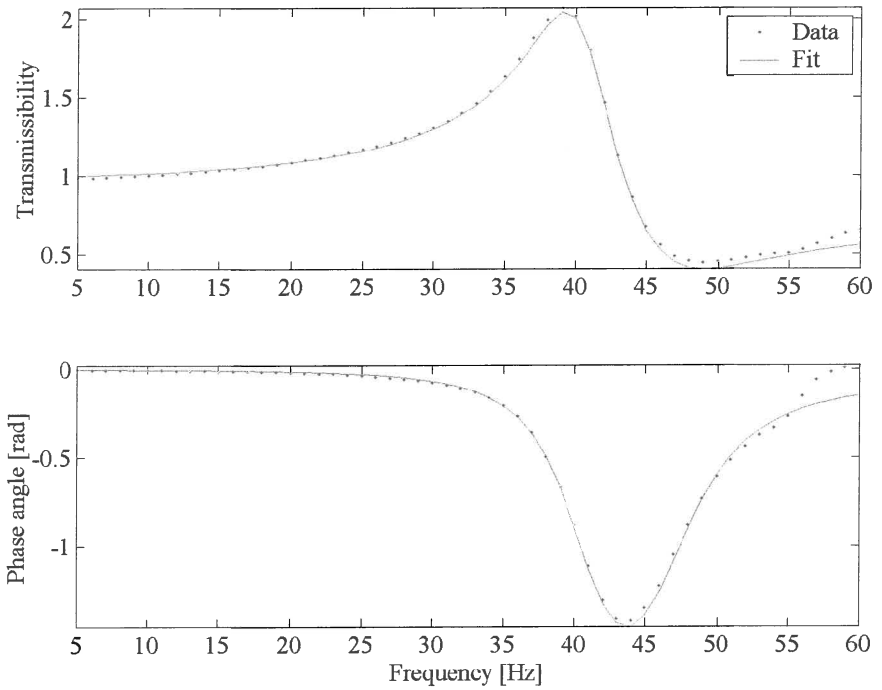

Figure 4.18 The 55 Shore A spring curve fit with $\eta = 0.1$ $m = 15$

Figure 4.18 shows the fit obtained using equation 4.36. The values obtained for the stiffness and damping were:

$$k_t(\omega) = 0.43 \times 10^4 \omega + 2.88 \times 10^6 \quad \textbf{(4.37)}$$

$$c_t(\omega) = 2.23\omega \quad \textbf{(4.38)}$$

The objective function could not be fitted successfully the 35 shore A spring's transmissibility data.

4.5 Conclusion

The methods used to characterise the absorber are in good agreement and it can be concluded that they are sound. The quality of the measured data was in some cases insufficient to obtain good fits of theoretical predictions. Halwes (1980) concluded that the properties of the elastomer could not economically be controlled to within ±10% of the target value. This study reiterated that the major obstacle for mass production of these absorbers would be the type of elastomer used. In practice changes to the port diameter after the manufacture of the spring will be necessary. Halwes did this by specifying the port diameter at the maximum stiffness expected. The spring stiffness was measured after manufacture and the port was reamed to compensate if the spring rate was less.

The transmissibility data clearly shows that the absorber can reduce the force transmitted by a single degree-of-freedom system significantly. The 35 Shore A spring reduced the isolation frequency by 7 Hz. The measurement techniques must be improved if accurate parameter extraction is desired.

CHAPTER 5

Design study

5.1 Introduction

In this chapter a vibration absorber will be designed for a screen application. The design methodology described in chapter 3 will be used, but in this case the isolation frequency will be 12.5 Hz. The chosen screen was designed for a sand washing plant. First the single degree-of-freedom screen model will be analysed. Then an absorber will be added. The effect will be discussed. Next a two degree-of-freedom screen model will be designed according to the SDRC guidelines given in chapter 1 (Riddle *et al.*, 1984). An absorber will then be added between the sub-frame and the ground to illustrate the improvement possible. To simplify the comparison, hysteretic damping will be assumed for both the screen and the absorber. The screen is fitted on steel coil springs with a loss factor of 0.01. It is further assumed that the combined viscous and material damping of the absorber can be represented by a loss factor of 0.1.

Finally the study will be concluded with recommendations for the design of absorbers for screens.

5.2 Single degree-of-freedom screens

5.2.1 Screen

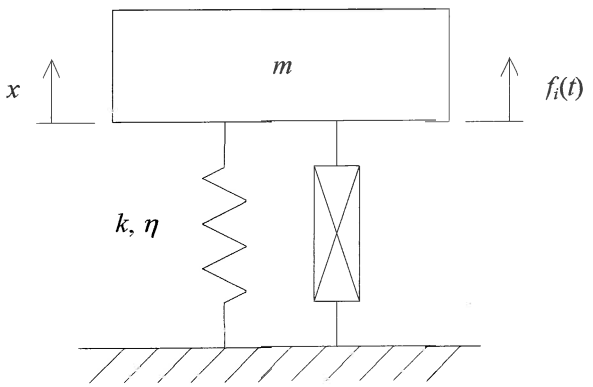

Figure 5.1 A single degree-of-freedom screen

According to the manufacturer two rotating eccentric mass excitation motors transfer 27 000 kg of force to the screen. The motors rotate at 750 rpm. The spring rate is given as 30.4 kg/mm and there are 4 springs on each corner. The screen has a 2-second run-up time, which is too short for any problematic transient response amplification. Run-down can take as long as 2 minutes and damping can therefore become important to reduce the response at resonance.

Table 5.1 Physical properties of the screen

Mass [kg]	m	13×10^3
Force amplitude[1] [N]	F_i	264.87×10^3
Stiffness[2] [N/m]	k	4.77×10^6
Spring loss factor	η	0.01
Operating speed [Hz]	f	12.5

[1] 27000×9.81, [2] $4\times4\times30.4\times10^3\times9.81$

Table 5.2 Operating characteristics the screen

Natural frequency [Hz]	f_n	3.05
Frequency ratio	$\frac{\omega}{\omega_n}$	4.1
Stroke amplitude [mm]	X	3.5
Acceleration [m/s^2]	$\omega^2 X$	2.21g
Static deflection [mm]	x_s	26.7
Dynamic force transmitted [N]	F_o	16758.55
Transmissibility [%]	$\lvert T_r \rvert$	6.327

Figures 5.2 and 5.3 show the response and force transmissibility of this design. The low damping of the spring can cause high amplitudes at the natural frequency during run-down.

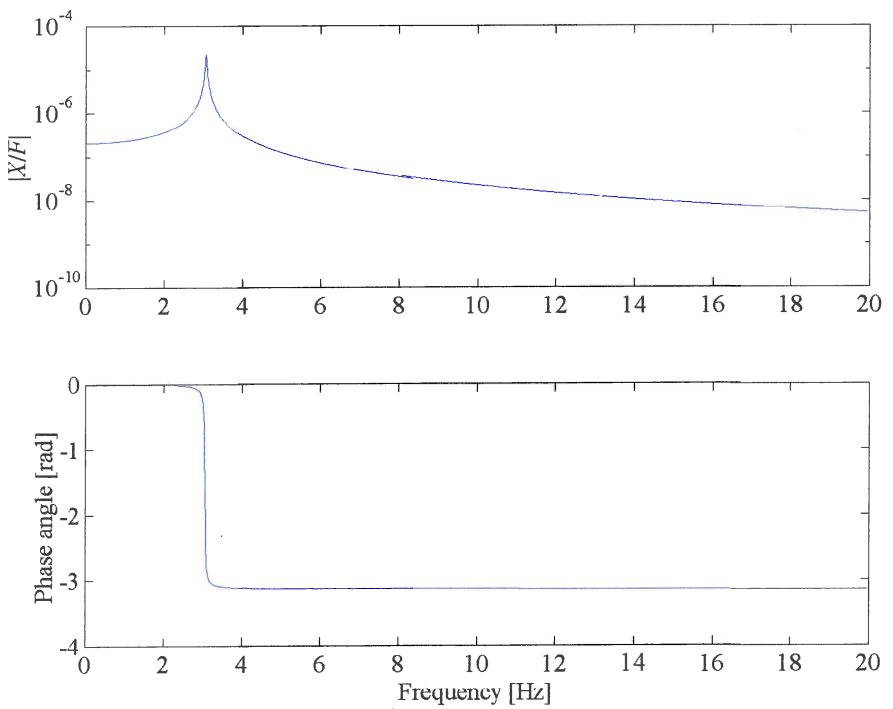

Figure 5.2 Response of the screen

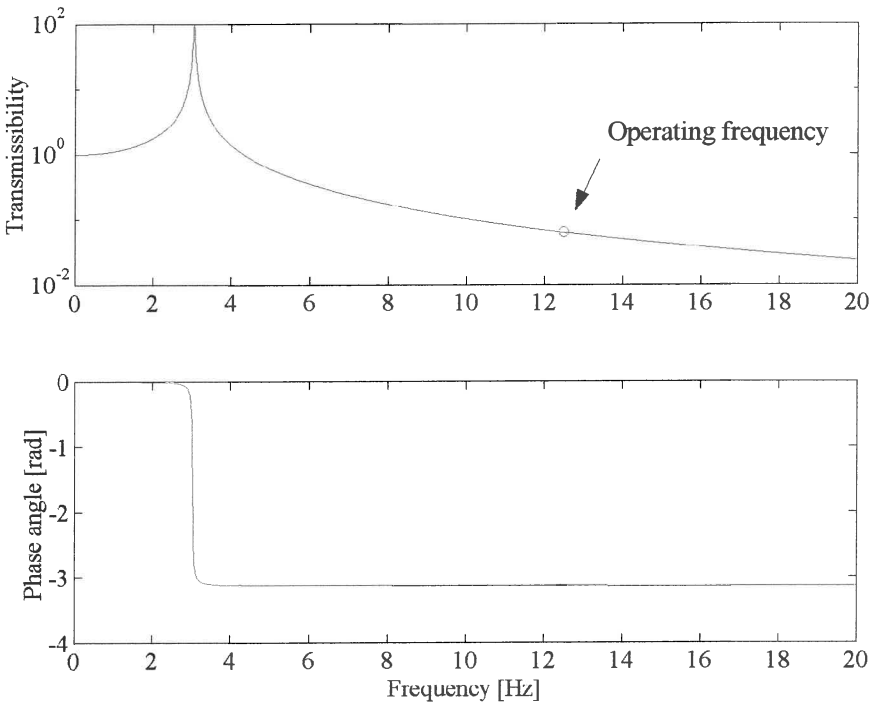

Figure 5.3 Transmissibility of the screen

The design of the screen was done in accordance with current practice and therefore the operating frequency is 4 times larger than resonance. Although the transmissibility is only 6%, a total of 16.8 kN is still transmitted to the support structure.

5.2.2 Screen with an absorber

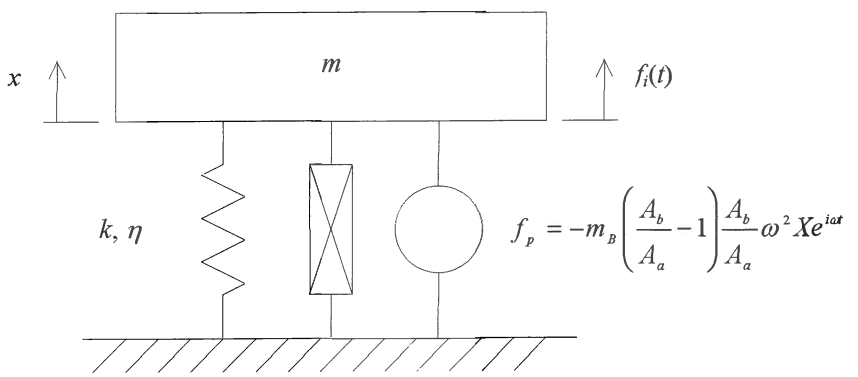

Figure 5.4 Screen fitted with a LIVE absorber

The force f_p in figure 5.4 is the force generated by the absorber (equation 2.59).

In chapter 3 it was shown that the best isolation would be achieved when the stiffness of the spring is as low as possible. For the screen application low stiffness would result in high static deflection. For a steel spring the static deflection will only become problematic at 125 mm (chapter 1). The LIVE absorber cannot accommodate high static deflection easily. The first problem is the available space, but more importantly the polyurethane's ultimate tensile strength must not be exceeded. Both these problems can be overcome if the static deflection is reasonably low. The experimental absorber was built to deflect only 10 mm, but with a softer material and a different geometry it will be possible to attain larger deflections. It is thought that a 20 mm deflection can still be accommodated in a design. The results are therefore listed for the best possible 20 mm deflection as well as for 26.7 mm in order to compare it to the previous result for the screen. The absorber was designed in accordance with the guidelines in chapter 3. The mass, force and forcing frequency is the same as before.

Table 5.3 Physical properties of the system

		$x_s = 20$	$x_s = 26.7$
Mass [kg]	m	13×10^3	13×10^3
Force amplitude [N]	F_i	264.87×10^3	264.87×10^3
Stiffness [N/m]	k	6.38×10^6	4.78×10^6
Spring loss factor	η	0.1	0.1
Operating speed [Hz]	f	12.5	12.5
Area ratio	A_r	36	36
Reservoir diameter [mm]	d_b	180	180
Absorber liquid density [kg/m^3]	ρ	1000	1000

Table 5.4 Design results and operating characteristics of the system

		$x_s = 20$	$x_s = 26.7$
Port length [mm]	l	290	217
Port diameter [mm]	d_a	30	30
Natural frequency [Hz]	f_n	3.52	3.05
Frequency ratio	$\frac{\omega}{\omega_n}$	3.55	4.1
Stroke amplitude [mm]	X	3.64	3.64
Acceleration [m/s^2]	$\omega^2 X$	2.29g	2.29g
Dynamic force transmitted [N]	F_o	2322	1738
Transmissibility [%]	$\lvert T_r \rvert$	0.797	0.597

At a static deflection of 20 mm the force transmitted to the support structure is 7.2 times less than a screen fitted with conventional isolators. Figures 5.5 and 5.6 show the response and transmissibility for the design.

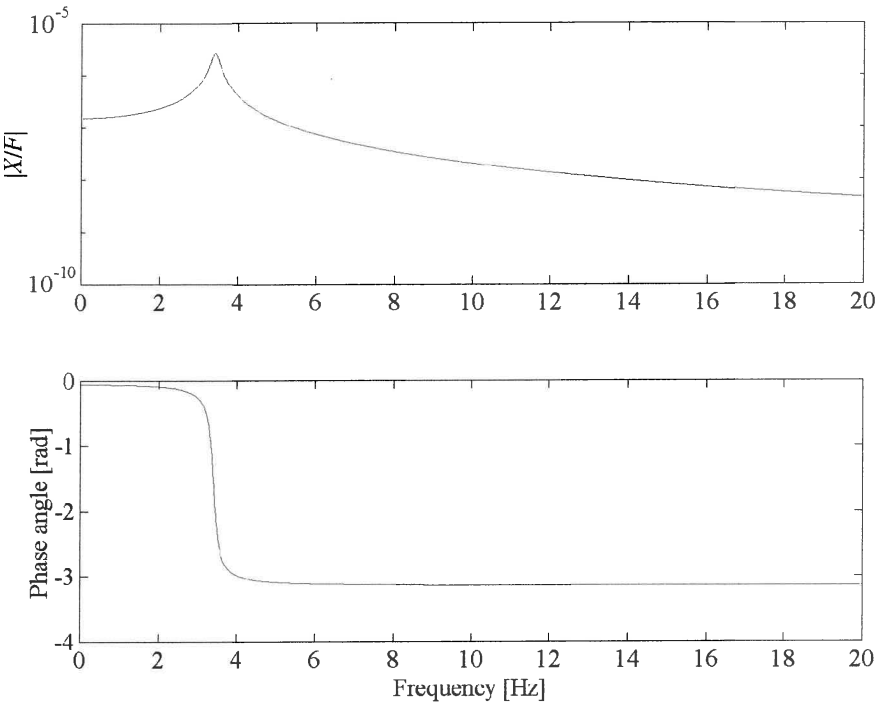

Figure 5.5 Response of the screen with an absorber fitted ($x_s = 20$ mm)

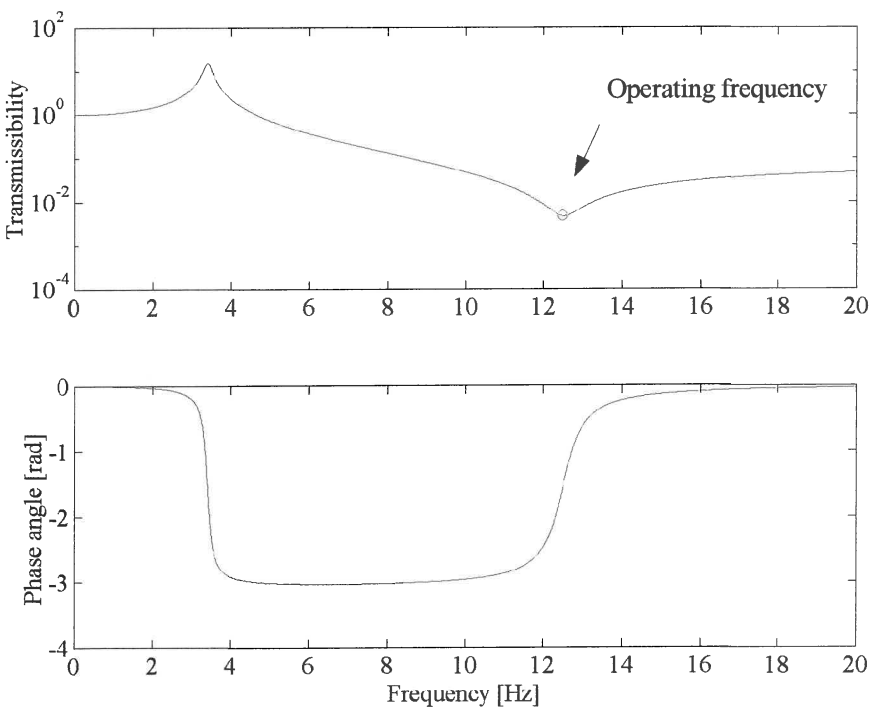

Figure 5.6 Transmissibility of a screen with an absorber fitted ($x_s = 20$ mm)

5.3 Two degree-of-freedom screens

5.3.1 Screen with a sub-frame

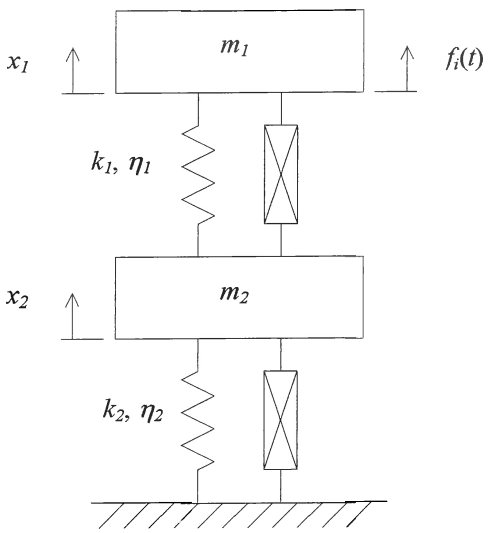

Figure 5.7 Screen with a sub-frame

Table 5.5 Physical properties of the screen with a sub-frame

		$x_2 = 20$ mm	$x_2 = 37.5$ mm
Screen mass [kg]	m_1	13×10^3	13×10^3
Sub-frame mass [kg]	m_2	16.9×10^3	16.9×10^3
Mass ratio	$\frac{m_2}{m_1}$	1.3	1.3
Screen stiffness [N/m]	k_1	4.77×10^6	4.77×10^6
Sub-frame stiffness [N/m]	k_2	14.67×10^6	7.82×10^6
Loss factor of the screen spring	n_1	0.01	0.01
Loss factor of the absorber spring	n_2	0.1	0.1
Static deflection of the screen [mm]	x_1	46.7	64.22
Stiffness ratio	$\frac{k_2}{k_1}$	3.07	1.64

The screen mass, stiffness, excitation force and frequency is the same as before. The sub-frame mass is 1.3 times the screen mass (chapter 1). The sub-frame stiffness was calculated using the permissible static deflection of a rubber spring, which was given as 15% of its free length (37.5 mm for a 250 mm spring) by Riddle *et al.* (1984).

Table 5.6 Operating characteristics of the screen with a sub-frame

		$x_2 = 20$ mm	$x_2 = 37.5$ mm
Natural frequencies [Hz]	f_1	2.53	2.15
	f_2	5.66	4.85
Frequency ratios	$\frac{\omega}{\omega_1}$	2.21	5.8
	$\frac{\omega}{\omega_2}$	4.94	2.57
Static deflection of the screen [mm]	x_1	46.7	64.2
Dynamic force transmitted [N]	F_o	2922	1442
Stroke amplitude [mm]	X_1	3.52	3.52
	X_2	0.198	0.183
Acceleration [m/s^2]	$\omega^2 X_1$	2.216g	2.215g
Transmissibility [%]	$\lvert T_r \rvert$	1.1	0.544

It will still be possible to achieve low transmissibility without using the upper bound of 130% of the screen mass for the sub-frame mass. Figure 5.8 shows that the gain in isolation will be less at high mass ratios. A 50% mass ratio will therefore already provide good isolation while not adding too much weight to the assembly. Figures 5.9 to 5.11 show the response and transmissibility for a system with a sub-frame deflection of 37.5 mm.

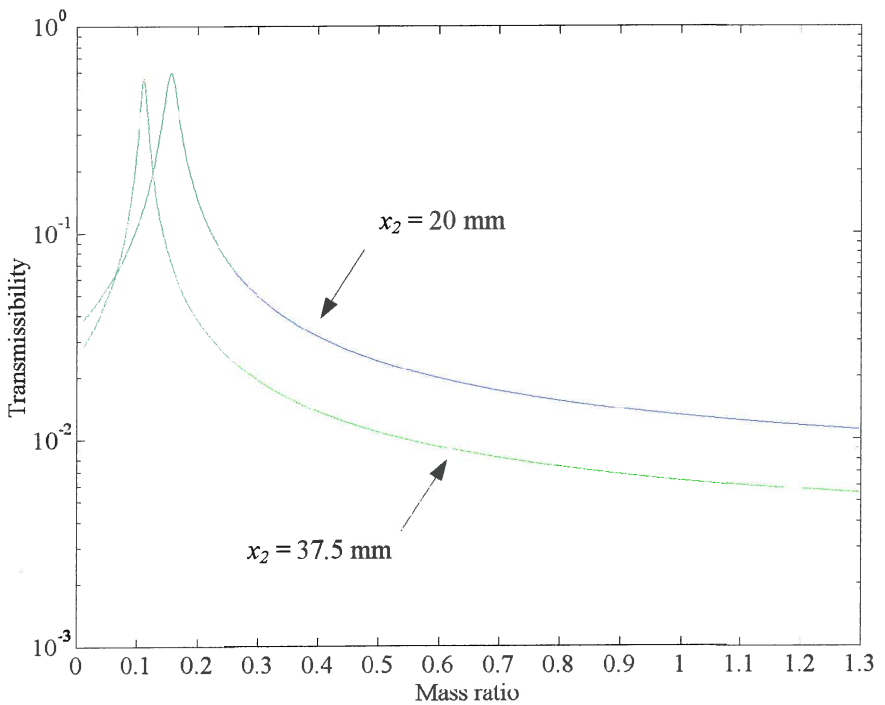

Figure 5.8 Transmissibility at 12.5 Hz as a function of mass ratio

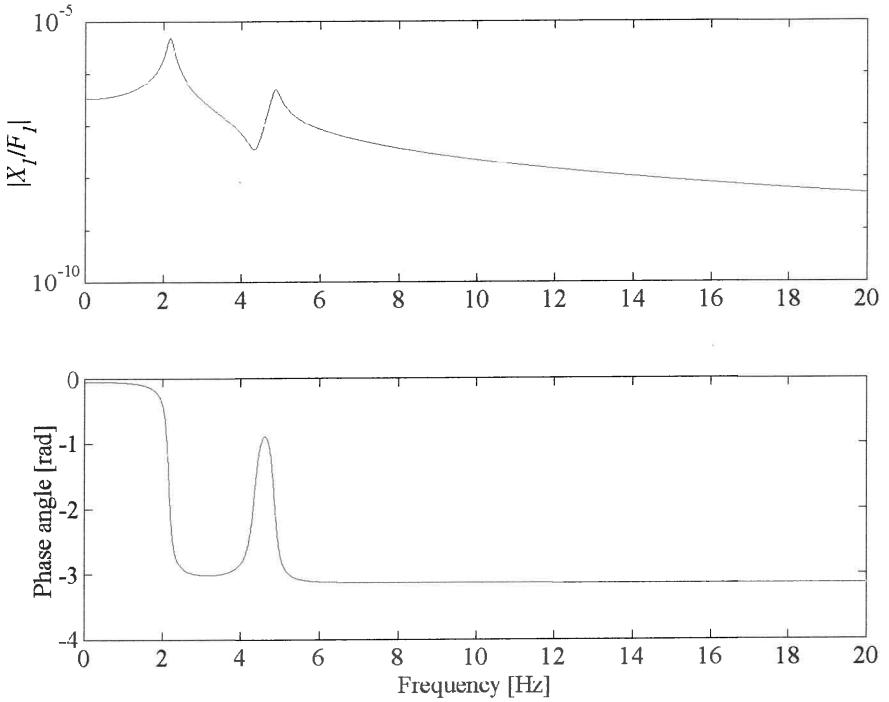

Figure 5.9 Response of the screen to the excitation force (x_2 = 37.5 mm)

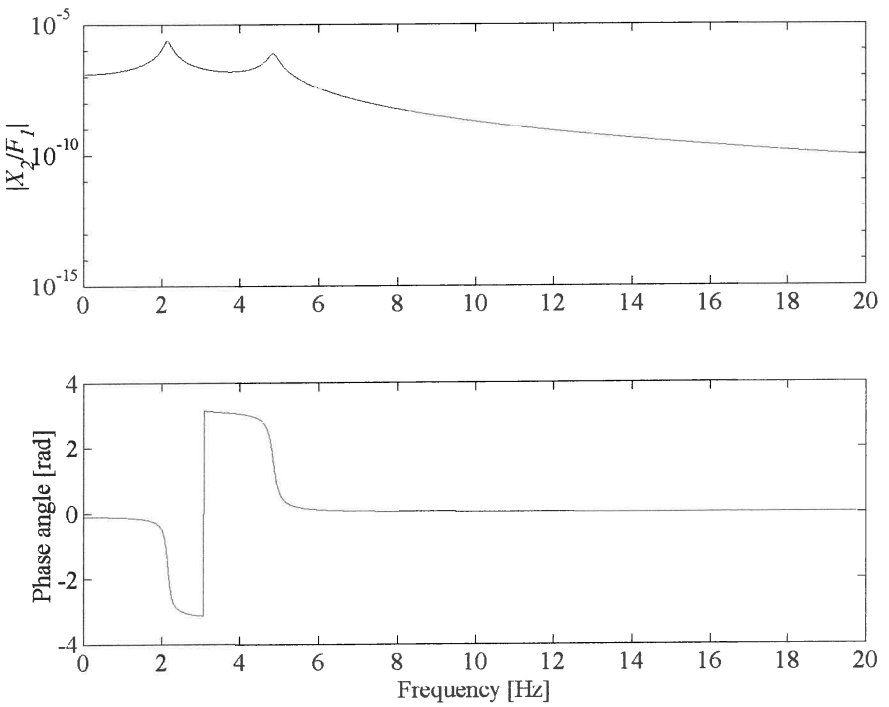

Figure 5.10 Response of the sub-frame to the excitation force (x_2 = 37.5 mm)

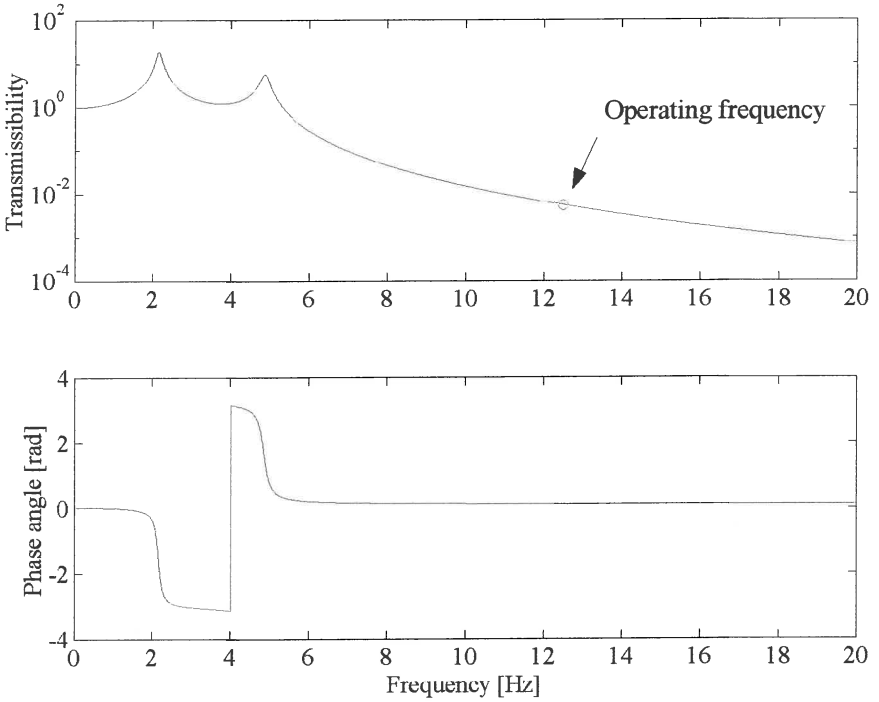

Figure 5.11 Transmissibility of a screen with a sub-frame (x_2 = 37.5 mm)

5.3.2 Screen with a sub-frame and an absorber

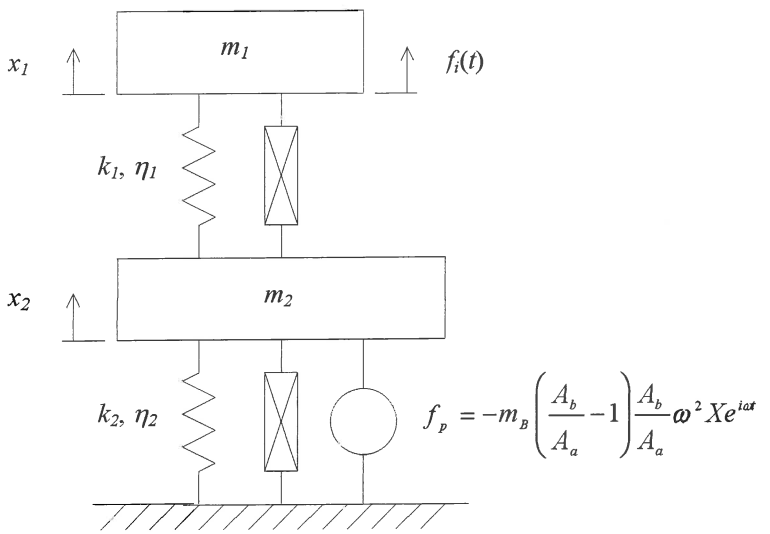

Figure 5.12 Screen with a sub-frame and a LIVE absorber

The force f_p in figure 5.12 is the force generated by the absorber.

Table 5.7 Physical properties of the system

		$x_2 = 20$ mm	$x_2 = 37.5$ mm
Screen mass [kg]	m_1	13×10^3	13×10^3
Secondary mass [kg]	m_2	1950	1950
Mass ratio	$\frac{m_2}{m_1}$	0.15	0.15
Screen stiffness [N/m]	k_1	4.77×10^6	4.77×10^6
Absorber stiffness [N/m]	k_2	7.33×10^6	3.91×10^6
Stiffness ratio	$\frac{k_2}{k_1}$	1.54	0.82
Loss factor of the screen spring	n_1	0.01	0.01
Loss factor of the absorber spring	n_2	0.1	0.1
Static deflection of the screen [mm]	x_1	46.7	64.22
Area ratio	A_r	36	36
Reservoir diameter [mm]	d_b	180	180
Absorber liquid density [kg/m^3]	ρ	1000	1000

Table 5.8 Design results and operating characteristics the system

		$x_2 = 20$ mm	$x_2 = 37.5$ mm
Port length	l	337	179
Port diameter	d_a	30	30
Natural frequencies [Hz]	f_1	2.33	1.99
	f_2	10.1	9.54
Frequency ratios	$\frac{\omega}{\omega_1}$	5.36	6.29
	$\frac{\omega}{\omega_2}$	1.23	1.31
Dynamic force transmitted [N]	F_o	1808	955
Stroke amplitude [mm]	X_1	3.67	3.67
	X_2	2.47	2.44
Acceleration [m/s^2]	$\omega^2 X_1$	2.3g	2.3g
Transmissibility [%]	$\lvert T_r \rvert$	0.679	0.36

In both these cases the response is lower than for a conventional sub-frame while only adding 15% of the screen mass to the assembly. The additional weight of m_2 will require higher absorber stiffness and therefore a longer port. A sub-frame with the same mass (15%) will have a transmissibility of 8%, which is even higher than a screen with conventional isolators. Figures 5.13 to 5.15 show the response and transmissibility of an absorber with a feasible 20 mm static deflection.

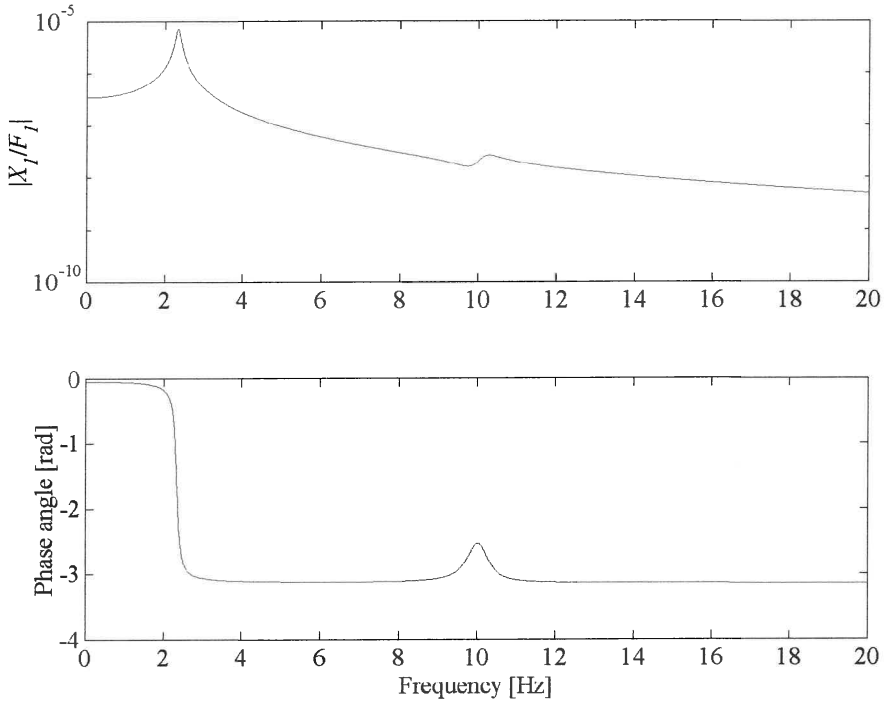

Figure 5.13 Response of the screen to the excitation force (x_2 = 20 mm)

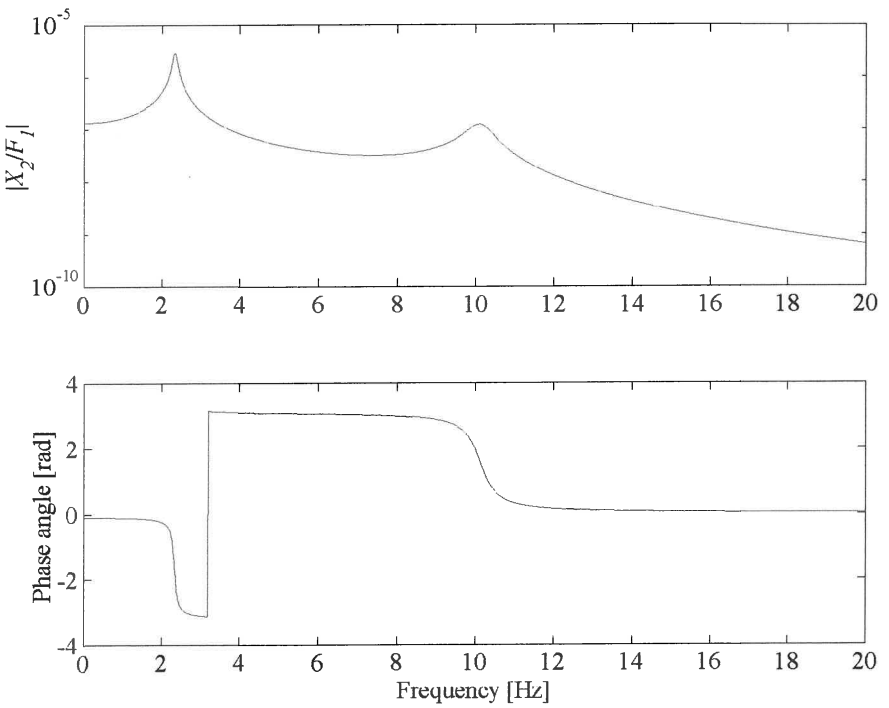

Figure 5.14 Response of the sub-frame to the excitation force (x_2 = 20 mm)

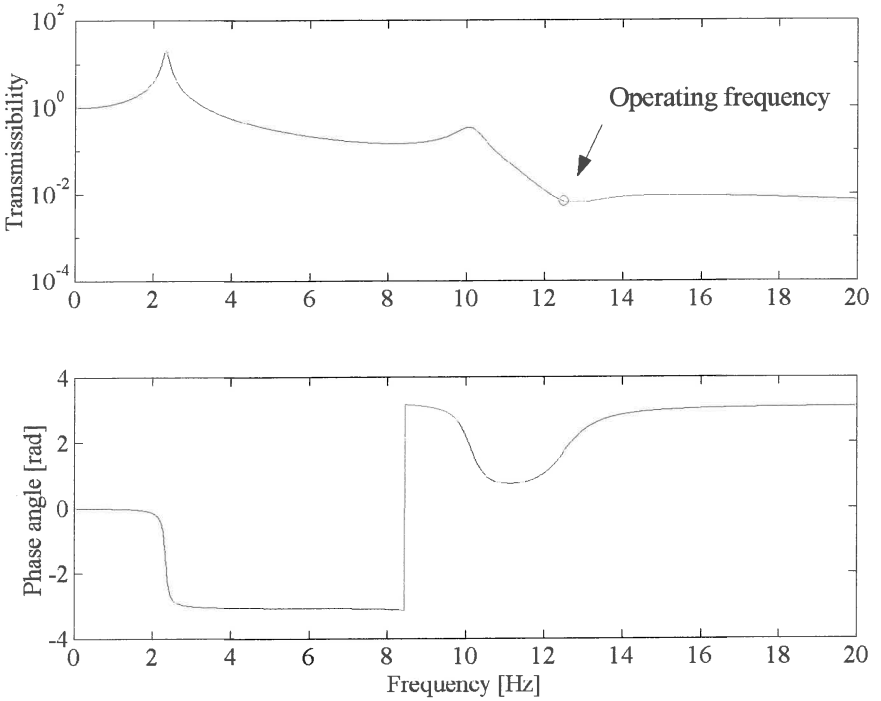

Figure 5.15 Transmissibility of the screen with an absorber fitted to the sub-frame (x_2 = 20 mm)

5.4 Conclusions

From the analysis presented in this chapter the following conclusions can be drawn:

- The single degree of freedom screen fitted with an absorber will offer the most benefit since good isolation can be achieved and there is no addition of mass to the system.
- The sub-frame fitted with an absorber will reduce the mass ratio for this type of design significantly. For applications where more isolation is needed than achievable with the single degree-of-freedom system this method is recommended.
- The damping of the absorber should be as low as possible.
- It is important that the absorber spring should be as soft as possible. It seems as if it will be difficult to design such a spring, but the anticipated problems can probably be overcome.
- The acceleration of the screen, which is the most important parameter affecting its operation, is not altered significantly using any of these methods.

Overall the liquid inertia vibration absorber has shown enough advantages over existing isolation methods for screens to warrant further development.

CHAPTER 6

Conclusions

Even though many industrial machines depend on vibration or oscillatory motion for their operation, such vibration may cause serious problems relating to their supporting structures, for instance fatigue damage. This study investigated how liquid inertia vibration absorbers can be used to attenuate the forces transmitted by vibrating screens.

In chapter 1 it was established that although vibration is essential to the proper working of a vibrating screen, the forces resulting from this operation are undesirable. Methods for the control of the vibration were presented. The current methods have certain drawbacks, which can be overcome with the use of vibration absorbers. Pendulum, hydraulic and liquid inertia absorbers were presented as possible solutions for screen isolation. The main advantage of these vibration absorbers is the excellent isolation that can be achieved with only a fraction of the weight increase associated with a sub-frame. The liquid inertia vibration eliminator (LIVE) absorber showed the most promise for this application because of its simple design and low maintenance requirements.

Next a detailed mathematical analysis of the LIVE system was presented. The effect of each variable on the system response was discussed. Arbitrary port inlet/outlet geometry was taken into account using Lagrange's equations. The viscous damping plays a very important role in the amount of isolation that can be achieved. The damping was analysed using CFD and methods for reduction were suggested. The lowest transmissibility resulted when the natural frequency was much smaller than the isolation frequency. This was found when the system mass is much larger than the absorber mass.

Chapter 3 showed how to design the LIVE absorber. Two methods for the design were discussed. The optimisation approach is recommended due to its ease of use. The numerous practical considerations for the design of these absorbers were highlighted. The possible absorber liquids were listed. Water was chosen as absorber liquid on cost and safety grounds. Considerable effort was made to predict the absorber stiffness. The summation of flat plate springs in series, representing the exact geometry, was found to be of adequate accuracy if compared to finite element results. The damping for the design was calculated and the addition of conical inlets/outlets reduced the amount of damping considerably. The viscous damping is a linear function of frequency. The inlets/outlets reduced the effective absorber mass and this reduction was compensated for by increasing the port length.

Chapter 4 discussed the methods used for the estimation of the spring stiffness and loss factor as well as the absorber transmissibility. The results showed that the stiffness was a function of time and that the spring rate could be described by an exponential decay function. The constant frequency excitation methods showed excellent agreement with sine sweep methods. The stiffness of the absorber was found to be a linear function of frequency. The absorber stiffness cannot be accurately predicted and in practice alteration to the port geometry will be

necessary after manufacture and testing of the spring. The loss factor for polyurethane was 0.12, which is considered to be low and did not vary appreciably with frequency. Elastomers with lower loss factors do exist although manufacturing these will be more difficult. Two springs were fitted to the absorber and both showed excellent transmissibility results. The softer spring had a transmissibility of 16% at 42 Hz, which was lower than the 55 Shore A as predicted. Softer springs and less damping can improve these results.

Chapter 5 presented and analysed two possible configurations showing how an absorber can be added to a screen. First the absorber was fitted to a screen and then to a sub-frame. The addition of a realistic absorber showed that the transmissibility could be reduced significantly. The absorber fitted directly to the screen showed the most promise since the addition of weight was negligible, while reducing the transmissibility with a factor of 7.2. Fitting the absorber to the sub-frame gave similar transmissibility results to that of a screen fitted with a sub-frame only, but the mass ratio was only 15%.

This study laid a sound mathematical base for the design of LIVE type vibration absorbers. Future work should include:

- The optimisation of the port geometry for the minimum amount of the flow damping. This should be done using CFD and an optimisation algorithm.
- A major design challenge remains the active control of the isolation frequency. Although some work has been done in this area, a cost-effective method hasn't been proposed yet.
- The bulk of any future work should be experimental testing of various absorber designs and isolation frequency control methods.
- An investigation of cost effective manufacturing of the absorber and specifically of the elastomeric spring should be undertaken.
- Alternative castable, low loss factor elastomers must be found.
- Physical configurations of absorbers in screen suspension systems must be investigated.
- A detailed cost comparison between conventional isolation systems and vibration absorbers must be made.

References

Agnes, G.S. 1997. Performance of nonlinear mechanical, resonant-shunted piezoelectric, and electronic vibration absorbers for multi-degree-of-freedom structures. *PhD Thesis*, Virginia Polytechnic Institute and State University.

Braun, D. 1980. Development of anti-resonance force isolators for helicopter vibration reduction, *Sixth European rotorcraft and powered lift aircraft forum*, Bristol, England, September 16-19.

Braun, D. 1988. Vibration isolator particularly of the anti-resonance type. *U.S. Patent 4,781,363.*

Brock, J.E. 1946. A note on the damped vibration absorber. *Transactions of the American Society of Mechanical Engineers A*, 284.

Davey, A.B., Payne, A.R. 1964. *Rubber in engineering practice*. London: Applied Science Publishers.

Den Hartog, J.P. 1956. *Mechanical vibrations*, Fourth Edition, New-York: McGraw-Hill.

Desanghere, G. & Vansevenant, E. 1991. An adaptive tuned vibration absorber, *Proceedings of the 10th IMAC*, p.1347-1352.

Desjardins, R.A. & Hooper W.E. 1980. Antiresonant rotor isolation for vibration reduction, *Journal of the American Helicopter Society*, Vol. 25, no. 3, July, p.46-55.

Desjardins, R.A. & Hooper, W.E. 1976. Rotor isolation of the hingeless rotor B0-105 and YUH-61A helicopters, *2nd European Rotorcraft and Powered Lift Aircraft Forum*, Buckeburg, F.R.G., September.

Desjardins, R.A., Ellis, C.W. & Sankewitsch, V. 1978. Vibration isolation system. *U.S. patent no. 4,088,042.*

Desjardins, R.A., & Sankewitsch, V. 1982. Vibration isolation system. *U.S. patent no. 4,311,213.*

Dumbaugh, G.D. 1984. The evolution of the first "universal" vibratory drive system for moving and processing bulk solid materials, *Bulk Solids Handling*, vol. 4, no. 1, March, p.125-140.

Ewins, D.J. 1995. *Modal testing: theory and practice*, Baldock: Research Studies Press.

Fischer, P., Karrer, H., Kamla, T. 1998. Tuning of vibration absorbers under wide band excitation by stochastic dynamic analysis, International conference on noise and vibration engineering, September 16-18.

Flannely, W.G. 1966. The dynamic anti-resonant vibration isolator. *22nd Annual AHS National Forum*, Washington, p.152-158.

Frahm, H. 1909. Device for damping vibrations of bodies, *U.S. Patent no. 989958.*

Franchek, M.A., Ryan, M.W. & Bernhard, R.J. 1995, Adaptive passive vibration control, *Journal of Sound and Vibration*, 189(5), p.565-585.

Frolov, K., Goncharevich, I. 1991. *Vibration technology theory and practice*. Boca Raton: CRC Press.

Gaffey, T.M. & Balke, R.W. 1976. Isolation of rotor induced vibration with the Bell focal pylon-nodal beam system. *Society of Automotive Engineers*. p.1-10.

Garibaldi, L. & Onah, H.N. 1996. *Viscoelastic material damping technology*, Torino: Becchis Osiride.

Gere, J.M. & Tomoshenko, S.P. 1991, *Mechanics of materials*. London: Chapman & Hall.

Greenway, M. 1983. Vibration in screening plants: designing out maintenance, *Proceedings of the 1983 Maintenance Management Convention*, October 17-19.

Halwes, D.R. et al., 1980. *Vibration suppression system, U.S. patent no. 4,236,607.*

Halwes, D.R., 1981. Total main rotor isolation system analysis, Bell Helicopter Textron, *NASA Contractor Report No. 165667*. Langley Research Center, Hampton, Virginia, June.

Heyns, P.S. & Van Niekerk, J.L. 1997. Vibrating screen technology: An overview of vibration control methods. LGI Report no LGI97/075.

Igusa, T. & Xu, K. 1991. Vibration reduction characteristics of distributed tuned mass dampers, *Proceedings of the 4th International Conference on Structural Dynamics: Recent Advances*, Southampton, 15-18 July, p.596-605.

ISO 7626. *Methods for the experimental determination of mechanical mobility*.

Johnson, D.A. 1991. Optimal dynamic absorber for transients - Application to the motion of a robot arm, *Proceedings of the 9th IMAC*.

Korenev, B.G. & Reznikov L.M., 1993. *Dynamic vibration absorbers theory and technical applications*, West Sussex: Wiley.

Mackie, K., Marais, C. & Heyns, M. 1997. The dynamic characteristics of type AB Neidhart systems. *LGI report no. 97/038*.

Maia, N.M.M. & Júlio, M.M.S. (Editors) 1998. *Theoretical and experimental modal analysis*. Baldock: Research Studies Press.

Margolis, D.L. & Baker, D. 1992. The variable fulcrum isolator: A low power, nonlinear, vibration control component. *Transactions of the ASME*, March, Vol. 114, p.148-154.

Nashif, A.D., Jones, D.I.G., Henderson, J.P. 1985. *Vibration damping,* New York: John Wiley & Sons.

O'Leary, J.J. 1969. Reduction in the vibration of the CH-47C helicopter using a variable tuning vibration absorber, *Shock and vibration symposium*, December.

Olgac, N. & Holm-Hansen, B.T. 1993. Vibration absorbers utilizing only position measurements for time varying excitation frequencies. *ASME Symposium on Mechatronics*.

Patankar, S.V. 1980. *Numerical heat transfer and fluid flow*, New York: McGraw-Hill.

Rao S.S. 1990. *Mechanical vibrations*, 2nd Edition, New York: Addison Wesley.

Rice, H.J. 1987. Stable design of asymmetric non-linear vibration absorbers. *Proceedings of the 5th IMAC*. p.1474-1478.

Riddle, T., Bates, G. & Thomas, G. 1984. Summary report on the design on nine isolation system subframes systems, *Structural Dynamics Research Corporation*, Ohio: SDRC.

Rita, A.D., McGarvey, J.H., Jones, R. 1976. Helicopter rotor isolation utilizing the dynamic antiresonant vibration isolator, *32nd Annual AHS National Forum*, Washington, May.

Shaw C.T. 1992. *Using computational fluid dynamics*, Englewood Cliffs: Prentice Hall.

Smith, M.R. & Stamps, F.N. 1988. Vibration isolation system, *US patent no. 5,788,029.*

Tsai, H.-C. & Lin, G.-C. 1994. Explicit formulae for optimum absorber parameters for force excited and viscously damped systems, *Journal of Sound and Vibration,* 176(5), p.585-596.

White, F.M. 1991. *Viscous fluid flow*, 2nd Edition, McGraw-Hill.

White, F.M. 1988. *Fluid Mechanics*, 2nd Edition, McGraw-Hill.

APPENDIX A

Mathematical model of a single D.O.F vibration absorber

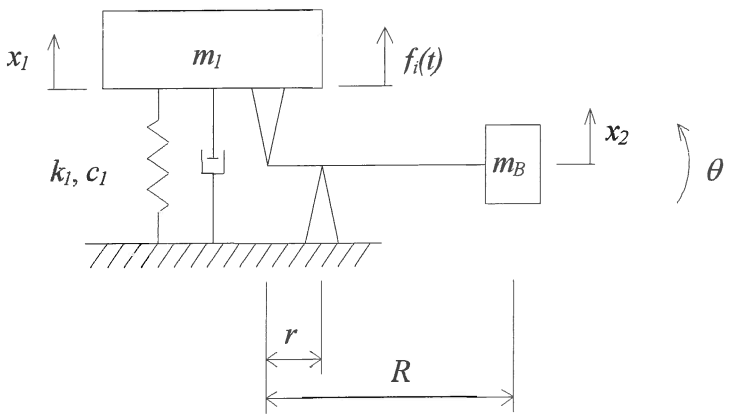

Figure A.1 A single D.O.F. vibration absorber system

The kinetic energy of the system in figure A.1 is given by equation A.1:

$$T = \frac{1}{2}\left(m_1\dot{x}_1^2 + m_B\dot{x}_2^2 + I_G\dot{\theta}^2\right) \qquad \textbf{(A.1)}$$

I_G is the moment of inertia of the mass m_B about its mass centre. The relation between x_3, θ, and x_2 are given by equations A.2 and A.3 (refer to figure A.2):

$$x_2 = \left(1 - \frac{R}{r}\right)x_1 \qquad \textbf{(A.2)}$$

$$\theta \approx -\frac{x_1}{r} \qquad \textbf{(A.3)}$$

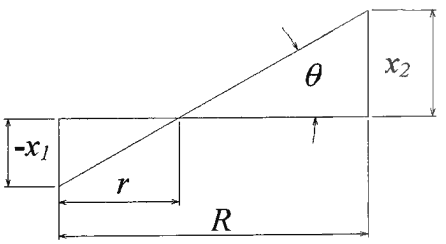

Figure A.2 Schematic of relationship between the variables

Substituting these relations in equation A.1 results in the following:

$$T = \frac{1}{2}\left(m_1 + \left(1 - \frac{R}{r}\right)^2 m_B + \frac{I_G}{r^2}\right)\dot{x}_1^2 \qquad \textbf{(A.4)}$$

From equation A.4 the kinetic term in the Lagrange's equations can be derived:

$$\frac{d}{dt}\left(\frac{\partial T}{\partial \dot{x}_1}\right) = \left(m_1 + \left(1-\frac{R}{r}\right)^2 m_B + \frac{I_G}{r^2}\right)\ddot{x}_1 \tag{A.5}$$

The elastic energy is given by:

$$V = \frac{1}{2}k_1 x_1^2 \tag{A.6}$$

From equation A.6 the potential energy term in the Lagrange's equations can be derived:

$$\frac{\partial V}{\partial x_1} = k_1 x_1 \tag{A.7}$$

The Rayleigh function is given by:

$$R = \frac{1}{2}c_1 \dot{x}_1^2 \tag{A.8}$$

From equation A.8 the damping term in the Lagrange's equations can be derived:

$$\frac{\partial R}{\partial \dot{x}_1} = c_1 \dot{x}_1 \tag{A.9}$$

The complete equation of motion (A.11) can be formulated by substituting the expressions in Lagrange's equations (A.10) with those found in equations A.5, A.7 and A.9.

$$\frac{d}{dt}\left(\frac{\partial T}{\partial \dot{x}_j}\right) - \frac{\partial T}{\partial x_j} + \frac{\partial V}{\partial x_j} = Q_j^{(n)} \qquad j = 1,2,\ldots,n \tag{A.10}$$

$$\left(m_1 + m_B\left(1-\frac{R}{r}\right)^2 + \frac{I_G}{r^2}\right)\ddot{x}_1 + c_1\dot{x}_1 + k_1 x_1 = F_0 \sin(\omega t) \tag{A.11}$$

The frequency response of the system to a force can be found by substituting the assumed solution and its derivatives (A.12, A.13 and A.14) as well as the harmonic force (A.15) into the equation motion (A.11). The frequency response to a force $F_j(i\omega)$ is shown in equation A.16.

$$x_j(t) = X_j e^{i\omega t} \tag{A.12}$$

$$\dot{x}_j(t) = i\omega X_j e^{i\omega t} \tag{A.13}$$

$$\ddot{x}_j(t) = -\omega^2 X_j e^{i\omega t} \tag{A.14}$$

$$f_j(t) = F_j e^{i\omega t} \tag{A.15}$$

$$X_1 = \frac{1}{-\omega^2\left[m_1 + m_B\left(1-\frac{R}{r}\right)^2 + \frac{I_G}{r^2}\right] + i\omega c_1 + k_1} F_1 \tag{A.16}$$

The transmissibility will be defined in terms of forces. For this purpose the force transmitted by the spring (F_v), the damper (F_d) and the dynamic force of the absorber (F_a) must be calculated. The first two are simply given by equation A.17 and A.18:

$$F_v = k_1 x_1 \tag{A.17}$$

$$F_d = c_1 \dot{x}_1 \tag{A.18}$$

The complete derivation of equation A.19 is shown in Appendix D.

$$F_a = -\left[m_B \left(1 - \frac{R}{r} \right) \frac{R}{r} - \frac{I_G}{r^2} \right] \ddot{x}_1 \tag{A.19}$$

The transmissibility is given in terms of the forces and as a function of frequency. Equations A.17 to A.19 are rewritten using equations A.12 to A.14 and added to arrive at the total force transmitted to the foundation. The force applied at mass m_1 is given by equation A.15. The transmissibility is therefore:

$$\begin{aligned} \frac{F_o}{F_i} &= \frac{\left[k_1 + i\omega c_1 + \omega^2 \left(m_B \left(1 - \frac{R}{r} \right) \frac{R}{r} - \frac{I_G}{r^2} \right) \right] X_1}{F_1} \\ &= \frac{k_1 + i\omega c_1 + \omega^2 \left[m_B \left(1 - \frac{R}{r} \right) \frac{R}{r} - \frac{I_G}{r^2} \right]}{k_1 + i\omega c_1 - \omega^2 \left[m_1 + m_B \left(1 - \frac{R}{r} \right)^2 + \frac{I_G}{r^2} \right]} \end{aligned} \tag{A.20}$$

Equation A.20 can be non-dimensionalised as follows:

$$|T_r| = \left\{ \frac{\left[1 - \left(\frac{\omega}{\omega_a} \right)^2 \right]^2 + \left[2\zeta \frac{\omega}{\omega_n} \right]^2}{\left[1 - \left(\frac{\omega}{\omega_n} \right)^2 \right]^2 + \left[2\zeta \frac{\omega}{\omega_n} \right]^2} \right\}^{\frac{1}{2}} \tag{A.21}$$

$$\phi = \tan^{-1} \left\{ \frac{2\zeta \frac{\omega}{\omega_n}}{1 - \left(\frac{\omega}{\omega_a} \right)^2} \right\} - \tan^{-1} \left\{ \frac{2\zeta \frac{\omega}{\omega_n}}{1 - \left(\frac{\omega}{\omega_n} \right)^2} \right\} \tag{A.22}$$

The following transmissibility plot of equation A.20 illustrates the effect of damping. The importance of low damping in the absorber is clearly evident.

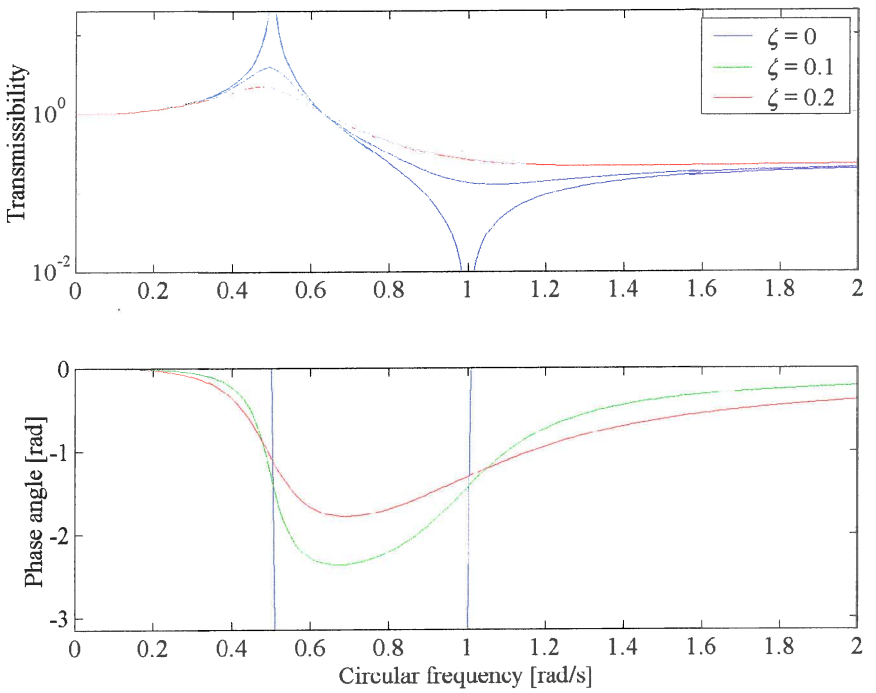

Figure A.3 Transmissibility plot of equation A.20 with $\omega_a = 1$, $\omega_n = 0.5$

The aim of the absorber is to minimise the force transferred to the foundation. This will be achieved when the numerator in the transmissibility equation (A.20) is equal to zero:

$$k_1 + i\omega c_1 + \omega^2\left[m_B\left(1-\frac{R}{r}\right)\frac{R}{r} - \frac{I_G}{r^2}\right] = 0 \qquad \textbf{(A.21)}$$

The non-trivial solution for the isolation frequency ($c_1 = 0$) is:

$$f_a = \frac{1}{2\pi}\sqrt{\frac{-k_1}{m_B\left(1-\frac{R}{r}\right)\frac{R}{r} - \frac{I_G}{r^2}}} \qquad \textbf{(A.22)}$$

The response of the screen to the applied force after the addition of the absorber is of critical importance since it will influence its effective operation. The response of the screen is given by equation A.16. From this equation it is evident that the response of the screen will be influenced by the addition of an absorber. The effect must be minimised through proper choice of parameters and the applied force must be adjusted to compensate.

The following figure illustrates the forced response of the system. The response at the isolation frequency can be low.

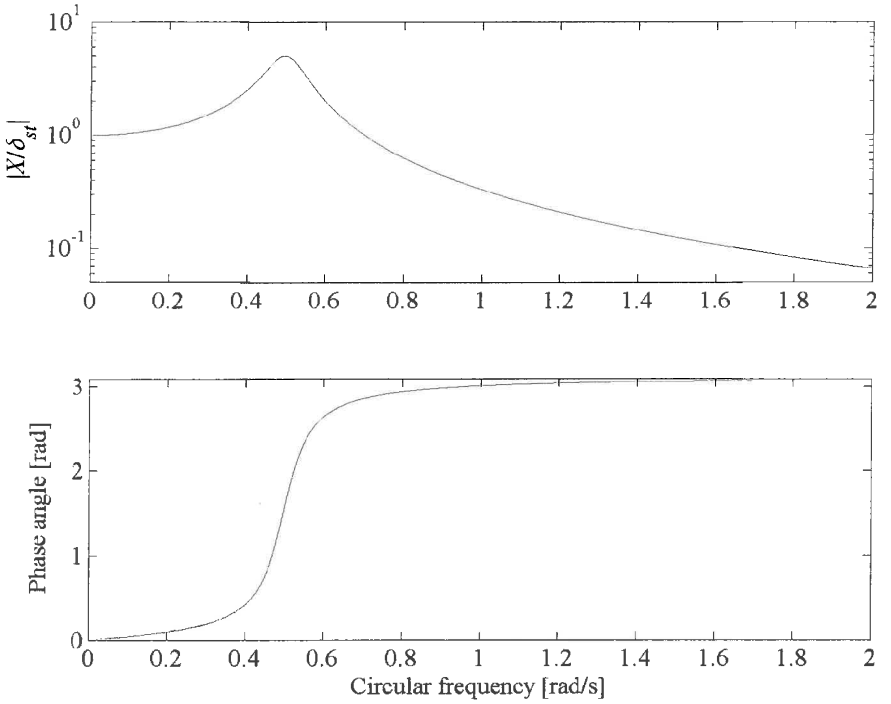

Figure A.4. A typical response of mass m_1 due to force F_1 with $\omega_a = 1$, $\omega_n = 0.5$ and $\zeta = 0.1$

The natural frequency can be seen on the FRF plot. The plot also shows the response of the system at the anti-resonant frequency (the exact point of anti-resonance might not be clear). The undamped natural frequency for this single degree-of-freedom system is given by equation A.23:

$$f_n = \frac{1}{2\pi}\sqrt{\frac{k}{m_1 + m_B\left(1-\frac{R}{r}\right)^2 + \frac{I_G}{r^2}}} \qquad \textbf{(A.23)}$$

APPENDIX B

Mathematical model of a two D.O.F. vibration absorber system

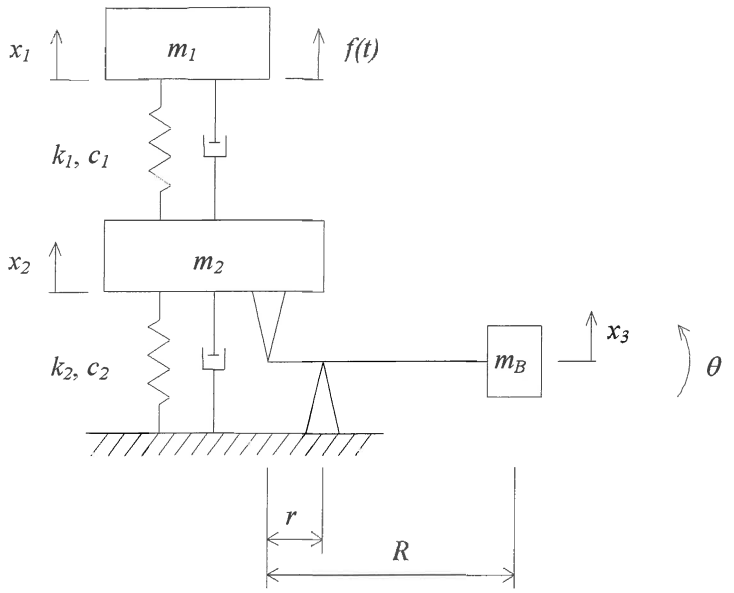

Figure B.1 A 2 degree-of-freedom vibration absorber system

The kinetic energy of the system in figure B.1 is given by equation B.1:

$$T = \frac{1}{2}\left(m_1\dot{x}_1^2 + m_2\dot{x}_2^2 + m_B\dot{x}_3^2 + I_G\dot{\theta}^2\right) \quad \textbf{(B.1)}$$

I_G is the moment of inertia of the mass m_B about its mass centre. The relation between x_3, θ, and x_2 are given by equations B.2 and B.3 (refer to figure B.2):

$$x_3 = \left(1 - \frac{R}{r}\right)x_2 \quad \textbf{(B.2)}$$

$$\theta \approx -\frac{x_2}{r} \quad \textbf{(B.3)}$$

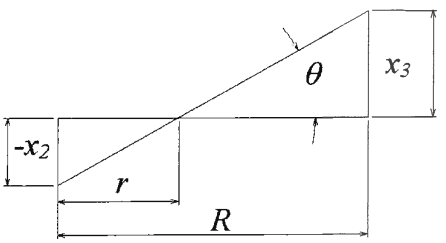

Figure B.2 Schematic of relationship between variables

Substituting these relations in equation B.1 results in the following:

$$T = \frac{1}{2}\left[m_1 \dot{x}_1^2 + \left(m_2 + \left(1 - \frac{R}{r}\right)^2 m_B + \frac{I_G}{r^2} \right) \dot{x}_2^2 \right] \tag{B.4}$$

From equation B.4 the kinetic terms in the Lagrange's equations can be derived:

$$\frac{d}{dt}\left(\frac{\partial T}{\partial \dot{x}_1}\right) = m_1 \ddot{x}_1 \tag{B.5}$$

$$\frac{d}{dt}\left(\frac{\partial T}{\partial \dot{x}_2}\right) = \left(m_2 + \left(1 - \frac{R}{r}\right)^2 m_B + \frac{I_G}{r^2} \right) \ddot{x}_2 \tag{B.6}$$

The elastic energy is given by:

$$V = \frac{1}{2}\left(k_1 (x_1 - x_2)^2 + k_2 x_2^2 \right) \tag{B.7}$$

From equation B.7 the elastic terms in the Lagrange's equations can be derived:

$$\frac{\partial V}{\partial x_1} = k_1 x_1 - k_1 x_2 \tag{B.8}$$

$$\frac{\partial V}{\partial x_2} = -k_1 x_1 + k_1 x_2 + k_2 x_2 \tag{B.9}$$

The Rayleigh function is given by:

$$R = \frac{1}{2}\left(c_1 (\dot{x}_1 - \dot{x}_2)^2 + c_2 \dot{x}_2^2 \right) \tag{B.10}$$

From equation B.10 the damping terms in the Lagrange's equations can be derived:

$$\frac{\partial R}{\partial \dot{x}_1} = c_1 \dot{x}_1 - c_1 \dot{x}_2 \tag{B.11}$$

$$\frac{\partial R}{\partial \dot{x}_2} = -c_1 \dot{x}_1 + c_1 \dot{x}_2 + c_2 \dot{x}_2 \tag{B.12}$$

The mass matrix is given by equations B.5 and B.6:

$$[M] = \begin{bmatrix} m_1 & 0 \\ 0 & m_2 + \left(1 - \frac{R}{r}\right)^2 m_B + \frac{I_G}{r^2} \end{bmatrix} \tag{B.13}$$

The stiffness matrix is given by equations B.8 and B.9:

$$[K] = \begin{bmatrix} k_1 & -k_1 \\ -k_1 & k_1 + k_2 \end{bmatrix} \tag{B.14}$$

The damping matrix is given by equations B.11 and B.12:

$$[C]=\begin{bmatrix} c_1 & -c_1 \\ -c_1 & c_1+c_2 \end{bmatrix} \tag{B.15}$$

The complete equation of motion (B.17) can be formulated by substituting the expressions in the Lagrange equation (B.16) with those found in equations B.5 and B.6, B.8 and B.9 and B.11 and B.12.

$$\begin{bmatrix} m_1 & 0 \\ 0 & m_2+\left(1-\frac{R}{r}\right)^2 m_B+\frac{I_G}{r^2} \end{bmatrix}\begin{bmatrix} \ddot{x}_1 \\ \ddot{x}_2 \end{bmatrix}+\begin{bmatrix} c_1 & -c_1 \\ -c_1 & c_1+c_2 \end{bmatrix}\begin{bmatrix} \dot{x}_1 \\ \dot{x}_2 \end{bmatrix}+\begin{bmatrix} k_1 & -k_1 \\ -k_1 & k_1+k_2 \end{bmatrix}\begin{bmatrix} x_1 \\ x_2 \end{bmatrix}=\begin{bmatrix} F_0\sin(\omega t) \\ 0 \end{bmatrix} \tag{B.16}$$

The frequency response of the system to a force vector can be found by substituting the assumed solution and its derivatives (A.12, A.13 and A.14) as well as the harmonic force (A.15) into the equation of motion (B.17). The frequency response to a force vector $F(i\omega)$ is shown in equation B.22.

$$\begin{bmatrix} X_1 \\ X_2 \end{bmatrix}=\begin{bmatrix} -\omega^2 m_1+i\omega c_1+k_1 & -i\omega c_1-k_1 \\ -i\omega c_1-k_1 & -\omega^2\left[m_2+m_B\left(1-\frac{R}{r}\right)^2+\frac{I_G}{r^2}\right]+i\omega(c_1+c_2)+k_1+k_2 \end{bmatrix}^{-1}\begin{bmatrix} F_1 \\ F_2 \end{bmatrix} \tag{B.17}$$

The response at m_2 can be found by calculating the inverse of the system matrix:

$$\frac{X_2}{F_1}=\frac{-a_{21}}{a_{11}a_{22}-a_{21}a_{12}}$$

$$=\frac{i\omega c_1+k_1}{\left(-\omega^2 m_1+i\omega c_1+k_1\right)\left(-\omega^2\left[m_2+m_B\left(1-\frac{R}{r}\right)^2+\frac{I_G}{r^2}\right]+i\omega(c_1+c_2)+k_1+k_2\right)-(i\omega c_1+k_1)^2} \tag{B.18}$$

The transmissibility will be defined in terms of forces. For this purpose the force transmitted by the spring (F_v), the damper (F_d) and the dynamic force of the absorber (F_a) must be calculated. The first two are given by equations B.19 and B.20:

$$F_v=k_2x_2 \tag{B.19}$$

$$F_d=c_2\dot{x}_2 \tag{B.20}$$

The complete derivation of equation B.21 is shown in Appendix D.

$$F_a=-\left[m_B\left(1-\frac{R}{r}\right)\frac{R}{r}-\frac{I_G}{r^2}\right]\ddot{x}_2 \tag{B.21}$$

The transmissibility is given in terms of the forces and as a function of frequency. Equations B.19 to B.21 are rewritten using equations A.12 to A.14 and added to arrive at the total force transmitted to the foundation. The force applied at mass m_1 is given by equation B.18. The transmissibility is therefore:

$$\frac{F_o}{F_i} = \frac{\left(k_2 + i\omega c_2 + \omega^2\left[m_B\left(1-\frac{R}{r}\right)\frac{R}{r} - \frac{I_G}{r^2}\right]\right)X_2}{F_1}$$

$$= \frac{(i\omega c_1 + k_1)\left(k_2 + i\omega c_2 + \omega^2\left[m_B\left(1-\frac{R}{r}\right)\frac{R}{r} - \frac{I_G}{r^2}\right]\right)}{\left(-\omega^2 m_1 + i\omega c_1 + k_1\right)\left(-\omega^2\left[m_2 + m_B\left(1-\frac{R}{r}\right)^2 + \frac{I_G}{r^2}\right] + i\omega(c_1+c_2) + k_1 + k_2\right) - (i\omega c_1 - k_1)^2} \quad \textbf{(B.22)}$$

The following transmissibility plot of equation B.27 illustrates the effect of c_2. The importance of low damping in the absorber is clearly evident.

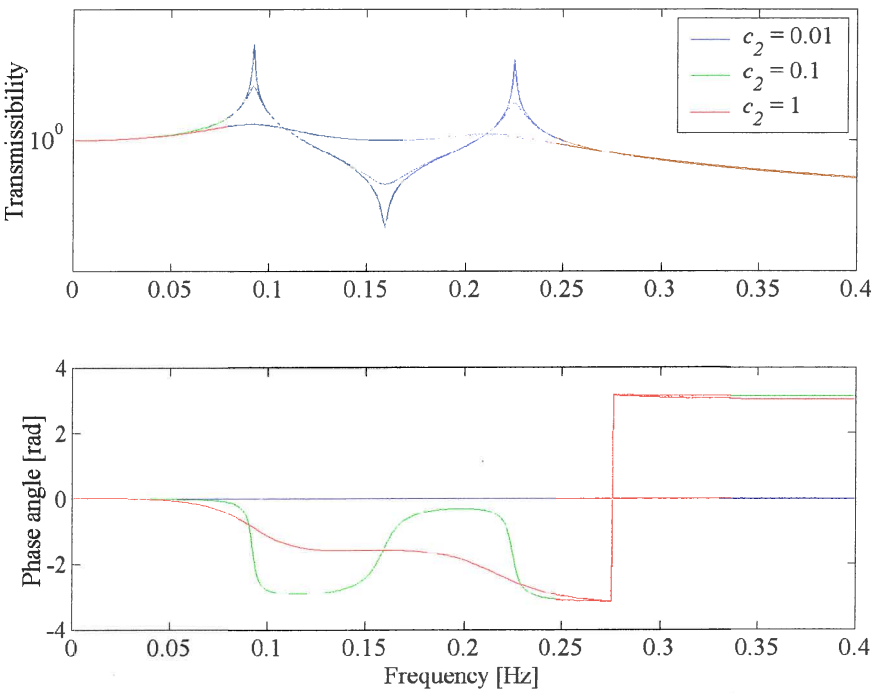

Figure B.3 A typical transmissibility plot of equation B.26 showing the effects of damping ($c_1 = 0$, $c_2 = 0.01$, $m_B = 0.5$, $m_1 = m_2 = k_1 = k_2 = 1$ and $R/r = 2$)

The aim of the absorber is to minimise the force transferred to the foundation. This will be achieved when the numerator in the transmissibility equation (B.22) is equal to zero:

$$k_2 + i\omega c_2 + \omega^2\left[m_B\left(1-\frac{R}{r}\right)\frac{R}{r}-\frac{I_G}{r^2}\right]=0 \qquad \textbf{(B.23)}$$

The non-trivial solution for the undamped isolation frequency ($c_2 = 0$) is:

$$f_a = \frac{1}{2\pi}\sqrt{\frac{-k_2}{m_B\left(1-\frac{R}{r}\right)\frac{R}{r}-\frac{I}{r^2}}} \qquad \textbf{(B.24)}$$

The response of the screen to the applied force after the addition of the absorber is of critical importance since it will influence its effective operation. The response of the screen is given by equation B.25. From this equation it is evident that the response of the screen will be influenced by the addition of an absorber. The effect must be minimised through proper choice of parameters and the applied force must be adjusted to compensate.

$$\frac{X_1}{F_1}=\frac{a_{22}}{a_{11}a_{22}-a_{21}a_{12}}$$

$$=\frac{-\omega^2\left[m_2+m_B\left(1-\frac{R}{r}\right)^2+\frac{I_G}{r^2}\right]+i\omega(c_1+c_2)+k_1+k_2}{\left(-\omega^2 m_1+i\omega c_1+k_1\right)\left(-\omega^2\left[m_2+m_B\left(1-\frac{R}{r}\right)^2+\frac{I_G}{r^2}\right]+i\omega(c_1+c_2)+k_1+k_2\right)-(i\omega c_1+k_1)^2} \qquad \textbf{(B.25)}$$

The following plot of equation B.25 illustrates the forced response of the system at mass m_1.

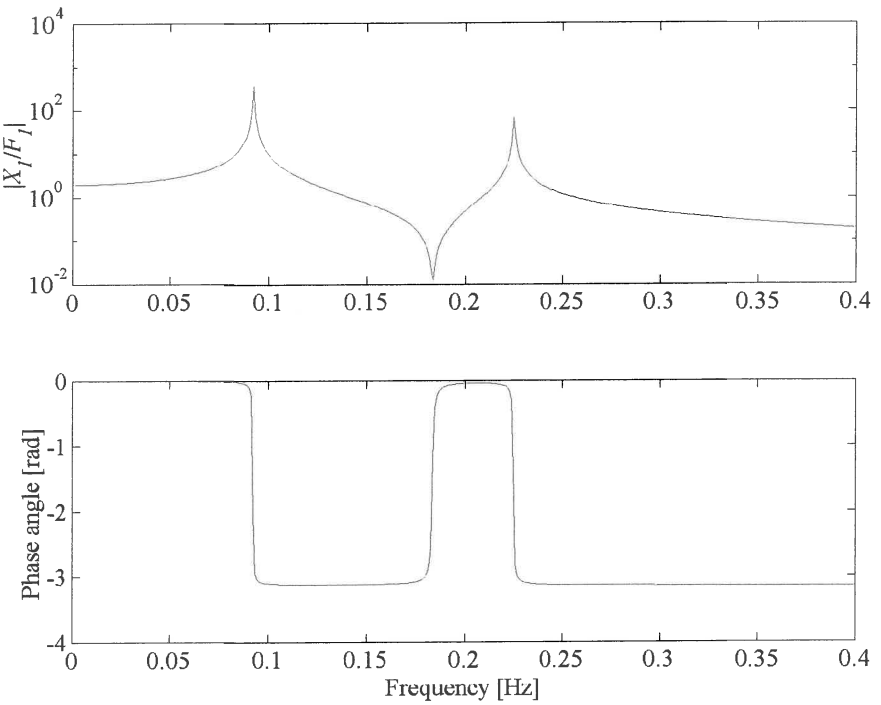

Figure B.4 A typical response of mass m_1 due to force F_1 (α_{11})
($c_1 = 0$, $c_2 = 0.01$, $m_B = 0.5$, $m_1 = m_2 = k_1 = k_2 = 1$ and $R/r = 2$)

The natural frequencies can be seen on both figure B.4 and B.5. The figures also show the response of the system at the isolation frequency (the exact point of isolation might not be clear). The natural frequencies cannot easily be found analytically but are rather calculated numerically with an eigenvalue approach.

The following plot of equation B.18 illustrates the forced response of the system at mass m_2. The 2 degree-of-freedom model can be used to model a screen mounted on an absorber.

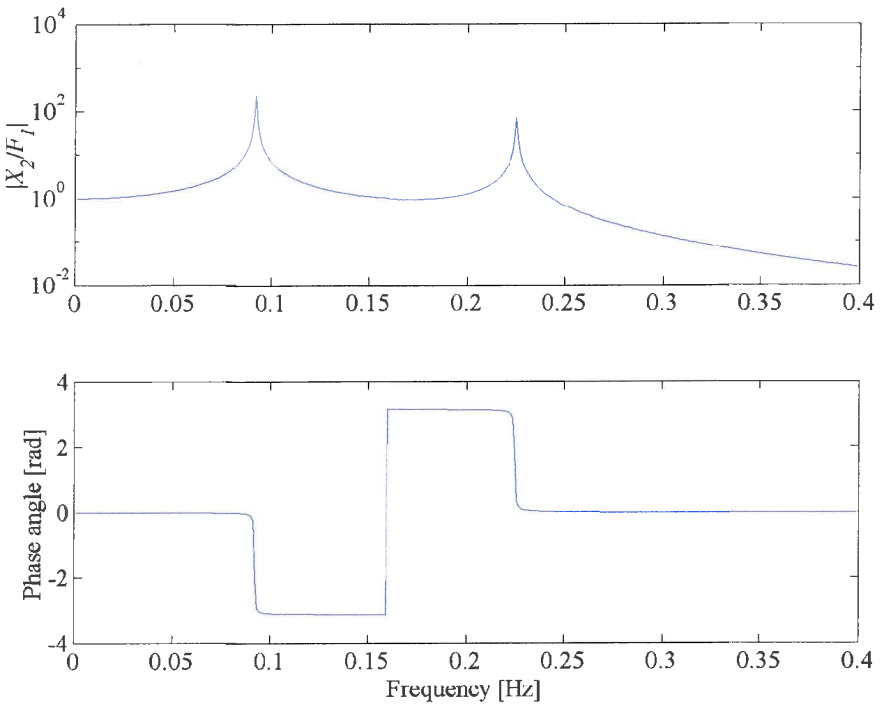

Figure B.5 A typical response of mass m_2 due to force F_1 (α_{21}) with $c_1 = 0$, $c_2 = 0.01$, $m_B = 0.5$, $m_1 = m_2 = k_1 = k_2 = 1$ and $R/r = 2$

APPENDIX C

Mathematical model of a 3 D.O.F. vibration absorber system

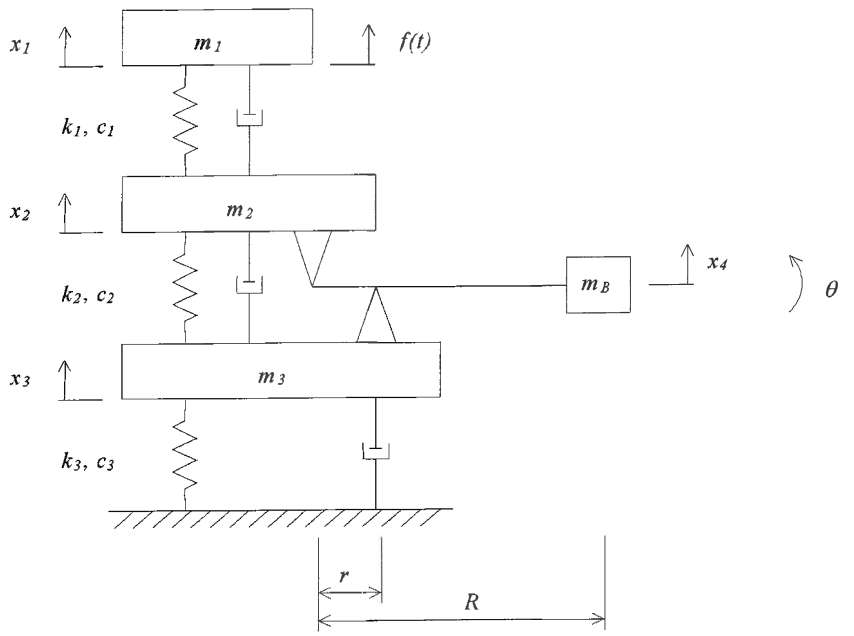

Figure C.1 A three degree-of-freedom system including a vibration absorber

The kinetic energy of the system in figure C.1 is given by equation C.1:

$$T = \frac{1}{2}\left(m_1\dot{x}_1^2 + m_2\dot{x}_2^2 + m_3\dot{x}_3^2 + m_B\dot{x}_4^2 + I_G\dot{\theta}^2\right) \qquad \textbf{(C.1)}$$

I_G is the moment of inertia of the mass m_B about its mass centre. The relation between x_4, θ, x_3 and x_2 are given by equations C.2 and C.3 (refer to figure C.2):

$$x_4 = \left(1 - \frac{R}{r}\right)x_2 + \frac{R}{r}x_3 \qquad \textbf{(C.2)}$$

$$\theta \approx \frac{x_3 - x_2}{r} \qquad \textbf{(C.3)}$$

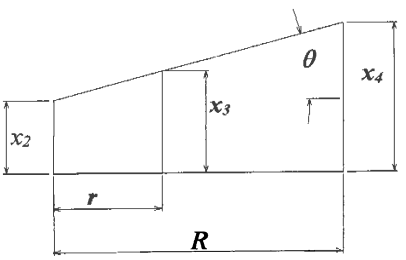

Figure C.2. Schematic of relationship between variables

Substituting these relations in equation C.1 results in the following:

$$T=\frac{1}{2}\left[m_1\dot{x}_1^2+\left(m_2+\left(1-\frac{R}{r}\right)^2 m_B+\frac{I_G}{r^2}\right)\dot{x}_2^2+\left(m_3+\left(\frac{R}{r}\right)^2 m_B+\frac{I_G}{r^2}\right)\dot{x}_3^2+\left(2\left(1-\frac{R}{r}\right)\left(\frac{R}{r}\right)m_B-2\frac{I_G}{r^2}\right)\dot{x}_2\dot{x}_3\right] \tag{C.4}$$

From equation C.4 the kinetic terms in the Lagrange's equations can be derived:

$$\frac{d}{dt}\left(\frac{\partial T}{\partial \dot{x}_1}\right)=m_1\ddot{x}_1 \tag{C.5}$$

$$\frac{d}{dt}\left(\frac{\partial T}{\partial \dot{x}_2}\right)=\left(m_2+\left(1-\frac{R}{r}\right)^2 m_B+\frac{I_G}{r^2}\right)\ddot{x}_2+\left(\left(1-\frac{R}{r}\right)\frac{R}{r}m_B-\frac{I_G}{r^2}\right)\ddot{x}_3 \tag{C.6}$$

$$\frac{d}{dt}\left(\frac{\partial T}{\partial \dot{x}_3}\right)=\left(m_3+\left(\frac{R}{r}\right)^2 m_B+\frac{I_G}{r^2}\right)\ddot{x}_3+\left(\left(1-\frac{R}{r}\right)\frac{R}{r}m_B-\frac{I_G}{r^2}\right)\ddot{x}_2 \tag{C.7}$$

The elastic energy is given by:

$$V=\frac{1}{2}\left(k_1(x_1-x_2)^2+k_2(x_2-x_3)^2+k_3x_3^2\right) \tag{C.8}$$

From equation C.8 the elastic terms in the Lagrange's equations can be derived:

$$\frac{\partial V}{\partial x_1}=k_1x_1-k_1x_2 \tag{C.9}$$

$$\frac{\partial V}{\partial x_2}=-k_1x_1+k_1x_2+k_2x_2-k_2x_3 \tag{C.10}$$

$$\frac{\partial V}{\partial x_3}=-k_2x_2+k_2x_3+k_3x_3 \tag{C.11}$$

The Rayleigh function is given by:

$$R=\frac{1}{2}\left(c_1(\dot{x}_1-\dot{x}_2)^2+c_2(\dot{x}_2-\dot{x}_3)^2+c_3\dot{x}_3^2\right) \tag{C.12}$$

From equation C.12 the damping terms in the Lagrange's equations can be derived:

$$\frac{\partial R}{\partial \dot{x}_1}=c_1\dot{x}_1-c_1\dot{x}_2 \tag{C.13}$$

$$\frac{\partial R}{\partial \dot{x}_2}=-c_1\dot{x}_1+c_1\dot{x}_2+c_2\dot{x}_2-c_2\dot{x}_3 \tag{C.14}$$

$$\frac{\partial R}{\partial \dot{x}_3}=-c_2\dot{x}_2+c_2\dot{x}_3+c_3\dot{x}_3 \tag{C.15}$$

The mass matrix is given by equations C.5, C.6 and C.7:

$$[M]=\begin{bmatrix} m_1 & 0 & 0 \\ 0 & m_2+\left(1-\frac{R}{r}\right)^2 m_B+\frac{I_G}{r^2} & \left(1-\frac{R}{r}\right)\frac{R}{r}m_B-\frac{I_G}{r^2} \\ 0 & \left(1-\frac{R}{r}\right)\frac{R}{r}m_B-\frac{I_G}{r^2} & m_3+\left(\frac{R}{r}\right)^2 m_B+\frac{I_G}{r^2} \end{bmatrix} \quad \textbf{(C.16)}$$

The stiffness matrix is given by equations C.9, C.10 and C.11:

$$[K]=\begin{bmatrix} k_1 & -k_1 & 0 \\ -k_1 & k_1+k_2 & -k_2 \\ 0 & -k_2 & k_2+k_3 \end{bmatrix} \quad \textbf{(C.17)}$$

The damping matrix is given by equations C.13, C.14 and C.15:

$$[C]=\begin{bmatrix} c_1 & -c_1 & 0 \\ -c_1 & c_1+c_2 & -c_2 \\ 0 & -c_2 & c_2+c_3 \end{bmatrix} \quad \textbf{(C.18)}$$

The complete equation of motion (C.20) can be formulated by substituting the expressions in the Lagrange's equations (A.10) with those found in equations C.5 to C.7, C.9 to C.11 and C.13 to C.15:

$$[M]\{\ddot{x}\}+[C]\{\dot{x}\}+[K]\{x\}=\{f\} \quad \textbf{(C.20)}$$

The frequency response of the system to a force vector can be found by substituting the assumed solution and its derivatives (A.12, A.13 and A.14) as well as the harmonic force (A.15) into the equation of motion (C.20). The frequency response to a force vector $F(i\omega)$ is shown in equation C.25.

The transmissibility is calculated numerically from equations C.21 and C.22

$$\begin{Bmatrix} X_1 \\ X_2 \\ X_3 \end{Bmatrix} = \left[-\omega^2[M]+i\omega[C]+[K]\right]^{-1}\begin{Bmatrix} F_1 \\ F_2 \\ F_3 \end{Bmatrix} \quad \textbf{(C.21)}$$

$$T_{ij}=\left|\frac{X_i}{X_j}\right| \quad \textbf{(C.22)}$$

The following transmissibility plot (T_{31}) described by equation C.22 illustrates the effect of c_2. The importance of low damping in the absorber is clearly evident. It is not always possible to see all the natural frequencies on the transmissibility plot. The position of the natural frequency is however extremely important and will be discussed later in this appendix.

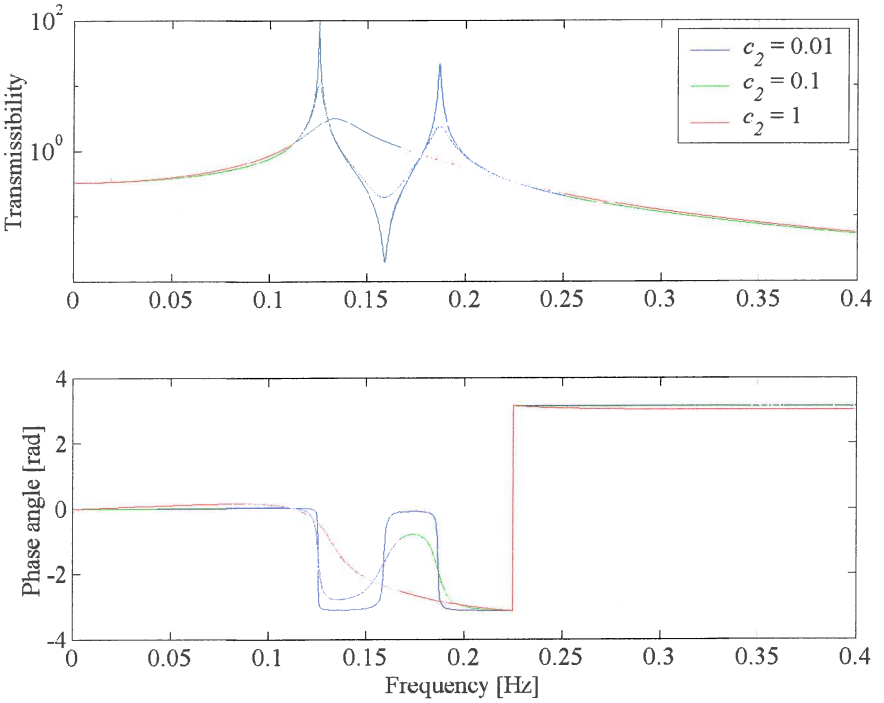

Figure C.3 A typical transmissibility plot of equation C.22 (T_{31}) showing the effects of damping ($c_1 = c_3 = 0$, $m_B = 0.5$, $m_3 = k_3 = k_2 = 1$, $I_G = 0$ and $R/r = 2$)

In order to be able to formulate an expression for the isolation frequency, an analytical expression will be found for the transmissibility between mass m_2 and mass m_3. Equation C.23 was found by substituting the assumed solution and its derivatives (A.12, A.13 and A.14) in the 3rd equation of the set of equations described by equation C.20.

$$\frac{X_3}{X_2} = \frac{k_2 + i\omega c_2 + \omega^2\left(m_B\left(1-\frac{R}{r}\right)\frac{R}{r} - \frac{I_G}{r^2}\right)}{k_2 + k_3 + i\omega(c_2 + c_3) - \omega^2\left(m_3 + m_B\left(\frac{R}{r}\right)^2 + \frac{I_G}{r^2}\right)} \qquad \textbf{(C.23)}$$

The aim of the absorber is to minimise the force transferred to the foundation by minimising the motion of mass m_3. This will be achieved when the numerator in the transmissibility equation (C.23) is equal to zero:

$$k_2 + i\omega c_2 + \omega^2\left(m_B\left(1-\frac{R}{r}\right)\frac{R}{r} - \frac{I_G}{r^2}\right) = 0 \qquad \textbf{(C.24)}$$

The non-trivial solution for the undamped isolation frequency ($c_2 = 0$) is:

$$f_a = \frac{1}{2\pi}\sqrt{\frac{-k_2}{m_B\left(1-\frac{R}{r}\right)\frac{R}{r} - \frac{I_G}{r^2}}} \qquad \textbf{(C.25)}$$

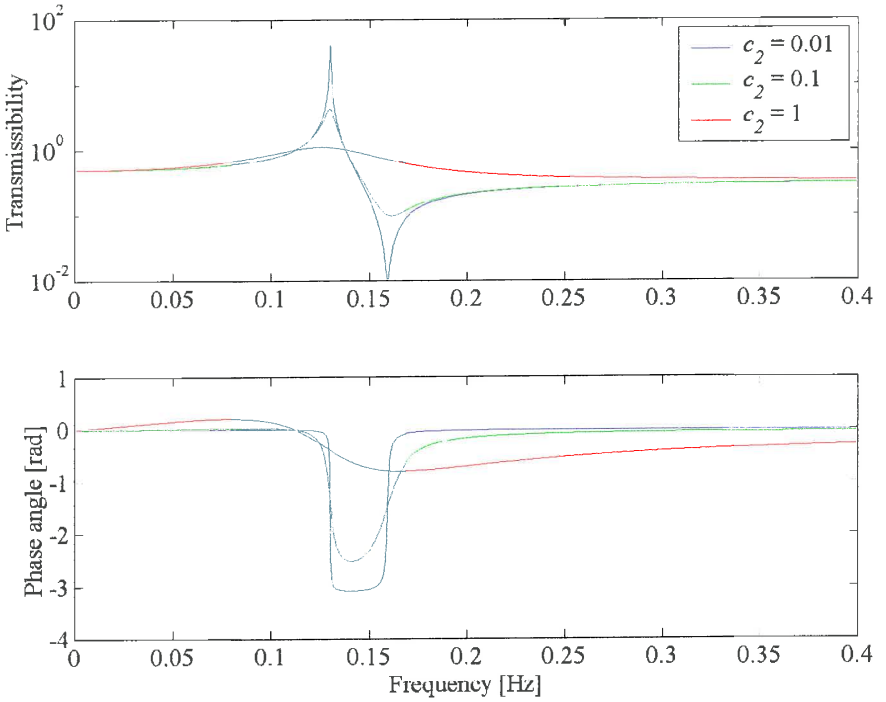

Figure C.4 A typical transmissibility plot of equation C.23 (T_{32}) showing the effects of damping ($c_1 = c_3 = 0$, $m_B = 0.5$, $m_3 = k_3 = k_2 = 1$, $I_G = 0$ and $R/r = 2$)

The response of the screen to the applied force after the addition of the absorber is of critical importance since it will influence its effective operation. The response of the screen is given by equation C.21. From this equation it is evident that the response of the screen will be influenced by the addition of an absorber. The effect must be minimised through proper choice of parameters and the applied force must be adjusted to compensate.

The following figures show the response at mass m_1 and m_3 due to a force acting on mass m_1. The three natural frequencies are clearly visible. The figures also show the response of the system at the anti-resonant frequency. Figure C.6 shows that mass m_3 has low response at anti-resonance.

The 3 DOF model can be used to model a screen mounted on an absorber when the stiffness of the support must be taken into account.

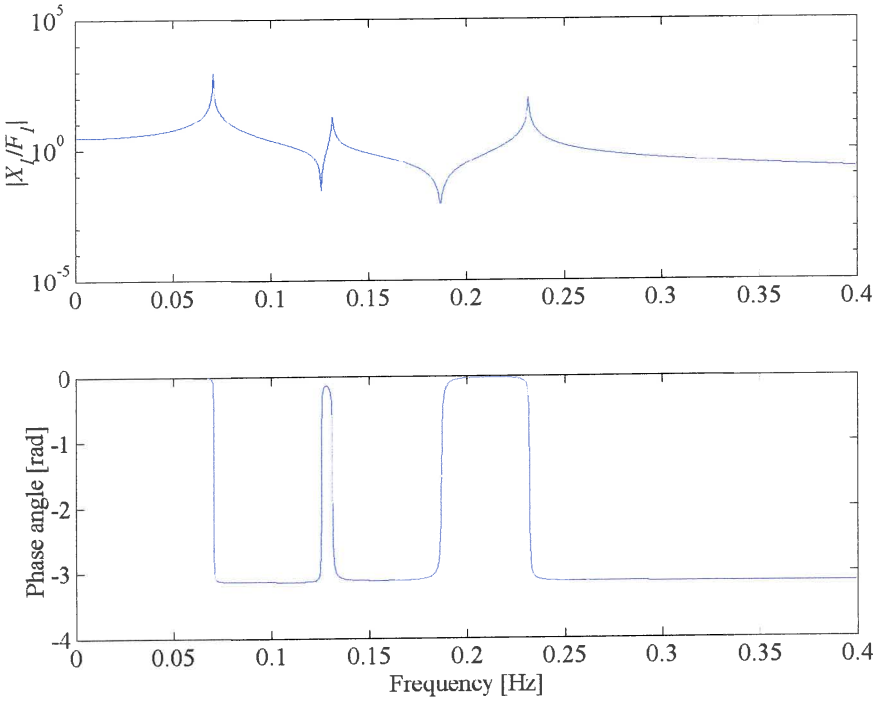

Figure C.5 The response of mass m_1 due to force F_1 (α_{11})
($c_1 = c_3 = 0$, $c_2 = 0.01$, $m_B = 0.5$, $m_1 = m_2 = m_3 = k_1 = k_2 = k_3 = 1$, $I_G = 0$ and $R/r = 2$)

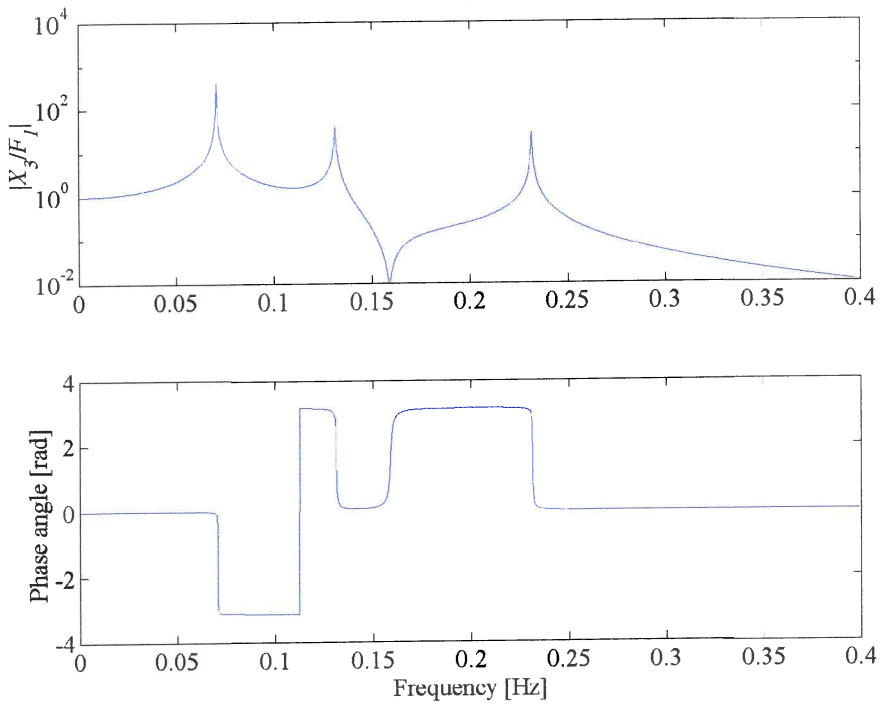

Figure C.6 The response of mass m_3 due to force F_1 (α_{31})
($c_1 = c_3 = 0$, $c_2 = 0.01$, $m_B = 0.5$, $m_1 = m_2 = m_3 = k_1 = k_2 = k_3 = 1$, $I_G = 0$ and $R/r = 2$)

APPENDIX D

Analysis of the inertial absorber force

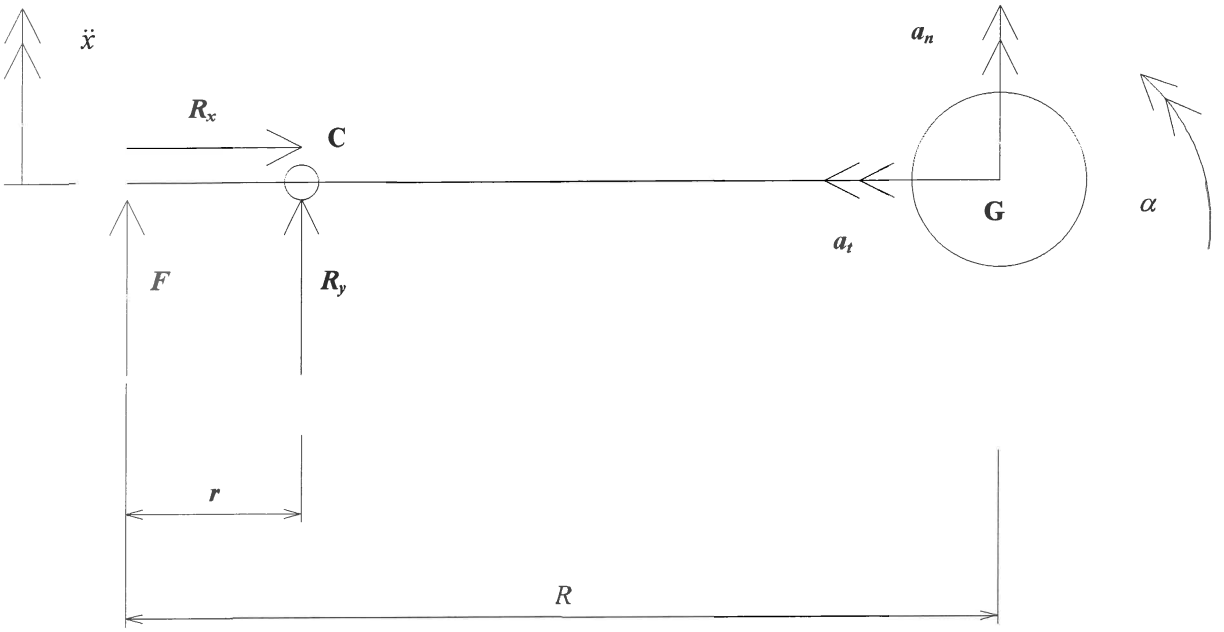

Figure D.2 Schematic of absorber pendulum

The sum of the moments about fixed pivot C is given by:

$$\begin{aligned}\Sigma M_C &= I_C\alpha \\ &= -Fr\end{aligned} \tag{D.1}$$

The sum of the forces in the x and y directions are:

$$\begin{aligned}\Sigma F_x &= -m_B a_t \\ R_x &= -m_B(R-r)\omega^2\end{aligned} \tag{D.2}$$

$$\begin{aligned}\Sigma F_y &= m_B a_n \\ F + R_y &= m_B(R-r)\alpha\end{aligned} \tag{D.3}$$

The trigonometric relationship between the linear and angular acceleration is given by:

$$\ddot{x} \approx -r\alpha \tag{D.4}$$

By substituting equation D.1 in equation D.3 the force R_y can be found as a function of the angular acceleration:

$$R_y = m_B(R-r)\alpha + \frac{I_C}{r}\alpha \tag{D.5}$$

The angular acceleration can now be substituted with the relationship given by equation D.4:

$$R_y = -\frac{m_B}{r}(R-r)\ddot{x} - \frac{I_C}{r^2}\ddot{x} \tag{D.6}$$

The following expression can be written for the moment of inertia about C using Steiner's theorem:

$$I_C = m_B(R-r)^2 + I_G \tag{D.7}$$

Substituting this relationship into equation D.6 results in:

$$\begin{aligned} R_y &= \left[-\frac{m_B}{r}(R-r) - \frac{m_B}{r^2}(R-r)^2 - \frac{I_G}{r^2} \right] \ddot{x} \\ &= \left[m_B\left(1-\frac{R}{r}\right)\frac{R}{r} - \frac{I_G}{r^2} \right] \ddot{x} \end{aligned} \tag{D.8}$$

APPENDIX E

Computational fluid dynamics analysis

E.1. Introduction

Viscous damping is a damping force that is proportional to the velocity of the fluid. To find the force it is necessary to solve the shear force on the port wall and the pressure drop across the port. Analytical equations that describe both these quantities were discussed in chapter 2, but they exist only for simple geometries. To find the total force acting on the port used in the final design computational fluid dynamics had to be used. The objective was to compare the final design with the theoretical model in order to show that a smooth inlet will reduce the amount of damping. The force found from the analytical equations was compared to CFD results for the theoretical case. This gave confidence in the method. The force acting on the port used in the final design was solved using CFD and compared to the theoretical case. This was a qualitative study and showed a marked improvement in the damping when a smooth inlet/outlet geometry was used.

E.2. Method and Model parameters

Computational fluid dynamics produce a prediction of how fluid will flow for a given situation (Shaw, 1992). To do this the numerical solutions to the equations that govern the flow must be solved. These equations can be found from the knowledge that mass and momentum must be conserved. The package used to solve the flow was STAR-CD. This package uses the finite volume method to solve the equations for the fluid flow, which is described in detail by Patankar (1980). Turbulence was included in the model using the k-ε turbulence model. This method calculates the kinetic energy k and the distribution of the dissipation rate of k denoted by ε.

The inputs needed by the CFD package are:

- the geometry of the flow domain including the computational mesh
- fluid properties
- boundary conditions
- solution control parameters

Due to its simplicity, the geometry for the theoretical model was created in STAR-CD. The geometry for the design was imported from CAD. A mesh of hexahedral cells was created. Only $1/8^{th}$ of the port was modeled to reduce the solution time. The fluid properties were the same for both models.

Table E.2 Fluid properties

Property	Value
Density [kg/m^3]	1000
Absolute viscosity	1×10^{-3}

The boundary condition was treated as a constant axial velocity inlet at the bottom and a constant axial velocity outlet at the top. It was assumed that the fluid flow would have the same velocity as the port that is forcing it. The port is moving relative to the sleeve and it is therefore possible to specify the boundary condition on the sleeve and keep the port fixed.

The velocity of the port is equal to the inlet velocity and is related to the amplitude and circular frequency by:

$$\dot{x}(t) = i\omega X e^{i\omega t}$$

By solving the damping for different inlet velocities, a lookup table can be constructed. For a fixed amplitude the damping coefficient is only a function of frequency.

The SIMPLE algorithm was used for the solution. The solution converged in 3000 iterations. The y^+ values were checked and fell within the acceptable range of 30 to 100.

The following two paragraphs will give detailed results for the two models. Graphical output of the CFD program is also included to give physical insight in the processes that cause damping.

E.3. Theoretical model

Figures E.1 to E.3 show the grid of hexahedral cells. A constant axial velocity outlet boundary condition was specified at the top and a constant axial velocity inlet at the bottom. The walls had a no-slip boundary condition. A symmetry plane was defined to reduce the size of the model. No flow is allowed perpendicular to this plane.

The port inlet and outlet are sudden contractions and expansions, which will create the maximum flow losses for this port and reservoir diameter.

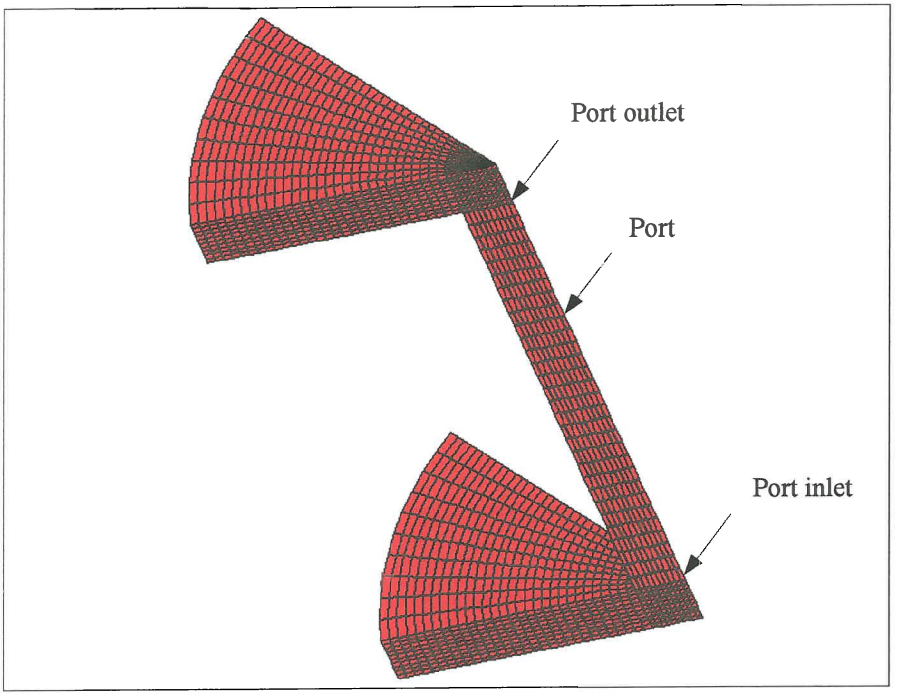

Figure E.1 3D grid for 1/8th of the flow region

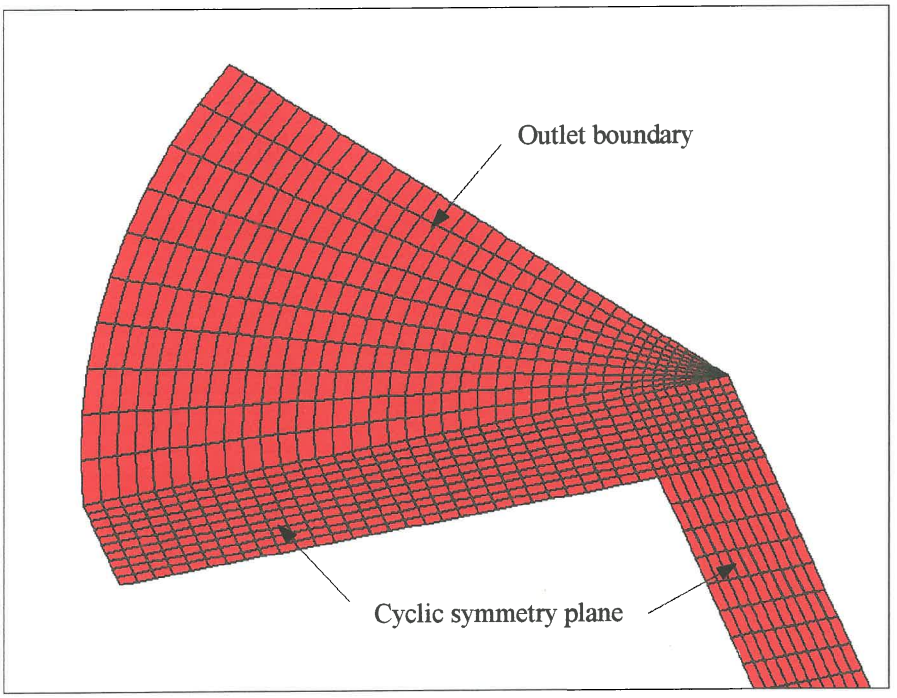

Figure E.2 Grid at the outlet

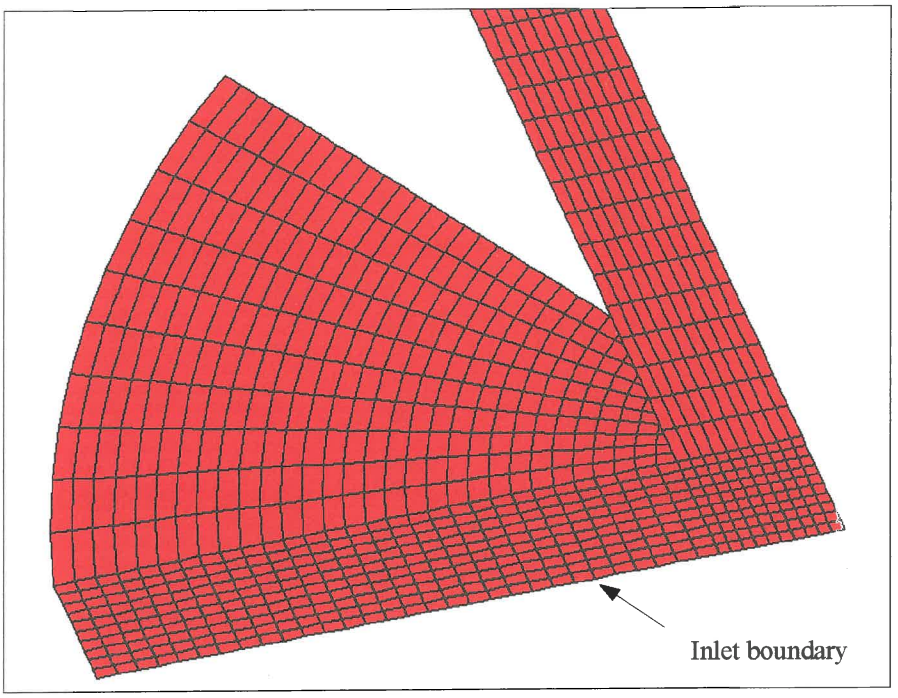

Figure E.3 Grid at the inlet

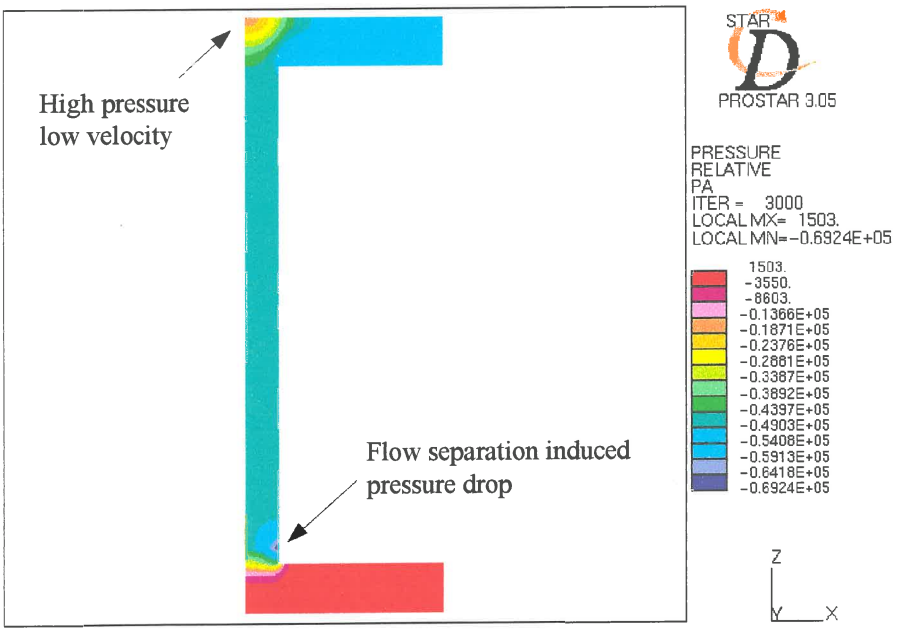

E.4 Relative pressure

On figure E.4 it can be seen that the flow separation at the inlet cause a pressure drop at the wall. The flow separation reduces the effective flow area, which accelerates the fluid. This condition can be seen in figure E.5 and E.7.

The wall had a no-slip boundary condition the effect of which can be seen in figure E.5.

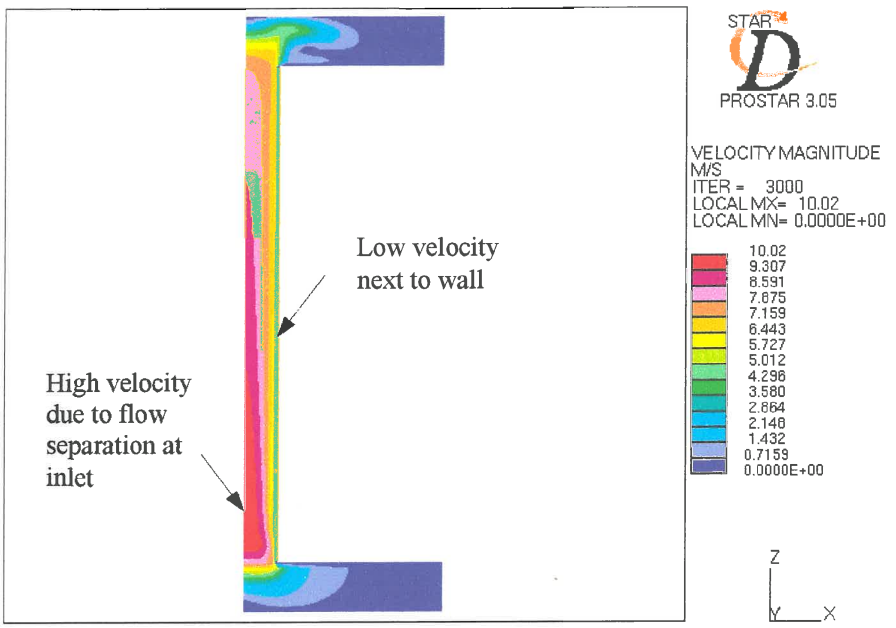

E.5 Velocity magnitude

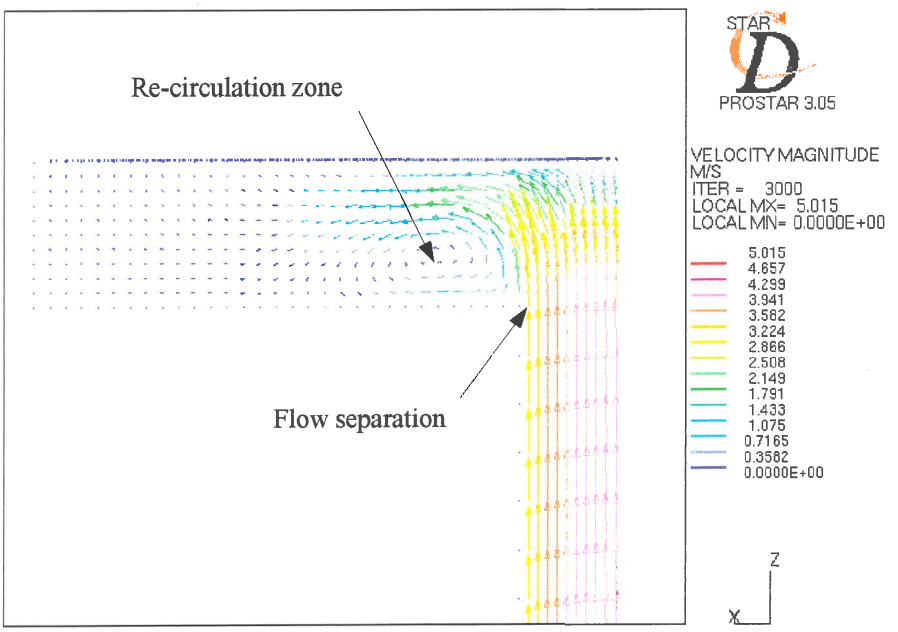

E.6 Velocity vectors at the outlet

Re-circulation at the outlet is caused by flow separation as can be seen in figure E.6. This condition will increase the damping.

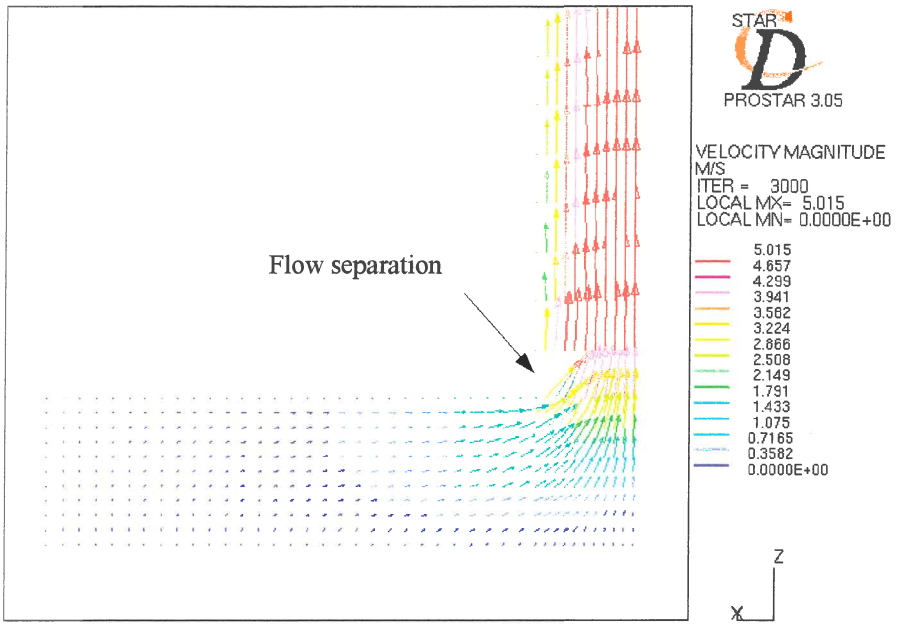

E.7 Velocity vectors at the inlet

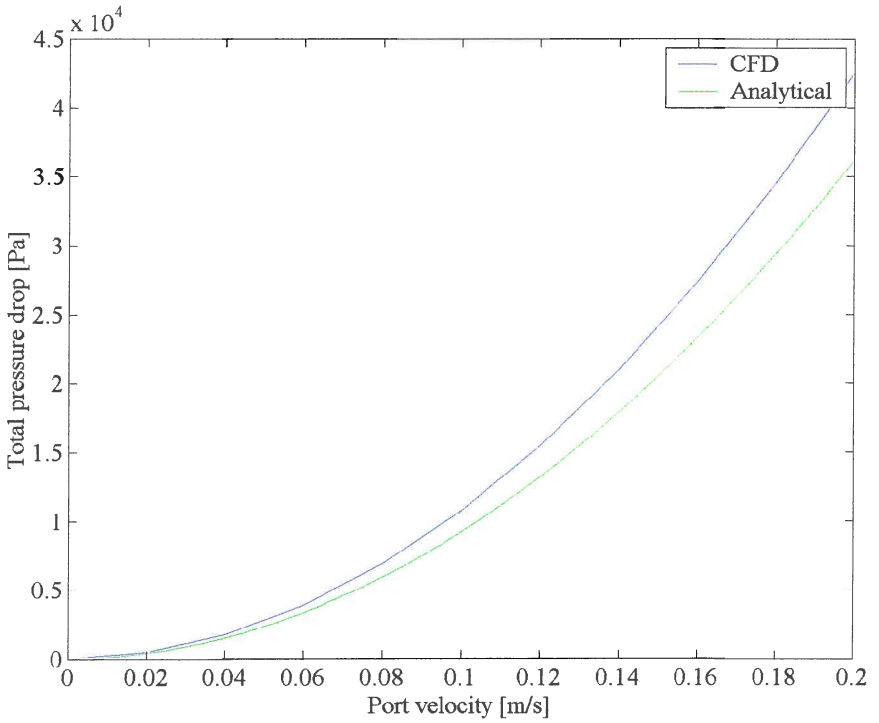

Figure E.8 Total pressure drop (Δp_T) as a function of port velocity ($\dot{x}$)

The total pressure drop is shown in figure E.8. The pressure drop at the outlet is shown in figure E.10 and is clearly much more that predicted analytically. The reason for this is the proximity of the boundary.

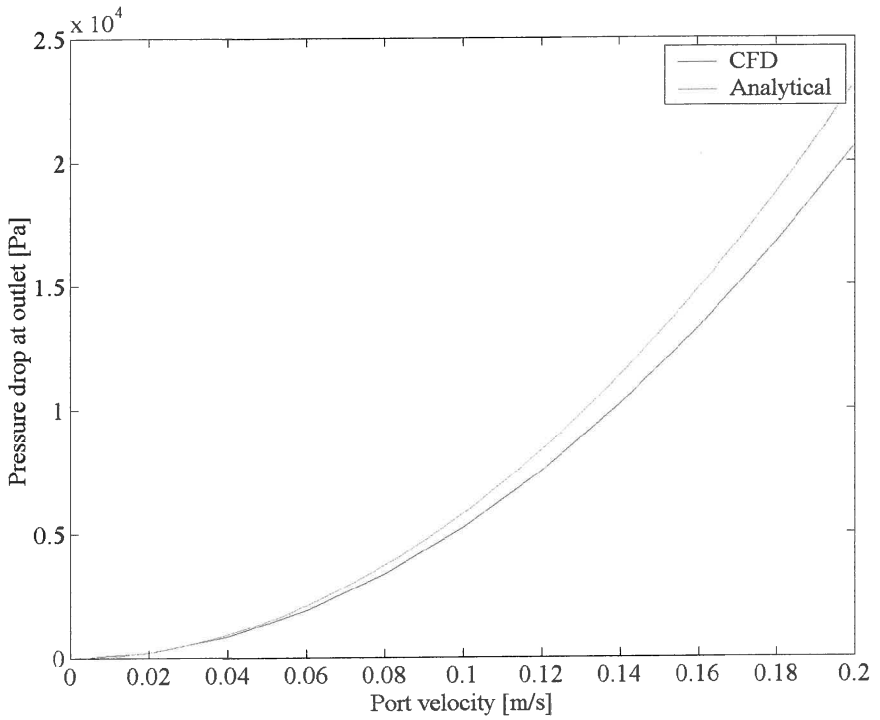

Figure E.9 The pressure drop at the outlet (Δp_o) as a function of port velocity ($\dot{x}$)

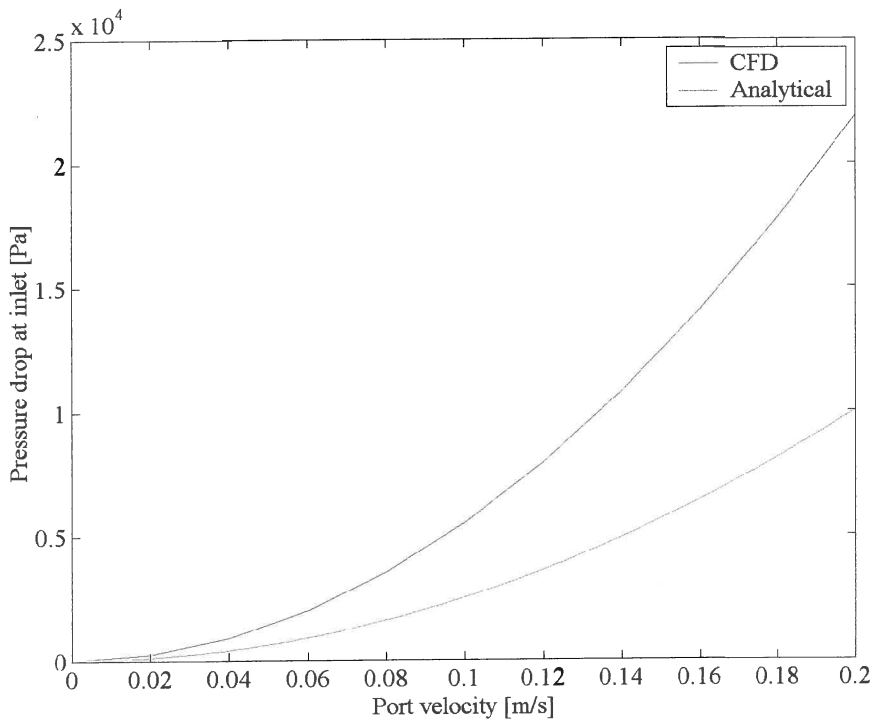

Figure E.10 The pressure drop at the inlet (Δp_i) as a function of port velocity ($\dot{x}$)

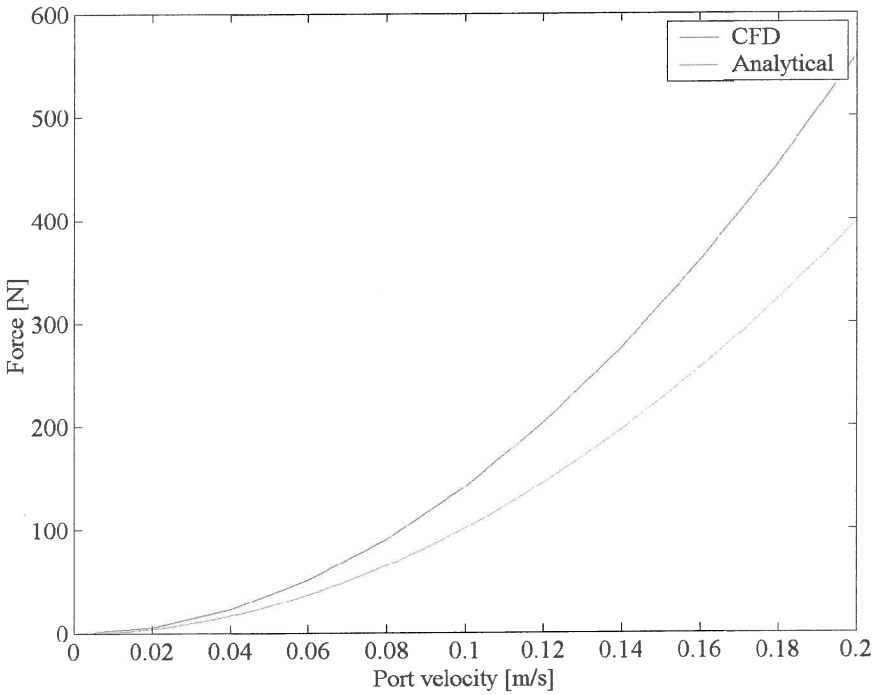

Figure E.11 Force in the z-direction (F_z) as a function of port velocity ($\dot{x}$)

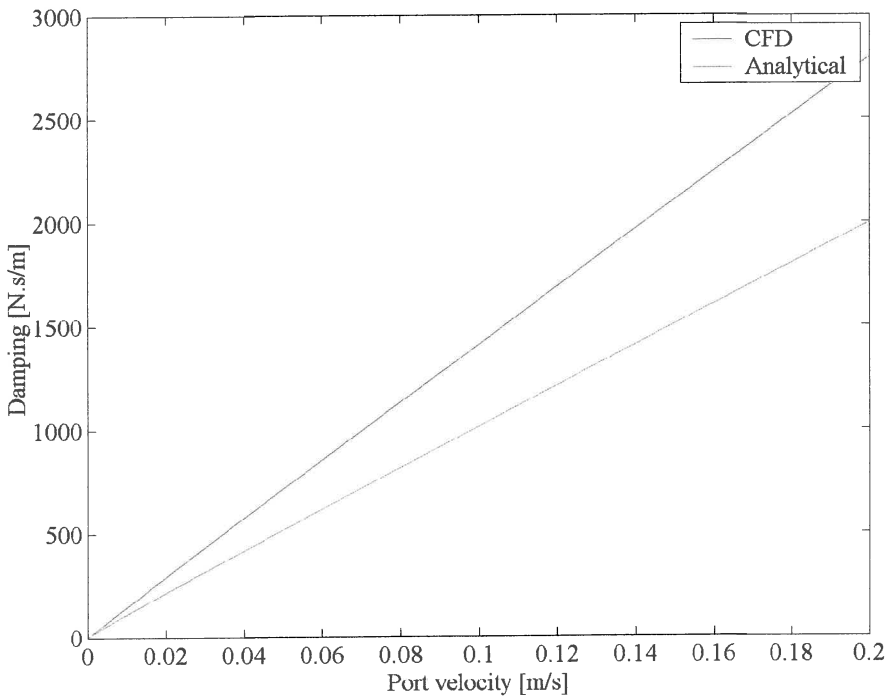

Figure E.12 Damping (c) as a function of port velocity ($\dot{x}$)

The pressure varies quadratically as can be expected from its relation with velocity (figure E.13) while the damping coefficient varies linearly as can be seen in figure E.12.

E.4. Design

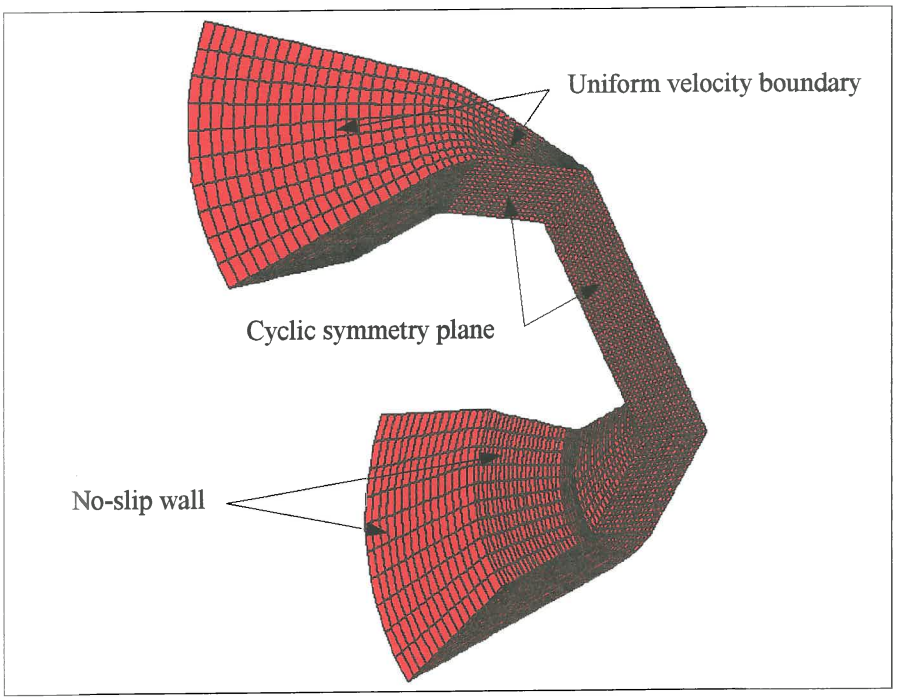

Figure E.13 3D grid for 1/8th of the flow region

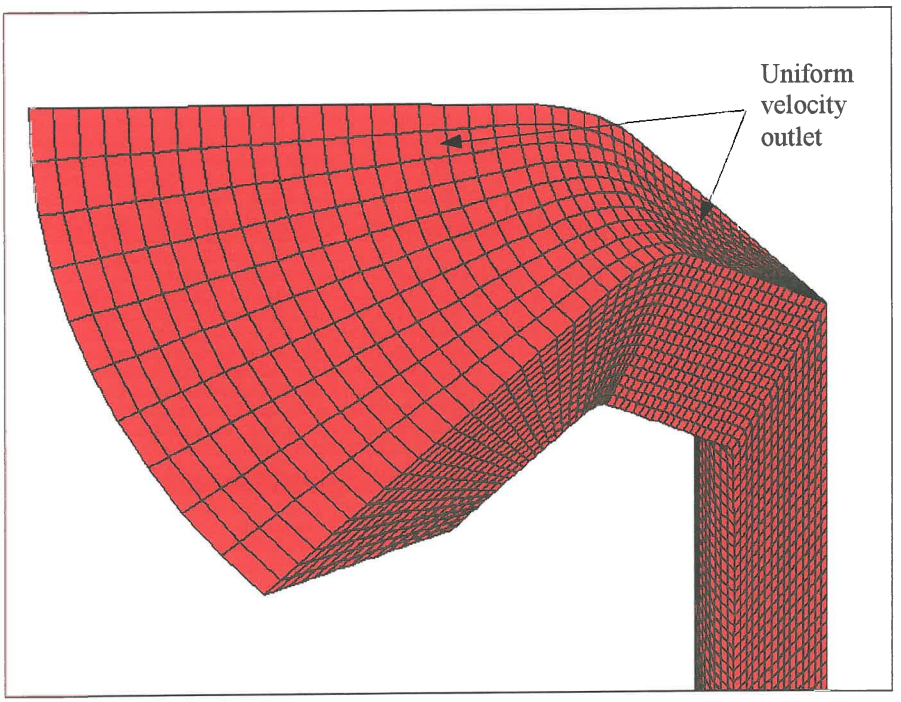

Figure E.14 Grid at the outlet

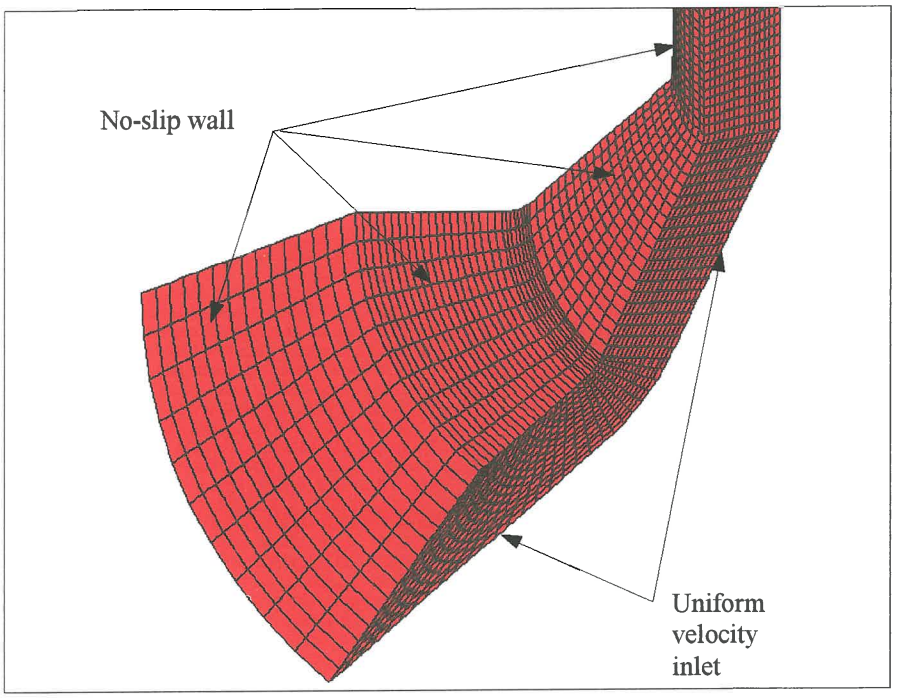

Figure E.15 Grid at the inlet

The mesh used for the final design is shown in figures E.13 to E.15. The boundary condition was a constant velocity in the z-direction on the ends of the grid. Figure E.16 show that the gradual change in area causes less flow disturbance.

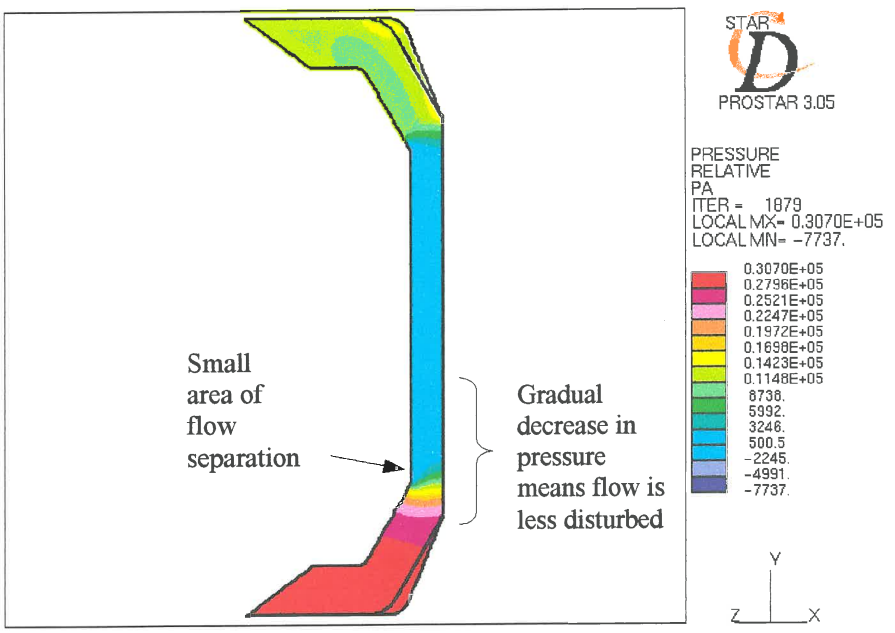

Figure E.16 Relative pressure

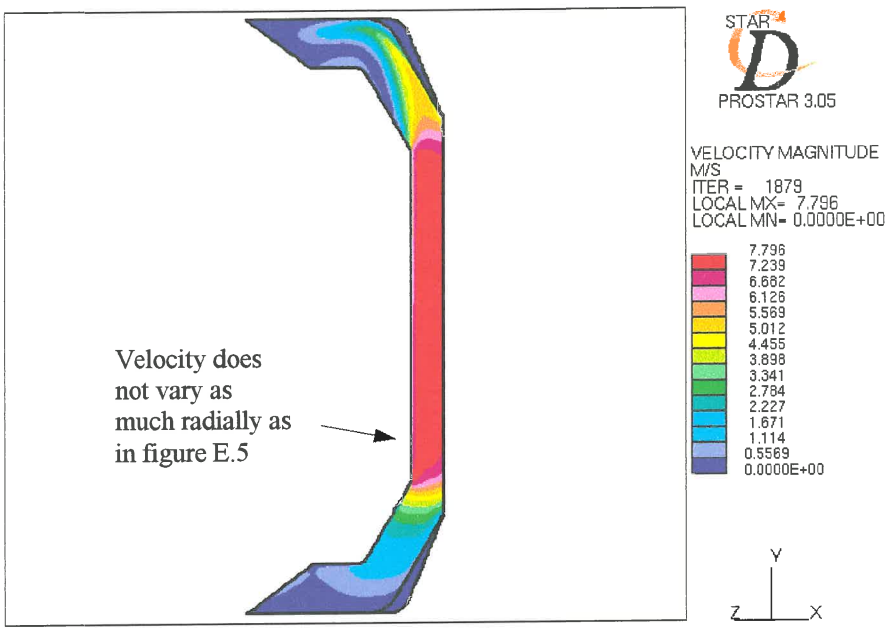

Figure E.17 Velocity magnitude

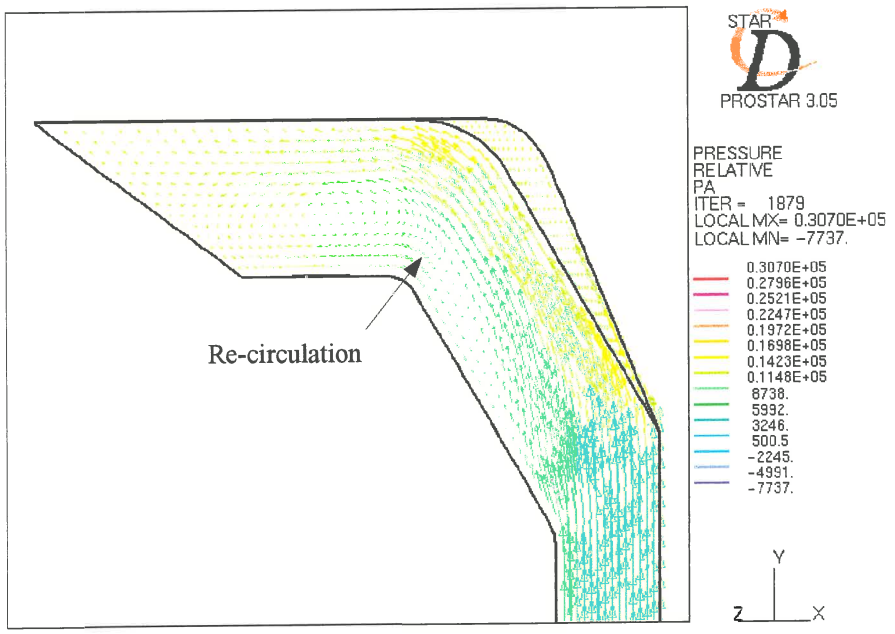

Figure E.18 Velocity vectors at outlet

Figures E.17 and E.18 show that the flow still gets separated at the outlet where a re-circulation region develops causing backward flow in the outlet. This will increase the damping. At the inlet (figure E.19) hardly any separation occurs.

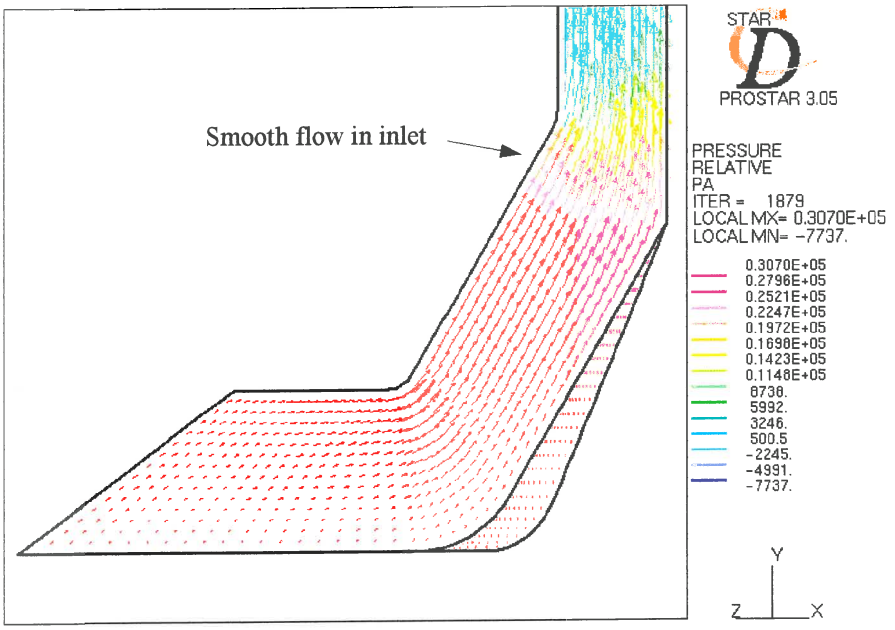

Figure E.19 Velocity vectors at inlet

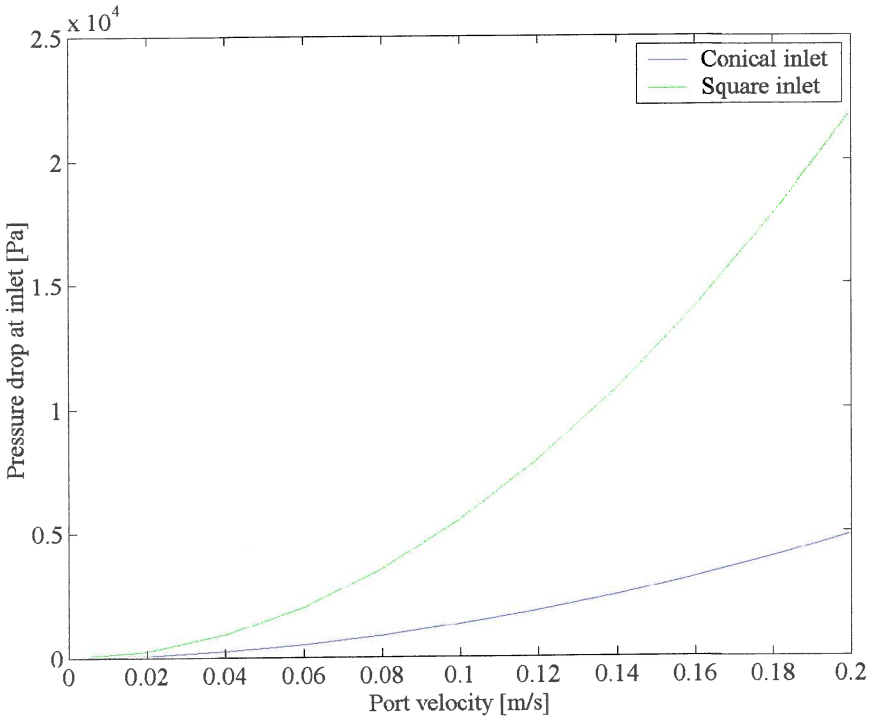

Figure E.20 The pressure drop at the inlet (Δp_o) as a function of port velocity ($\dot{x}$)

Figure E.20 shows that the pressure drop at the inlet is far less than for square inlets/outlets. The pressure drop decrease at the outlet is not as dramatic (figure E.21).

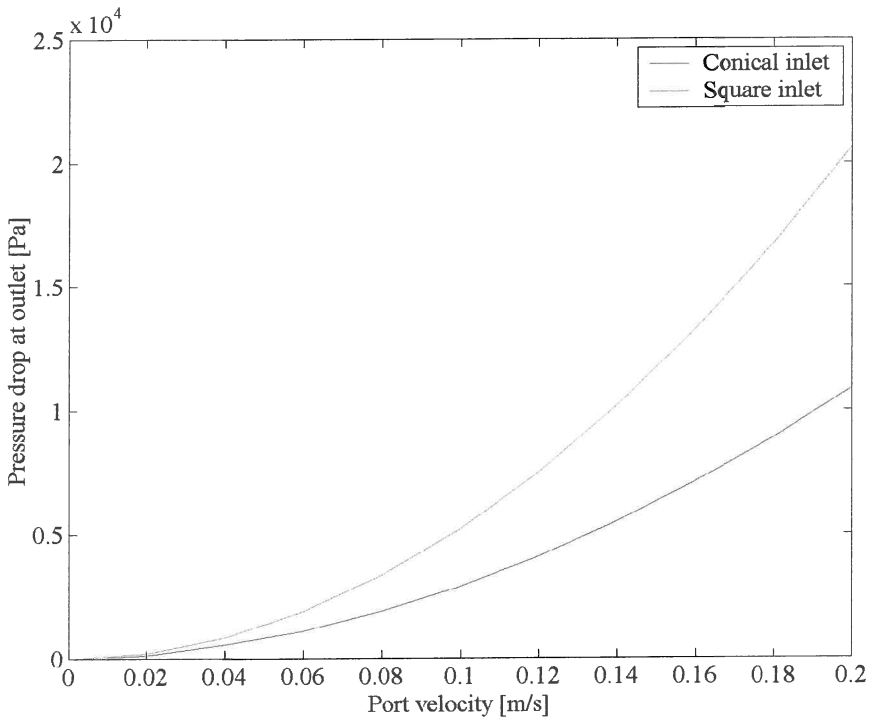

Figure E.21 The pressure drop at the outlet (Δp_o) as a function of port velocity ($\dot{x}$)

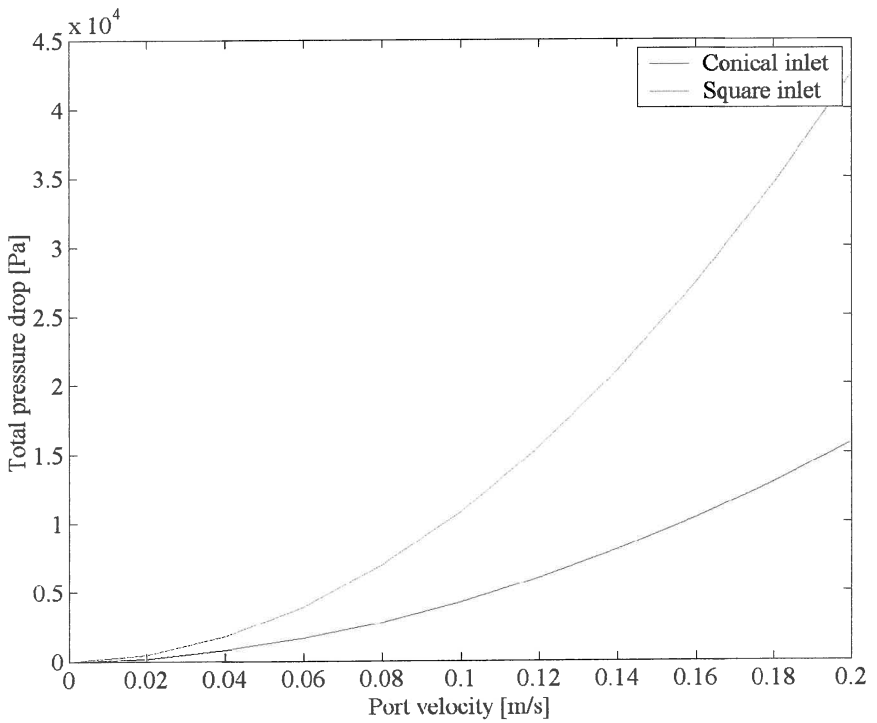

Figure E.22 Total pressure drop (Δp_i) as a function of port velocity ($\dot{x}$)

Figure E.22 shows that changes to the inlet/outlet geometry can have a major impact on the total pressure drop.

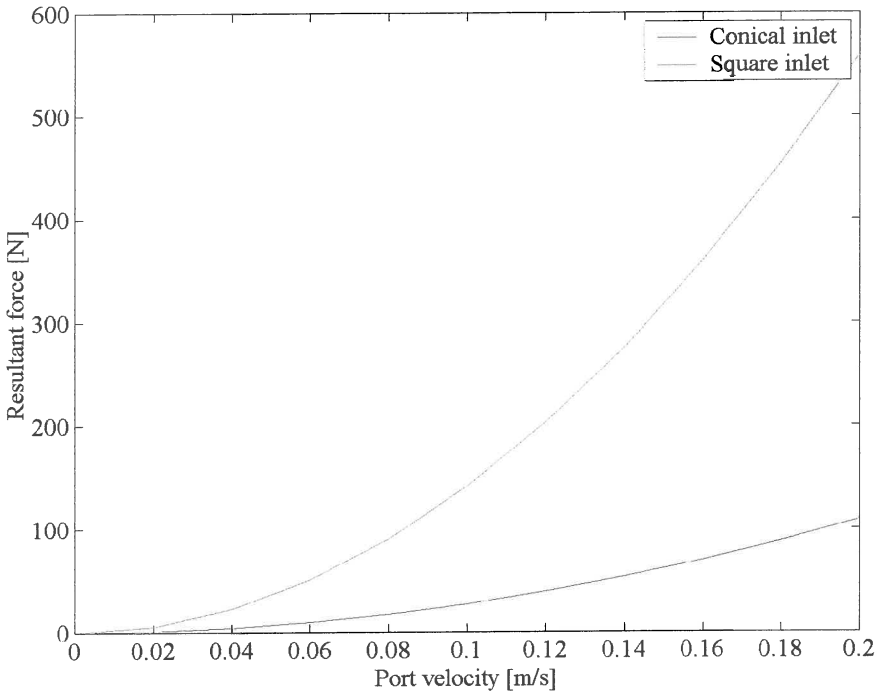

Figure E.23 Force in the z-direction (F_z) as a function of port velocity ($\dot{x}$)

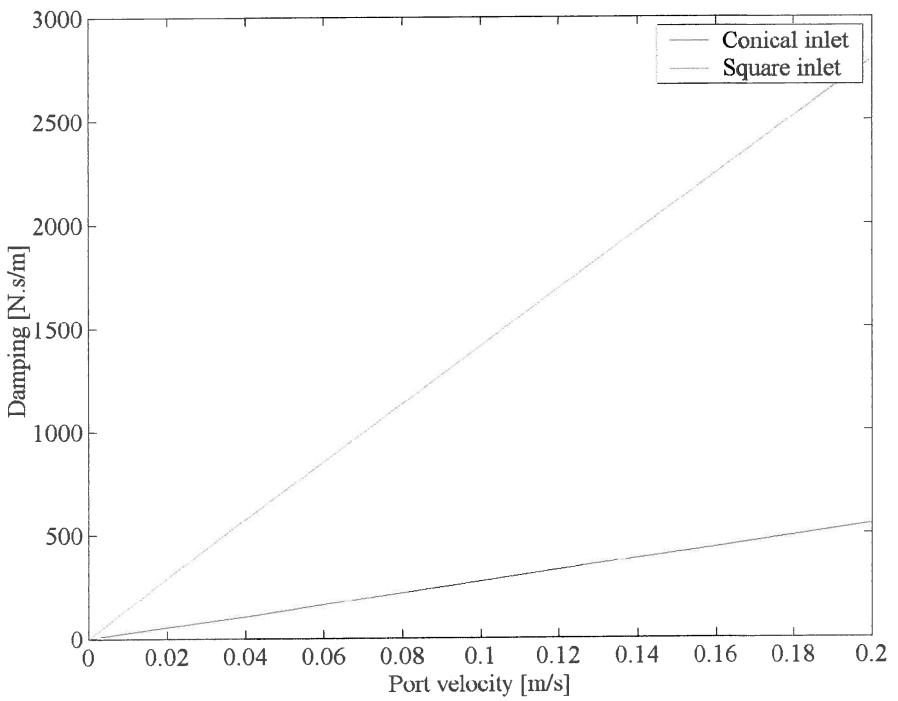

Figure E.24 Viscous damping (c) as a function of port velocity ($\dot{x}$)

The conical inlets/outlets reduced the viscous damping significantly as can be seen in figure E.24.

E.5. Conclusion

The CFD analysis proved to be worthwhile. The total pressure drop of the design is 2.5 times less than the theoretical model. The viscous damping coefficient is 5 times less. The design was done only with knowledge based on theory and empirical data and further improvements are therefore possible. Manufacturability also played a major role in the eventual choice of geometry. The port geometry can however be optimized using CFD. Optimization of the port geometry could significantly reduce damping further and is recommended for a future study.

APPENDIX F

Detail design

F.1. Component mass

Table F.1 Component mass

Item	#	Solid model [kg]	Actual [kg]
M14 threaded rod	2		0.00766
Lid	1	4.45	4.18
M8 allencap	6		0.02132
Washer	6		0.00125
Connector	1	17.6	16.98
Connector block 1	1	1.1	1.12
Connector block 2	1	1.1	1.10
M10 flat head socket screw	2		0.00234
M8 flat head socket screw	4		0.00186
Sleeve	1	8.41	7.92
O-ring	2		0.0036
Top plug	1	3.68	3.70
M6	1		0.0066
Washer	1		0.001
Spring	1	1.14	0.9
Port	1		4.74
Bottom plug	1	3.68	3.64

Table F.2 Volume

Item	Solid model [L]
Spring	1.071
Port	0.078
Reservoir	0.110
Total fluid	0.298

Table F.3 Density

	[kg/m^3]
Polyurethane	1060
Steel	7850
Water	1000

System mass 15.28 kg

F.2. Detail of the tuning port

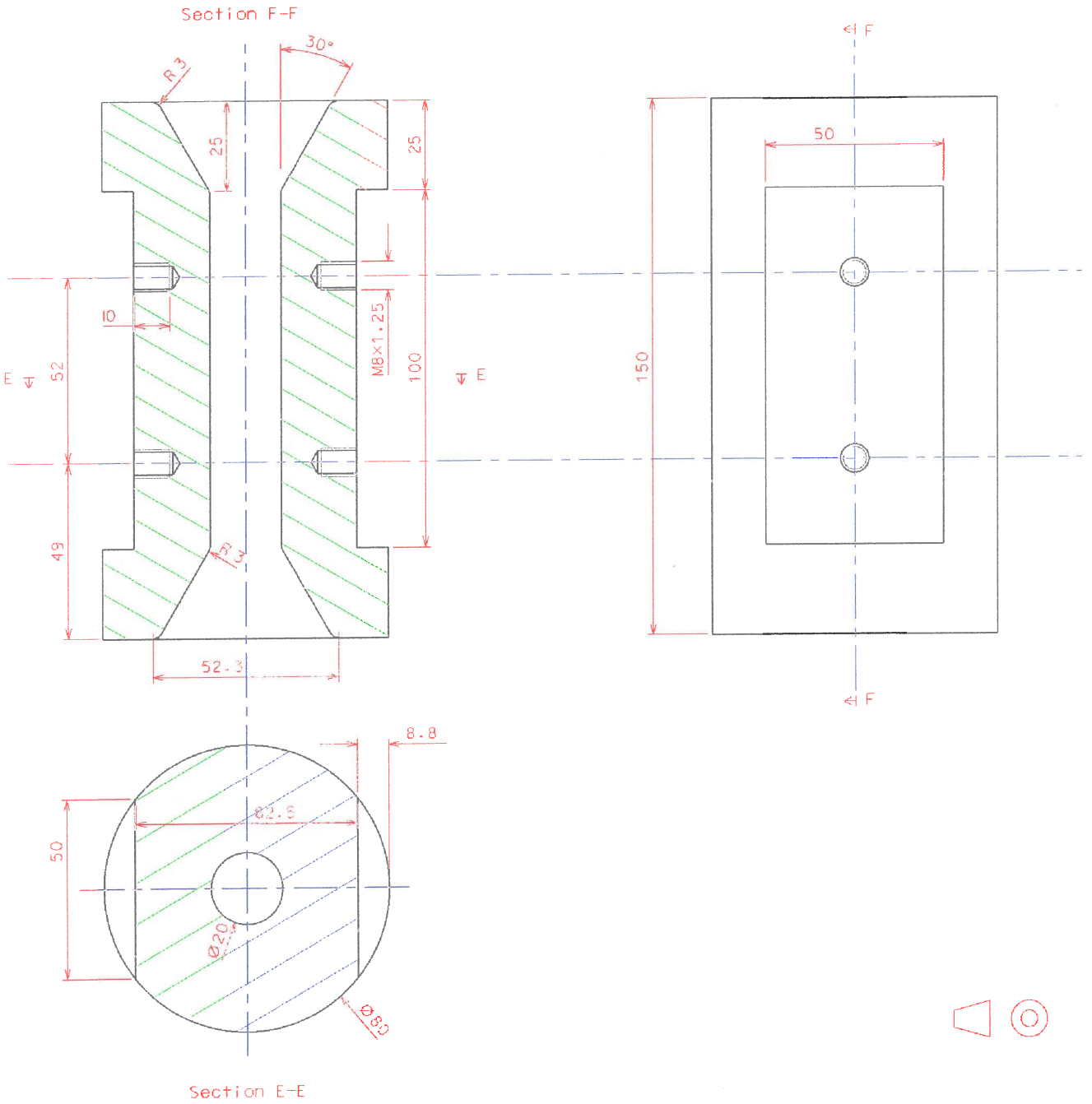

APPENDIX G

Test results of an absorber with a 55-Shore A spring

Table I.2. Test results for stiffness [MN/m].

	Hysteresis loop equation			Sine curve fit		
Frequency [Hz]	k_0	k_∞	$\Delta k/k_0$ [%]	k_0	k_∞	$\Delta k/k_0$ [%]
5	3.06	2.98	2.51	3.05	3.03	0.49
10	3.40	3.24	4.47	3.39	3.23	4.63
15	3.54	3.38	4.67	3.54	3.36	5.00
19	3.63	3.53	2.84	3.63	3.54	2.64
26	4.14	4.10	1.06	4.15	4.10	1.22
30	4.65	4.26	8.56	4.66	4.25	8.73
35	4.51	4.19	7.08	4.50	4.19	6.94
40	5.06	4.88	3.60	5.06	4.89	3.38

Curve fit not successful, $\Delta k = k_0 - k_\infty$

Table I.3. Average test results for stiffness [MN/m].

Frequency [Hz]	k_0	k_∞	$\Delta k/k_0$ [%]
5	3.05	3.01	1.50
10	3.39	3.24	4.55
15	3.54	3.37	4.83
19	3.63	3.53	2.74
26	4.15	4.10	1.14
30	4.66	4.25	8.64
35	4.50	4.19	7.01
40	5.06	4.88	3.49

Table I.4. Test results for the loss factor.

	Average peak method			Phase shift from curve fit			Energy method		
Frequency [Hz]	η_0	η_∞	$\Delta\eta/\eta_0$ [%]	η_0	η_∞	$\Delta\eta/\eta_0$ [%]	η_0	η_∞	$\Delta\eta/\eta_0$ [%]
5	0.27	0.27	1.78	0.28	0.27	4.42	0.34	0.32	4.31
10	0.42	0.40	2.98	0.42	0.41	3.79	0.46	0.45	3.02
15	0.48	0.47	1.73	0.49	0.48	2.39	0.51	0.50	1.70
19	0.50	0.50	0.62	0.50	0.50	1.38	0.53	0.51	3.15
26	0.53	0.52	2.33	0.53	0.53	-0.01	0.55	0.54	1.89
30	0.56	0.52	6.68	0.56	0.52	6.55	0.57	0.53	6.84
35	0.51	0.51	0.57	0.52	0.51	0.77	0.51	0.51	0.01
40	0.54	0.53	2.22	0.54	0.49	9.52	0.57	0.55	2.42

Curve fit not successful, $\Delta\eta = \eta_0 - \eta_\infty$

Table I.5. Average results for the loss factor.

	η_0	η_∞	$\Delta\eta/\eta_0$ [%]
5	0.30	0.29	3.57
10	0.43	0.42	3.26
15	0.49	0.48	1.94
19	0.51	0.50	1.74
26	0.53	0.53	1.41
30	0.56	0.52	6.69
35	0.51	0.51	0.45
40	0.55	0.52	4.70